Multifunctional nanostructured materials for next generation photovoltaics

Author

Wu, Congcong, Wang, Kai, Batmunkh, Munkhbayar, Bati, Abdulaziz SR, Yang, Dong, Jiang, Yuanyuan, Hou, Yuchen, Shapter, Joseph G, Priya, Shashank

Published

2020

Journal Title

Nano Energy

Version

Accepted Manuscript (AM)

DOI

10.1016/j.nanoen.2020.104480

Multifunctional Nanostructured Materials for Next Generation Photovoltaics

Congcong Wu[a,b,1], Kai Wang[b,1], Munkhbayar Batmunkh[c,d,1], Abdulaziz S. R. Bati[c], Dong Yang[b], Yuanyuan Jiang[b], Yuchen Hou[b], Joseph G Shapter[c,*], Shashank Priya[b,*]

[a] Hubei Collaborative Innovation Center for Advanced Organic Chemical Materials, Key Laboratory for the Green Preparation and Application of Functional Materials, Hubei Key Laboratory of Polymer Materials, School of Materials Science and Engineering, Hubei niversity, Wuhan 430062, China

[b] Materials Science and Engineering, Penn State, University Park, PA 16802, United States

[c] Australian Institute for Bioengineering and Nanotechnology, The University of Queensland, St Lucia Brisbane, Queensland 4072, Australia

[d] Centre for Clean Environment and Energy, Griffith University, Gold Coast, Queensland 4222, Australia

* Corresponding authors: j.shapter@uq.edu.au (J. G. Shapter); sup103@psu.edu (S. Priya)

[1] These authors contributed equally to this work.

Keywords: Nanostructured Materials; Photovoltaics; Application; 3rd Generation Solar Cells

Abstract: Next generation photovoltaics such as dye sensitized solar cells, perovskite solar cells and organic solar cells, generally termed as the "third-generation photovoltaic technologies", will have great impact on the photovoltaic technology deployment. These emerging photovoltaic cells are generally layer-structured devices, consisting of nanostructured layers with multifunctionalities of charge collection, extraction and photoconversion. Nanostructured layers including anode/cathode buffer layers, interfacial modification layers, and photon active layers are usually synthesized by various physical and chemical deposition techniques. Due to multiple coupling effects in these nanostructured materials, the layered cells have shown great potential for enhanced photovoltaic efficiency. Advanced nanotechnology fabrication approaches have accelerated the design and development of novel nanostructured materials, which is driving the advancements in solar cell performance. The nanomaterials and nanostructures critically impact the optical and electronic properties of the functional layers by modulating their morphology, microstructure, and surface states, thereby influencing the output voltage and conversion efficiency. In this review, we provide detailed discussion on recent developments in nanostructured materials and illustrate the designs for their integration with emerging "third-generation photovoltaic technologies". A comprehensive discussion is provided on the role of nanostructures, functionalities, and effectiveness of various nanomaterials in improving the performance of solar cells, including dye sensitized solar cells, perovskite solar cells and organic solar cells. Throughout the review, discussions are included addressing the remaining challenges and new opportunities.

CONTENT

1. Introduction

With the rapid growth in global population and modern technologies, our daily energy consumption has reached unprecedented levels. It is estimated that the global energy consumption will increase by ~50% by 2040 [1]. Today, 80% of the world's energy supply is derived from fossil fuels (coal, oil, and gas). In addition to the ever-increasing fossil fuel price, the combustion of fossil fuels has been thought to cause the greenhouse effect that is influencing the climate change. Thus, there is growing emphasis on developing alternative energy sources that will be able to meet the current and future energy demands.

Renewable energy sources such as wind, solar, hydro and geothermal are the promising alternatives. Until recently, hydroelectric power and wind energy have been the fastest growing technology but are limited by deployment and cost issues. Converting solar energy into electricity *via* photovoltaic (PV) devices (i.e., solar cells) is another rapidly growing avenue, as the sun light is an inexhaustible energy source[2,3]. Advances in solar technologies have seen a surge in the efficiency and power density [4]. PV technologies can be classified into three groups for historical reasons: *(i)* The "first-generation PV", based on silicon (Si) semiconductors[5] are technically mature, with the best power conversion efficiency (PCE) of ~26%[6] at the laboratory level. This approach has dominated the PV market with 91% of the market share. *(ii)* The "second-generation PV", is mostly based on thin-film inorganic semiconductors,[7] which only have a 9% market share due to their high manufacturing cost. The maximum efficiency of the "second-generation PV" is ~23% [6]. Although these first two generation PVs are commercially available, their manufacturing process is inherently complex and expensive.[8] Considering the need for providing large amount of electricity, low-cost PV techniques are urgently required. In order to meet cost and performance targets, the emerging *(iii)* "third-generation PVs" including dye sensitized solar cells (DSSCs), perovskite solar cells (PSCs), organic photovoltaic (OPV) and quantum-dot sensitized solar cells (QDSSCs) have been introduced.[9] The main features of the "third-generation PVs" are simple manufacturing, low cost and high performance.[6] Additional features such as flexibility and light-weight can enable additional applications such as potable power source, indoor light harvesters, and solar wings for drones.

Nanostructured functional materials are required for improving the PV efficiencies as well as reducing the cost. So far, a wide range of nanomaterials including semiconducting oxides, nanocarbons, one-dimensional (1D), two-dimensional (2D) and three-dimensional (3D) materials

have been employed in buffer layers, interfacial modification layers and photoactive layers. **Fig. 1** shows the timeline of the three PV generations along with multiple nanomaterials and nanostructures that have been successfully employed in the 3rd generation PVs. Herein, we review important breakthroughs and recent advances that have been made in the emerging PV techniques including DSSCs, PSCs, and OPVs using nanostructured materials. After a brief overview of each type of PV systems, important research mechanisms controlling the performance in each aspect of these PVs is discussed. The review concludes by providing perspectives on the remaining challenges and future opportunities.

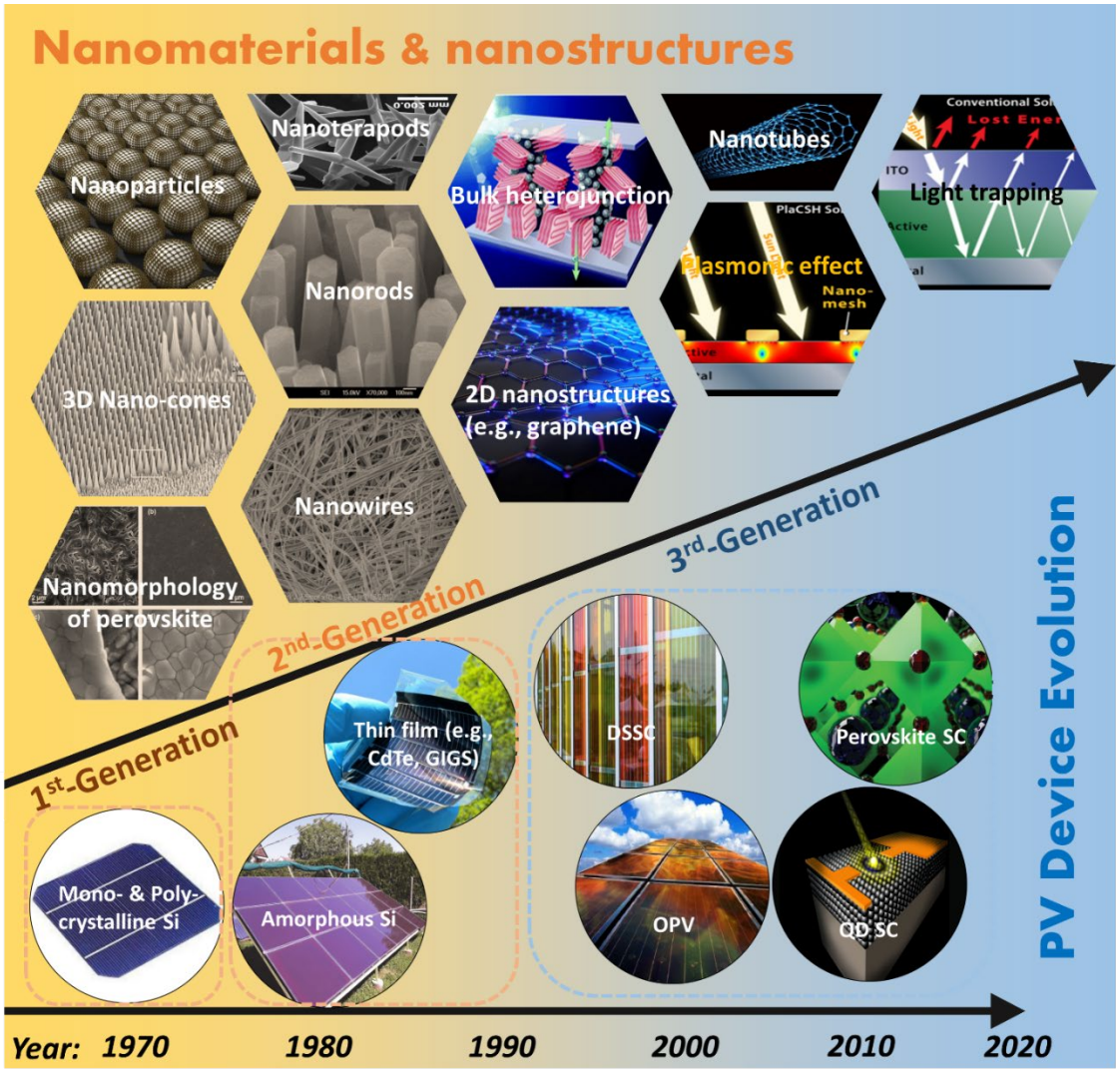

Fig. 1. Timeline of the three PV generations along with multiple nanomaterials and nanostructures that have been successfully employed in the 3rd generation PVs including the DSSCs, OPVs, Perovskite PVs, and QD PVs. Credits are given to various online resources for the adaption in this figure.

2. Dye Sensitized Solar Cells

Dye sensitized solar cells (DSSCs) have a number of unique features, such as easy fabrication, low-cost, semi-transparency *etc.,* making them an attractive thin film PV technology to supplement the traditional solar cell market.[10–13] The organic dyes and their photo-response was first discovered in 1968.[14] At the early stage, various dye sensitizers were investigated in terms of their photoelectrochemical properties, while the corresponding power conversion efficiency (PCE) struggled from 0.5% to 2.5%.[15–17] This is because of the use of bulk flat semiconductor electrodes that adsorb only a monomolecular layer of dye sensitizer hence resulting in poor light absorption (< 1%). Later in 1991, a nanostructured TiO_2 layer was employed to adsorb the dye, where the enlarged surface area dramatically increased the number of the dye molecules and thus an improved light absorption. For example, Grätzel's group utilized a 10 μm thick mesoporous nanocrystalline TiO_2 film combined with a ruthenium-based sensitizer, and obtained a conversion efficiency of ~ 8% for the DSSCs.[18] Next, we describe detailed functionality of nanomaterials and their effects on performance of the DSSCs.

DSSCs are generally composed of photo-anode, electrolyte and counter electrode. The photo-anode is constructed using a mesoporous layer sensitized by dye molecules. A monolayer of dye molecule is incorporated on the surface of nanocrystalline particles. The electrolyte is used to regenerate the oxidized dye and transport redox couple to the counter electrode, as illustrated in **Fig. 2a** [19,20]. The most commonly used electrolyte in high-efficiency DSSC is the triiodide/iodide (I_3^-/I^-) in liquid solvent or polymer matrix. When a photon impinges on the dye molecules, the excited electrons in dye jump from the HOMO (highest occupied molecular orbital) to LUMO (lowest unoccupied molecular orbital) ($S^0 \rightarrow S^*$). As the energy level of LUMO of dye sensitizer is higher than the conduction band (CB) of TiO_2, the excited electrons will transport to the CB (conduction band) of TiO_2. Subsequently, the electrons flow through the external working circuit and reach the counter electrode. The redox couple (I_3^-/I^-) in electrolyte regenerates the dye through the reaction $3I^- \leftrightarrow I_3^- + 2e^-$, and the newly formed I_3^- diffuses to the counter electrode, where it can be regenerated into I_3^- ions. The platinum layer coated on the conducting counter electrode works as the catalyst for the reaction, $I_3^- + 2e^- = 3I^-$, as illustrated in the schematic operation of DSSCs (**Fig. 2b**) [21–23].

The strategy to improve the performance of DSSCs is to increase the incident light absorption and enable effective charge carrier separation and transport. All these aspects are

closely related with the nanostructure of the photo-anode. Mesoporous oxides film such as TiO_2, ZnO, SnO_2 and Nb_2O_5 are the preferred photo-anode materials.[24,25] The internal surface area and porosity of the mesoporous film have a critical impact on the dye chemisorption, which determines the photocurrent generation. In addition, the morphology and structure of the photo-anode crucially affect the charge transfer kinetics. Continuous semiconductor networks are interpenetrated with *p*-type materials, providing an individual conductive path for both electrons and holes. The photo-anode needs to be electronically accessible for charge carriers to percolate across the mesoscopic network. On the other side, the counter electrode provides active sites to collect holes and regenerate the *p*-type species. The catalytic nanomaterials and the nanostructure features of the counter electrode affect the current delivery from the electrolyte as well as the overpotential at the electrolyte/counter electrode interface. Next, we introduce various nanostructured materials that have been used or have the potential to be used in DSSCs electrodes, describing their unique properties and the advantages as an electrode. Further, we provide guidance on development of nanomaterials that plays important role in photovoltaic performance.

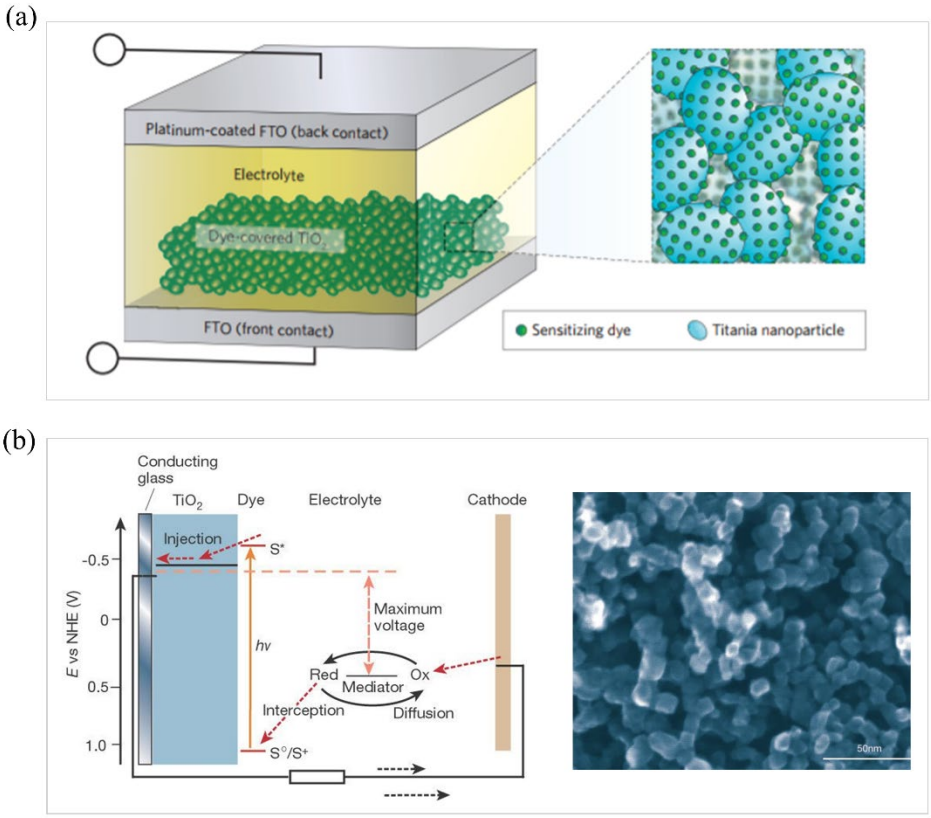

Fig. 2. (a) Schematics of the dye sensitized solar cells (DSSCs), which comprises of the transparent glass substrate, TiO_2 mesoporous photo-anode, electrolyte and platinum based counter electrode. Adapted from reference [12], with permission of © 2012 Macmillan Publishers Limited. **(b)** Illustration of the operational

mechanism for the DSSCs and scanning electron micrograph (SEM) of the surface of a mesoporous anatase TiO_2 film. Adapted from reference [25], with permission of © 2001 Macmillan Magazines Ltd.

2.1 Nanostructured photo-anode materials for DSSCs

Semiconductor nanoparticles with dimensions of ~20 nm were initially used to prepare the mesoporous film as photo-anode, which has enough surface area to adsorb sensitizer molecules and also serve as the electron transport channel for charge transport. It is commonly believed that the charge transport through the mesoporous film can be described by the random walk model, thus the electrons may recombine with holes in the *p*-type material or trapped when traveling across the particle boundaries. To address this issue, various novel nanostructured materials have been synthesized. The structure, morphology, orientation, and crystallinity was tailored with the aim to improve the charge transfer properties and surface area simultaneously. In this section, we are going to introduce one-dimensional (1D), three-dimensional (3D) and nanocomposite materials and their application in the photo-anode for DSSCs.

2.1.1 One-dimensional nanostructure

To address the low electron transport rate of TiO_2 nanoparticles, 1D nanostructure materials such as nanotubes, nanowires, and nanorods *etc.* could be promising substitutes for nanoparticles. One-dimensional nanomaterials can provide oriented fast electron transport pathways, and reduce the charge recombination at the surface states, defects and grain boundaries. These 1D materials have been intensively investigated and applied in DSSCs.

Nanotubes. Nanotube materials such as carbon, boron nitride, and oxides *etc.* are of great research interest for application in energy-related devices, among which TiO_2 nanotube shows great potential to be used as the photo-anode material in DSSCs. The TiO_2 nanotubes can be synthesized through different routes. The TiO_2 nanotubes first used in DSSCs were synthesized by a "surfactant template-assisted method". A single phase of anatase TiO_2 nanotubes with outer and inner diameters of about 10 and 5 nm and a length of 30-500 nm were fabricated. The TiO_2 nanotube based DSSCs showed more than ~2× improvement in the current density compared to conventional cells because of the higher internal surface area, which results in 4.88% PCE with a 4 μm thick nanotube-powder film layer.[26] Typically, the "hydrothermal method" is the most commonly used method to fabricate 1D nanomaterials, but Kasuga et al. introduced the first "chemical method" to fabricate TiO_2. Briefly, they first treated the TiO_2-SiO_2 powder with an

aqueous solution of 10 M NaOH at 110 °C for 20 h and then HCl aqueous solution to exchange the Na^+. This results in nanotubes with an outer diameter of 8 nm and a length of 100 nm. The formation mechanism is shown by TEM results (**Fig. 3a**), where the nanoparticles experienced a gradual transformation into the tube-shaped nanomaterials. During this process, the alkali solution treatment leads to the formation of Ti-O-Na and Ti-OH sheets. Subsequent dehydration of the Ti-OH bonds by HCl decreases the bond distance from one Ti to the neighboring Ti at the surface, resulting in the folding of the sheets into nanotubes.[27,28] Based on this method, high specific surface area TiO_2 nanotubes have been fabricated and PCE of the corresponding DSSC was obtained to be ~7%.[29,30]

Even though high specific surface area can be obtained from the hydrothermal method, the resultant TiO_2 nanomaterials typically exhibit powder-like feature, requiring further processing including paste preparation, film deposition, and annealing to obtain a qualified photo-anode layer. During these procedures (e.g., grinding and high-temperature annealing), the morphology of the nanotube can be easily changed or even damaged. In addition, the nanotubes are randomly stacked within the photo-anode layer, which could change the direction of electron transport and result in less electron collection at the conductive substrate. From this point of view, the well-aligned TiO_2 nanotube array that is vertically aligned with the substrate (**Fig. 3b**) is a better choice. Typically, anodization is the method to synthesize TiO_2 nanotube array on a Ti foil. The Ti foil and Pt are used as working and counter electrode, respectively, both of which are placed in a solution bath containing fluoride ions. Upon applying the voltage, the fluoride ions move towards the Ti working electrode and etch the Ti foil forming distributed voids. After reaching equilibrium between the inward and outward fluoride etching, the tube-like structure can be formed on the Ti foil. The TiO_2 nanotube array on the TiO_2 foil substrate is directly used as the photo-anode of DSSCs (**Fig. 3b**), where both inner and outer tube walls can be active sites to adsorb dye molecules.

The challenge in the application of TiO_2 nanotube array in DSSCs is the lower surface area compared with nanoparticles, which is on the order of several hundred nanometers. Schmuki et al. fabricated the nanotubes (with a diameter of approximately 100 nm, wall thickness of 15 nm, tube length of 2.5 μm and 500 nm, respectively) using the etching process that obtained DSSCs with only 0.036% PCE.[31] Since then, the improvement of the surface area by increasing the aspect ratio has become the priority in synthesizing TiO_2 nanotube arrays.[32,33] The geometry of TiO_2 nanotube arrays can be tuned by the anodization parameters, such as electrolyte, voltage, time,

substrate roughness *etc.* For example, Grimes et al. used an ethylene glycol (EG) based electrolyte anodized at 60 V for 17 h, which resulted in the formation of the nanotube arrays with a length of 220 μm, average inner diameter of 110 nm and an aspect ratio of approximate 1400, as shown in **Fig. 3c**. The achievement of the ultra-high aspect ratio is due to the utilization of organic solvents with high dielectric constant, which allows for a larger potential window for nanotube formation. Since the 220 μm nanotube arrays is hard to handle, the DSSC using 20 μm length nanotube arrays was fabricated and exhibited a PCE of 6.9% [34]. Normally, the length of TiO_2 nanotube can be increased by increasing fluoride concentration and applied voltage, however, that will also enlarge the pore size of the tube thereby compensating the tube length. Diau et al. combined potentiostatic and galvanostatic approaches to grow a TiO_2 nanotube array with length of 70 μm on the Ti foil substrate. They tested the DSSCs with TiO_2 nanotube with a length of 15–57 μm, and the best performance cell was obtained from the 30 μm nanotube exhibiting 7.6% efficiency.[35]

Due to the opaque nature of Ti foil, the TiO_2 nanotube array/Ti foil photo-anode can only be applied in a backside illumination architecture. In this case, the light illuminates from the counter electrode, passes through the Pt catalyst, electrolyte, and then reaches the TiO_2 nanotube and dye sensitizer. This always results in significant light loss. To address this issue, the transfer of TiO_2 nanotubes from Ti foil onto fluorine-doped tin oxide (FTO) glass is the solution. Wang et al. reported the free-standing TiO_2 nanotube membranes that were detached from the Ti foil and bonded on to the FTO glass.[36] As shown in **Fig. 3d**, after immersing the sample in H_2O_2 for 15 s, the entire TiO_2 nanotube membrane can be detached from Ti foil and transferred on to FTO glass substrate. Based on this technique, the conversion efficiency of front illuminated DSSCs with TiO_2 nanotube cell reaches a high value of 9.02%. In contrast, Grimes et al. reported the fabrication of transparent TiO_2 nanotube array films on the transparent conducting oxide glass with lengths between 0.3 and 33.0 mm using an electrochemistry approach. **Fig. 3e** shows a 20-mm-thick titanium film deposited on FTO glass, and the front illuminated DSSCs based on this TiO_2 nanotube yielded a PCE of 6.9%.[37]

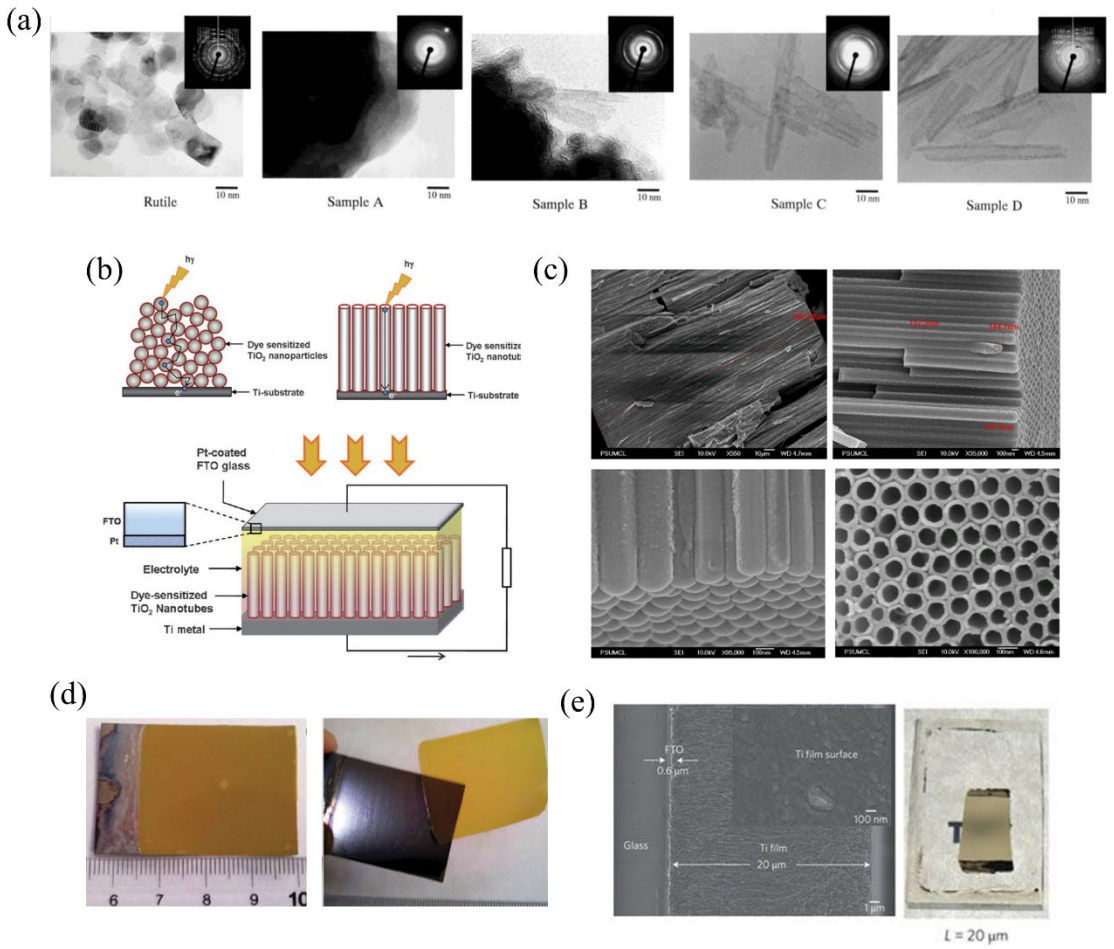

Fig. 3. (a) TEM images and selected-area electron diffraction (SAED) patterns of the rutile raw material and reaction products at different synthesis steps (sample A, B, C and D was obtained when the conductivity of the supernatant reached 10 mS/cm, 70 μS/cm, 800 μS/ cm and 5 μS/cm, respectively) Adopted from reference [27], with permission of © 1999 WILEY-VCH Verlag GmbH,. **(b)** Schematic representation of DSSCs using TiO_2 nanotubes array grown on a Ti substrate, and the comparison of the electron pathways through nanoparticulate and nanotubular structured TiO_2, adopted from reference [38] with permission of © 2010 The Royal Society of Chemistry. **(c)** The cross-section, bottom, and top SEM images of a nanotube array sample grown at 60 V in an ethylene glycol electrolyte containing 0.25 wt% NH_4F, adopted from reference [34], with permission of © 2007 IOP Publishing Ltd. **(d)** Digital images of the TiO_2 nanotube arrays before and after detaching from the Ti foil, respectively. Adopted from reference [36], with permission of © 2013 Elsevier B.V. **(e)** SEM and digital images of a 20 μm long nanotube array (pore size, 95 nm; wall thickness, 10 nm), adopted from reference [37], with permission of © 2009 Macmillan Publishers Limited.

Nanowires and nanorods. Similar to the nanotubes, the use of one-dimensional nanowires or nanorods is intended to increase the electron diffusion length and improve the charge collection efficiency. The study of nanowire/nanorod is mainly focused on ZnO and TiO_2, with the aim to simultaneously increase the surface area and maintain an efficient carrier collection. Yang's group fabricated a ZnO nanowire array in aqueous solution using a seeded growth process. The 10-15

nm thick ZnO film was first deposited on the FTO glass. The nanowires grew from these nuclei *via* the thermal decomposition of a zinc complex. Based on this method, uniform ZnO nanowire with length around 16 μm can be synthesized (**Fig. 4a**). Each individual nanowire displayed a high electron diffusivity of D_n = 0.05-0.5 cm^2 s^{-1}, which is hundred times higher than the nanoparticles. However, the DSSC with the ZnO nanowire array exhibited poor performance, with a relatively low PCE of 1.5%.[39] Aydil et al. also synthesized ZnO nanowire using solution chemistry method and metalorganic chemical vapor deposition, but only obtained a PCE of 0.3% and 0.5% respectively.[40,41] In distinct contrast to nanotubes, the nanowires or nanorods can only provide outer surfaces to adsorb the sensitizer, so the main reason for the low PCE of DSSCs is the insufficient surface area for dye adsorption and the low light absorption. In order to increase the surface area of ZnO nanowires, Gao et al. reported a new liquid-phase chemical process to grow ultralong ZnO nanowire arrays. The process effectively suppresses the homogeneous nucleation which usually leads to the formation of particles. As a result, ZnO nanowires with length over 30 μm were synthesized within 10 h. However, even with 33 μm ZnO nanowire, the corresponding DSSCs still showed the low conversion of 2.1%.[42] Following this work, Gao and coworkers reported an newly developed solution to grow multilayer assemblies of ZnO nanowire arrays, possessing a high internal surface area that is >5× larger than that of single-layer ZnO nanowire arrays, as shown in **Fig. 4b**. Multilayers of ZnO nanowires can be stacked to avoid fusion at the root of nanowire arrays, providing high surface area. The DSSCs with 4 layers of ZnO nanowire arrays showed the efficiency of 7%, demonstrating a significant advancement in this field.[43] In addition to the chemical method, Boschloo et al. also reported a metal organic vapor deposition (MOCVD) method to synthesize the well-ordered and single-crystalline ZnO arrays with low defect density. This design accelerated the electron transport, providing two orders of magnitude faster (~30 μs) response than that in nanoparticles.[44]

The problem of ZnO is the instability in acidic dye solution, thus the DSSCs assembled with ZnO normally show poor performance compared to that of TiO_2. However, due to the different crystalline structure, the growth of TiO_2 nanowire films with proposed orientation and excellent crystallinity is more difficult than ZnO. Aydil and coworkers reported a simple hydrothermal method for the growth of oriented single-crystalline rutile TiO_2 nanorods on FTO substrates. The nanorod morphology such as diameter, length, and density can be well controlled through the hydrothermal parameters. As shown in **Fig. 4c**, high-resolution transmission electron

microscopy (HRTEM) shows complete crystallinity along their entire lengths with scattering spacing of d_{110} = 3.2 Å and d_{001} = 2.9 Å, which are consistent with the lattice parameters of rutile phase.[45] Lin et al. also demonstrated the single-crystalline rutile TiO_2 nanorods arrays with thickness up to 30 μm grown on FTO substrates by a one-pot hydrothermal method. In their work, it was found that the etching treatment could significantly increase the roughness of the nanorods, hence increasing the internal surface area. Benefitting from the etching process, there is a boost in the device efficiency, reaching a value of 7.91% for the TiO_2 nanorod based DSSCs (**Fig. 4d**).[46] Regarding the morphology of the nanowire/rod arrays, Kuang et al. reported a self-assembled multi-layered TiO_2 nanowire/rod with tunable wire/rod length from 15 to 55 μm. This nanostructure consisted of a bottom layer made of densely packed TiO_2 nanowires, an intermediate layer made of hierarchical TiO_2 nanowires with short nanorods branches, and an upper layer made of loose TiO_2 nanowires, as illustrated in **Fig. 4e**. Such a design is advantageous in the large surface area for sufficient dye adsorption, excellent electron transport, and a pronounced light-scattering effect that can further improve the light absorption. As a result, a high PCE of 9.40% is obtained in the corresponding DSSCs, which is significantly higher than that using nanoparticles (7.23%).[47]

The one-dimensional nanomaterials possess superior charge transport properties compared to the nanoparticles, while the low internal surface area remains the limitation for the 1D nanomaterials to be used as the photo-anode. Development of nanostructured materials with improved surface area and super electrical properties is still the research interest in this area. Briefly, the aspect ratio, surface roughness, and multilayer designs have shown the effectiveness in improving performance. The directional electron transport in 1D materials also provides the opportunities for reducing the energy loss. However, for an efficient DSSC, novel nanostructured materials are still needed.

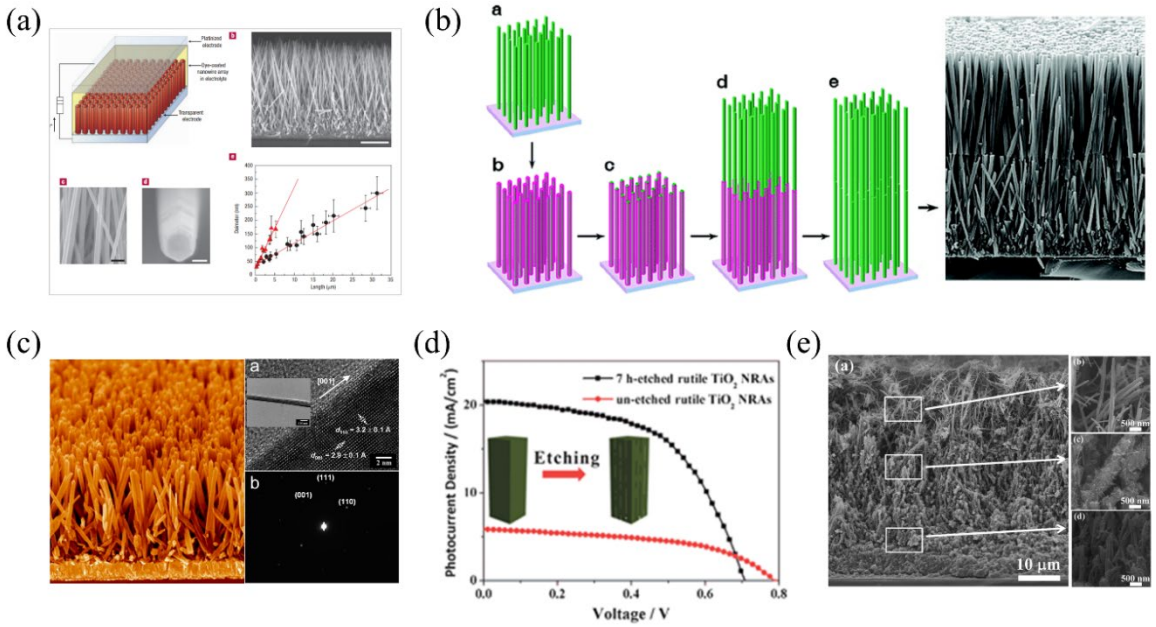

Fig. 4. (a) Schematic of the ZnO nanowire based DSSCs, the SEM image of cleaved nanowire array on FTO, magnified view of the oriented wires and single nanowire, and wire length against diameter with (circles) and without (triangles) PEI added to the growth bath. Adopted from reference [39] with permission of © 2005 Nature Publishing Group. (b) Schematics and SEM cross-sectional image of the two-layer assembly of ZnO nanowire arrays on TCO, adopted from reference [43] with permission of 2011 American Chemical Society. (c) SEM image of the oriented rutile TiO_2 nanorod film grown on FTO substrate and HRTEM image of a single TiO_2 nanorod, adopted from reference [45] with permission of © 2009 American Chemical Society. (d) The impact of etching treatment on the photovoltaic performance of TiO_2 nanorod based DSSCs, adopted from reference [46] with permission of © 2013 The Royal Society of Chemistry. (e) The cross-sectional SEM images of multi-layered TiO_2 nanowire on FTO glass, which shows the upper, intermediate and bottom layer, adopted from reference [47] with permission of © 2014 The Royal Society of Chemistry.

2.1.2 Facet-dependent nanostructure

The surface chemistry of the inorganic nanocrystals has a crucial impact on the surface properties such as adsorption, catalysis and chemical transport. Surfaces with high reactivity normally diminish during the crystal growth process due to the surface energy minimization. For instance in the anatase TiO_2 crystals, ~ 94% of the facets are {101} which is thermodynamically stable and only a very small fraction exhibits the reactive {001} facets.[48–50] Lu et al. have demonstrated that the fluorine-terminated surfaces can alter the crystal growth, making the {101} facets more energetically preferable. As shown in **Fig. 5a**, a systematic mechanism investigation found that the surface termination with F atoms yields the lowest surface energies (γ) for both {001} and {101} surfaces, the F termination makes {001} surfaces more stable than the {101} surfaces. Based on this theoretical calculation, titanium tetrafluoride (TiF_4) solution and hydrofluoric acid

(HF) were used to synthesize modulated crystals, and the flat square anatase TiO_2 crystals with a high percentage of {001} facets were obtained.[50] Xie et al. used hydrofluoric acid solution as the solvent and synthesized the anatase TiO_2 nanosheets with 89% exposed {001} facets.[51] This result provides a method to achieve anatase TiO_2 crystals with a high percentage of reactive {001} facets, which have promising applications in solar cells.

Yu and co-workers synthesized the 2D anatase TiO_2 nanosheets with exposed {001} facets and utilized them in DSSCs.[52] Results have shown that TiO_2 with different nanostructures can have a big effect on the efficiency. For example, using TiO_2 nanosheets, nanoparticles, and P25, the corresponding DSSCs showed efficiencies of 4.56%, 4.24% and 3.64%, respectively. The highest PCE comes from the DSSCs using TiO_2 nanosheets, which is attributed to the improved crystalline features, high pore volume, large particle size and enhanced light scattering effect. Wang et al. also synthesized the nanosized anatase TiO_2 single crystals with different percentages of exposed {001}.[53] The study revealed the evolution of the morphology of the nanocrystals as a function of the HF concentration. The fluorine ions can dramatically reduce the surface energy of the {001} facets, promoting the exposure of the {001} facets in TiO_2 single crystals. Thus, the geometrical evolution of the TiO_2 nanocrystals can be considered as the relative expansion of {001} facets with the increase of the HF concentration, as shown in **Fig. 5b**. Correspondingly, the PCE of DSSCs increases with the percentage of {001} facets, where PCEs of 7.47%, 8.14% to 8.49% were achieved from DSSCs using TiO_2 nanocrystals with 10%, 38% and 80% exposed {001} facets, respectively. TiO_2 nanocrystals with a high percentage of {001} facets usually have larger particles size than the commonly used P25 particles. Yang et al. reported a two-step hydrothermal reaction method to synthesize the anatase TiO_2 nanoparticles with 34% exposed {001} facets. With further F^- incorporation, the device efficiency increased to 7.06%, which is a significant increment compared to the original 3.47% from the device without F^-.[54]. In addition to the traditional hydrothermal method, Feng and co-workers explored a microwave hydrothermal process to synthesize the TiO_2 nanocrystals from exfoliated titanate nanosheet precursors with a lepidocrocite-like structure. They revealed that the {010} faceted anatase nanocrystals exhibited higher photocatalytic activity and device efficiency compared to P25 nanocrystals.[55]

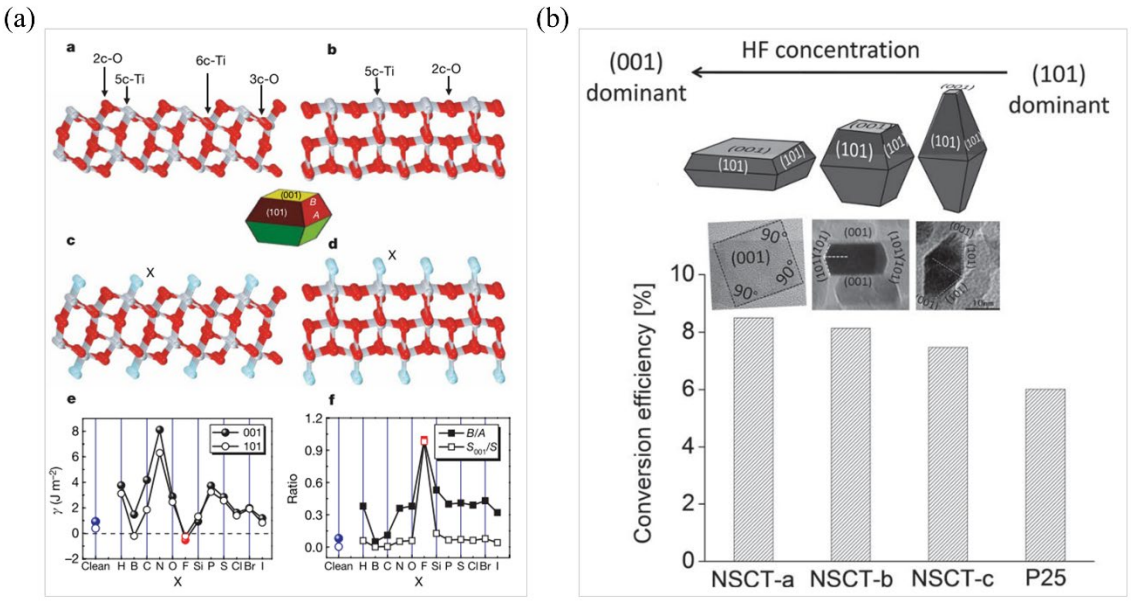

Fig. 5. (a) Slab models and calculated surface energies of anatase TiO_2 (001) and (101) surfaces, which shows the unrelaxed (001) and (101) surfaces with and without foreign atoms, adopted from reference [50] with permission of © 2008 Nature Publishing Group. (b) Schematic of the correlation between the particle morphology and the photoconversion efficiency of the nanosized anatase TiO_2 single crystals with different percentages of exposed (001) facets, adopted from reference [53] with permission of © 2011 WILEY-VCH Verlag GmbH & Co. KGaA, Weinheim.

Another example of the application of {001} faceted nanocrystals is the assembly of {001} sheets into TiO_2 spheres. Zhao et al. synthesized the micro-size anatase TiO_2 spheres with exposed mirror-like plane of {001} facets and demonstrated the application of such microspheres for photoanode in DSSCs. But the insufficient light absorption led to an average PCE of 7.91%.[56] Xu et al. reported the synthesis of hierarchically mesoporous microspheres consisting of over 90% {001} faceted nanosheets from different TiF_4 concentrations, as shown in **Fig. 6a**. These microspheres not only work as the light scattering layer but also provide a large surface area for dye loading. The nanosheet architectures can minimize the grain interface effect and the anatase {001} surfaces with high surface energy can effectively absorb the (COOH) groups. This results in a conversion efficiency of 7.51%, which is 43% higher than the standard Degussa P25 photoanode [57]. Yang and co-workers reported a yolk@shell nanostructure, which is typically recognized as a nanostructure consisting of interior core, void space, and permeable outer shell.[58] The yolk@shell hierarchical TiO_2 spheres (YSHS) possess a permeable shell self-assembled by ultrathin anatase TiO_2 nanocrystals with nearly 90% exposed {001} facets. The growth mechanism of the yolk@shell structure is illustrated in **Fig. 6b**. As the solvothermal reaction proceeds, the

solid spheres shrink and the newly formed spike-like nanoparticles assemble around the solid spheres. Due to the more negative band edge of (001) facets, the open circuit voltage (V_{OC}) was increased to 0.76 V, resulting in a PCE of 6.01%.

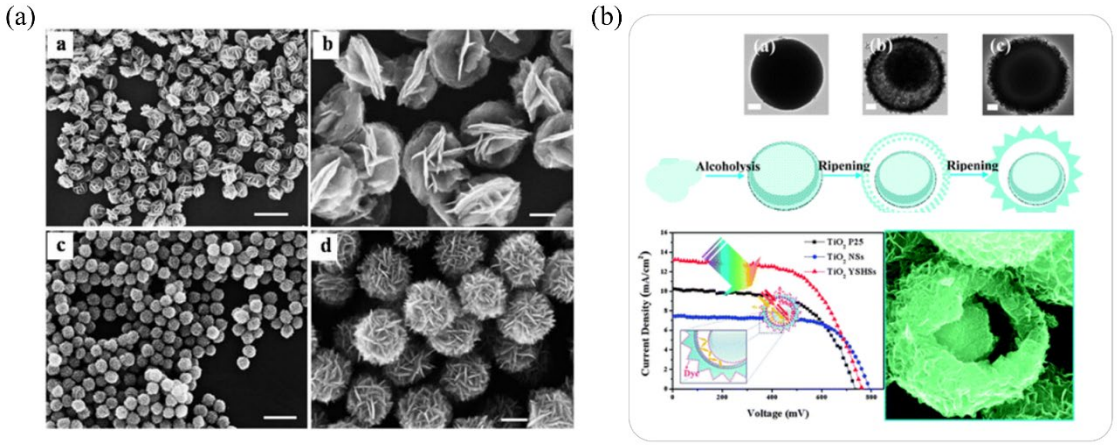

Fig. 6. (a) SEM images of the hierarchically structured TiO_2 nanosheets prepared at different TiF4 concentrations: 10 mM (upper row) and 30 mM (bottom row), adopted from reference [57] with permission of © 2011 The Royal Society of Chemistry. (b) TEM images and schematic illustration of the TiO_2 spheres and TiO_2 YSHSs obtained through solvothermal reaction with different times: 2 h, 12 h, 24 h (from left to right) and the J-V curves of the DSSCs with P25, TiO_2 spheres and TiO_2 YSHS, adopted from reference [58] with permission of © 2011 The Royal Society of Chemistry.

2.1.3 Nanocomposites

The function of the photo-anode in DSSCs is to adsorb the dye sensitizer and facilitate transport of the electrons. Hence, the composition, crystallinity, morphology of the materials have crucial impacts on these two functions. In some cases, one single material with a homogeneous morphology is not a perfect candidate to fulfill these two functions. In contrast, the nanocomposite photo-anode that combines the materials with different compositions, morphologies, and properties can be a promising platform. Researchers have focused on optimizing the optical and electrical properties and demonstrated various promising nanocomposite materials, including metal oxide/metal oxide, metal oxide/carbon and metal oxide/metal.

Metal oxide/Metal oxide. Various metal oxide combination, such as TiO_2 with Al_2O_3, MgO, SnO and ZnO have been fabricated for the photoanode material in DSSCs.[59–64] The composite of the TiO_2/ZnO has attracted particular interest due to the complementary properties between these two materials. The TiO_2 is favorable to adsorb dye molecules and has high chemical stability, while ZnO has high electron mobility, so the strategies such as surface coating, decoration, mixing

were attempted to combine these two aspects to achieve the combinatory effect.[65] Agrios et al. reported a nanocomposite photo-anode consisting of ZnO nanorods coated with TiO_2 nanoparticles using the wet-chemical methods. The ZnO nanorods were synthesized by chemical bath deposition, and the TiO_2 nanoparticles were coated uniformly over the nanorods by electrostatic layer-by-layer (LbL) deposition as shown in **Fig. 7a**, which provided ZnO nanorods with different amount of TiO_2 nanoparticles.[66] The nanocomposite benefits from the combination, as 1D ZnO nanorods provide fast electron transport pathways, while the coated TiO_2 nanoparticles provide enough surface area for dye loading. Gao and coworkers have reported the synthesis of multilayer arrays of vertically aligned ZnO nanowires directly on transparent conductive oxides. Subsequently, they grew a self-assembled TiO_2 monolayer onto the ZnO nanowires, as demonstrated in **Fig. 7b**. This nanocomposite structure circumvents the wire fusion problem in order to increase the surface area of ZnO nanowires, which coupled with the solid electrolyte of Spiro-OMeTAD gave rise to a PCE of 5.65% for the corresponding device.[67]

Since ZnO has a wider band gap (3.37 eV) compared to TiO_2 (3.2 eV), the utilization of ZnO to modify TiO_2 nanotube is another possible approach for reducing the charge recombination. TiO_2 nanotubes were synthesized on the Ti foil through anodization and the ZnO nanoparticles were induced *via* electrodeposition technique, where the coated ZnO can block the holes from the electrolyte and minimize the charge carrier recombination.[68,69] The formation of a heterojunction between the components is another important feature in the nanocomposite structure. Wang et al. reported a hybrid structure where the ZnO nanowires were inserted in the TiO_2 nanoparticles film.[70] The built-in potential at the heterojunction promoted the electron diffusion from the TiO_2 nanoparticles to ZnO nanowires, as illustrated in **Fig. 7c**. Based on this nanocomposite structure, the corresponding DSSCs exhibited a PCE of 8.44%, showing a 26.9% improvement compared with the TiO_2 nanoparticle based cell.

In addition to ZnO, SnO is another popular semiconductor to couple with TiO_2 and form the nanocomposite photo-anode. Similar to ZnO, SnO has higher electron mobility and wider band gap even larger than that of TiO_2, but the DSSC based on a single layer of SnO showed very poor device efficiency, owing to the very fast interfacial charge carrier recombination.[71] Cao and co-workers reported TiO_2-coated multilayered SnO_2 hollow microspheres (TiO_2-SnO_2) as a bifunctional photoelectrode material in DSSCs. As shown in **Fig. 7d**, the outer-shell diameters of spherical particles are in the range of 1~2 μm and the inner TiO_2 spheres have a diameter of 500

nm.[72] This nanocomposite structure overcomes the low V_{OC} of SnO photo-anode and increases the short circuit current (J_{SC}) due to the increased active surface area and the improved light scattering effect in the hollow spherical structure, resulting in a 5.65% efficiency. Kim and coworkers reported the TiO_2 nanosheets modified SnO nanotube [73] and SnO hollow spheres [74], respectively, to improve dye loading and charge transfer. A high PCE of 8.2% can be obtained for the hierarchical double-shell nanostructures consisting of an inner SnO_2 hollow spheres surrounded by outer TiO_2 nanosheets.

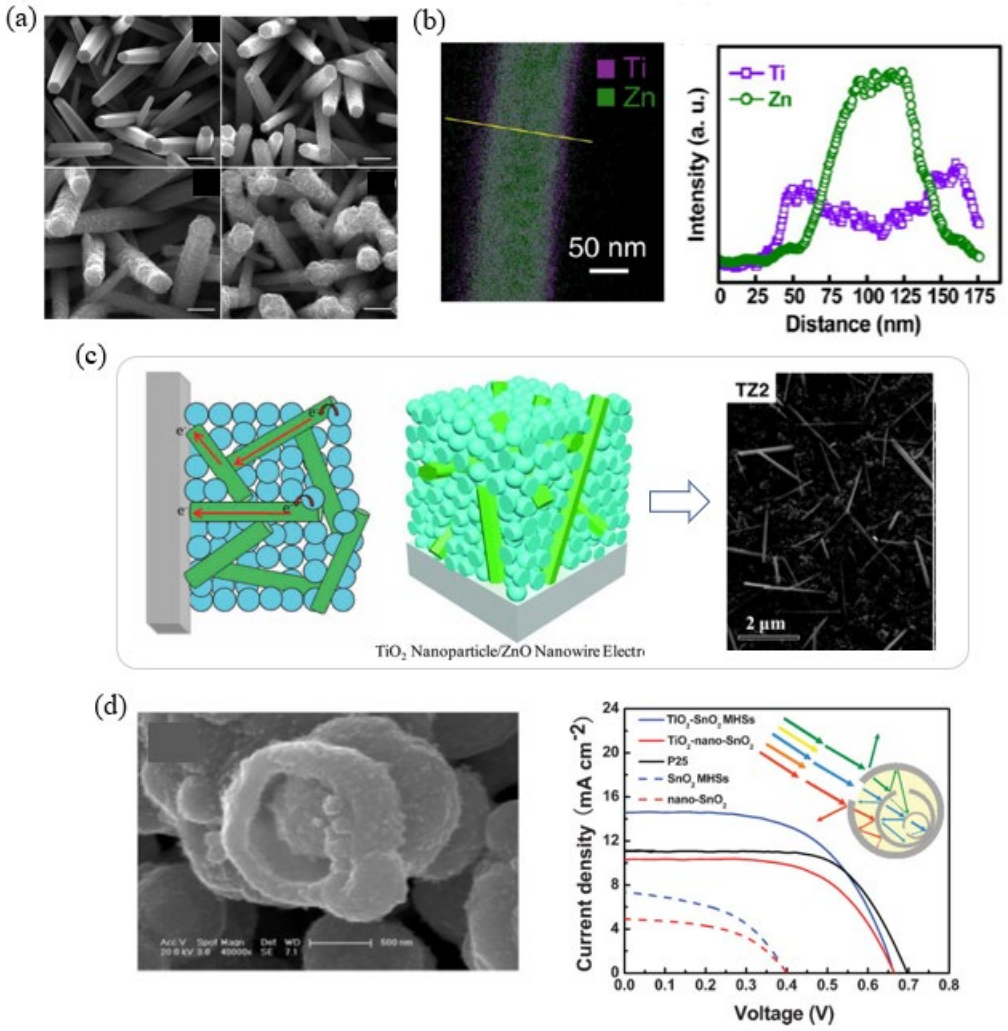

Fig. 7. (a) SEM images of ZnO nanorods coated with zero, one, three, or five layers of TiO_2 nanoparticles. Adopted from reference [66] with permission of © 2012 American Chemical Society (b) STEM elemental mapping image of TiO-coated ZnO nanowires and the line scan EDX profile obtained along the yellow dotted line, adopted from reference [67] with permission of © 2012 American Chemical Society. (c) Schematic illustration of electron transport in the nanoparticle/nanowire composite electrode and the SEM of the nanoparticle/nanowire composite film, adopted from reference [70], with permission of © 2012 WILEY-VCH Verlag GmbH & Co. KGaA, Weinheim. (d) SEM images of TiO_2-SnO_2 multilayered hollow

microspheres and J-V curve of DSSCs with different photo-anode structure, adopted from reference [72], with permission of © 2009 WILEY-VCH Verlag GmbH & Co. KGaA, Weinheim.

Metal oxide/Metal. Plasmons are generated when incident light excites coherent oscillation of the free electrons in metal nanoparticles such as Ag and Au.[75,76] This effect can cause intense absorption and enhanced local electromagnetic field, which have been used in DSSCs to improve the light absorption and PCE. There are several mechanisms in understanding the enhancement of the light absorption by the metallic plasmons: *(i)* metallic nanoparticles work as light scattering objects to scatter the photons within the film; *(ii)* metallic nanoparticles work as the subwavelength antennas where the plasmonic near-field is coupled to the semiconductor, which enhances the effective absorption cross-section; *(iii)* the metallic film on the back surface can couple the sunlight into the surface plasmon polaritons (SPPs) at the metal/semiconductor interface.[77] Based on these theories, various methods has been conceived to induce the metallic nanoparticle to couple with the TiO_2 photo-anode. Hupp et al. dispersed the Ag nanoparticles in TiO_2 networks *via* photoreduction of Ag^+ from dissolved $AgNO_3$. The PCE was improved by 25%, partially due to the increased dye loading upon the Ag incorporation, and the enhancement of the localized surface plasmon resonance (LSPR) behavior.[78] In addition to the light absorption, Wang et al. used Au nanoparticles that were inlaid in the TiO_2 layer and found that the quasi-Fermi level can be tuned to be lower by controlling the mass ratio of Au and TiO_2, as shown in **Fig. 8a**. As a result, the DSSC based on TiO_2 photo-anode with 0.168% Au displayed a PCE of 10.1% with V_{OC} of 863 mV, which is 97 mV higher than the conventional TiO_2 photo-anode.[79] Au nanoparticles with the TiO_2 nanowires also modify the optical properties of the photo-anode and improve the PCE further.[80,81]

McGehee et al. developed a one-step direct imprinting process for incorporating plasmonic silver nanodome arrays in the back reflectors of solid-state DSSCs, as illustrated in **Fig. 8b**.[82] A quartz master template with nanodome pattern was embossed into the film of TiO_2 nanoparticles and ethyl cellulose. After annealing, the nanodome pattern can be formed in the TiO_2 film, and then Ag was thermally evaporated on the surface of the device. In this nanostructure, the nanodome array of Ag back electrode played two roles in enhancing the light absorption by the light scattering effect and surface plasmon polariton effect. With the use of C220 dye, a PCE of 5.93% was obtained with 16% increment in J_{SC}. The metal nanoparticles in the photo-anode layer made contact with the dye molecules while also being exposed to the electrolyte, which risks charge

carrier recombination and electrolyte corrosion. Therefore, instead of directly using metal nanoparticles, core-shell particles were implemented in photo-anode for the plasmonic effect. Belcher et al. synthesized Ag@TiO_2 core-shell nanostructures and incorporated them in TiO_2 photo-anode, where the TiO_2 shell layer can block the charge recombination and prevent electrolyte corrosion. With a decrease in the thickness of TiO_2 photo-anode, the device efficiency was improved from 7.8% to 9%.[83] As an extension of this study, Belcher and co-workers found the localized surface plasmon resonance frequencies could be tunable depending upon the core-shell structure. As shown in **Fig. 8c**, they synthesized Ag@TiO_2 (AgT), Au@TiO_2 (AuT) and multiple-core-shell TiO_2-Au-TiO_2 nanoparticles and achieved maximum device efficiencies of 10.1%, 10.3%, and 10.8% for AgT, AuT, and TAuT NPs-incorporated DSSCs, respectively.[84] The core-shell structure is normally coupled with plasmonic effect and photo-charging effect, so in order to isolate these two effects and study the impact of each on the photovoltaic performance, Kamat et al. synthesized SiO_2- and TiO_2-capped Au nanoparticles, respectively. The SiO_2, as an insulator, acts as a barrier to prevent electron charging of the metal core, exhibiting only surface plasmon effects; while the TiO_2, as a semiconductor, is capable of transporting electrons to the Au core and thus charging the core in the Au@TiO_2-core@shell nanoparticles. As a result, the Au@SiO_2 in DSSC produces higher photocurrent owing to the plasmonic effect, resulting in higher PCE of 10.2% as compared to 9.8% for Au@TiO_2 (**Fig. 8d**).[85]

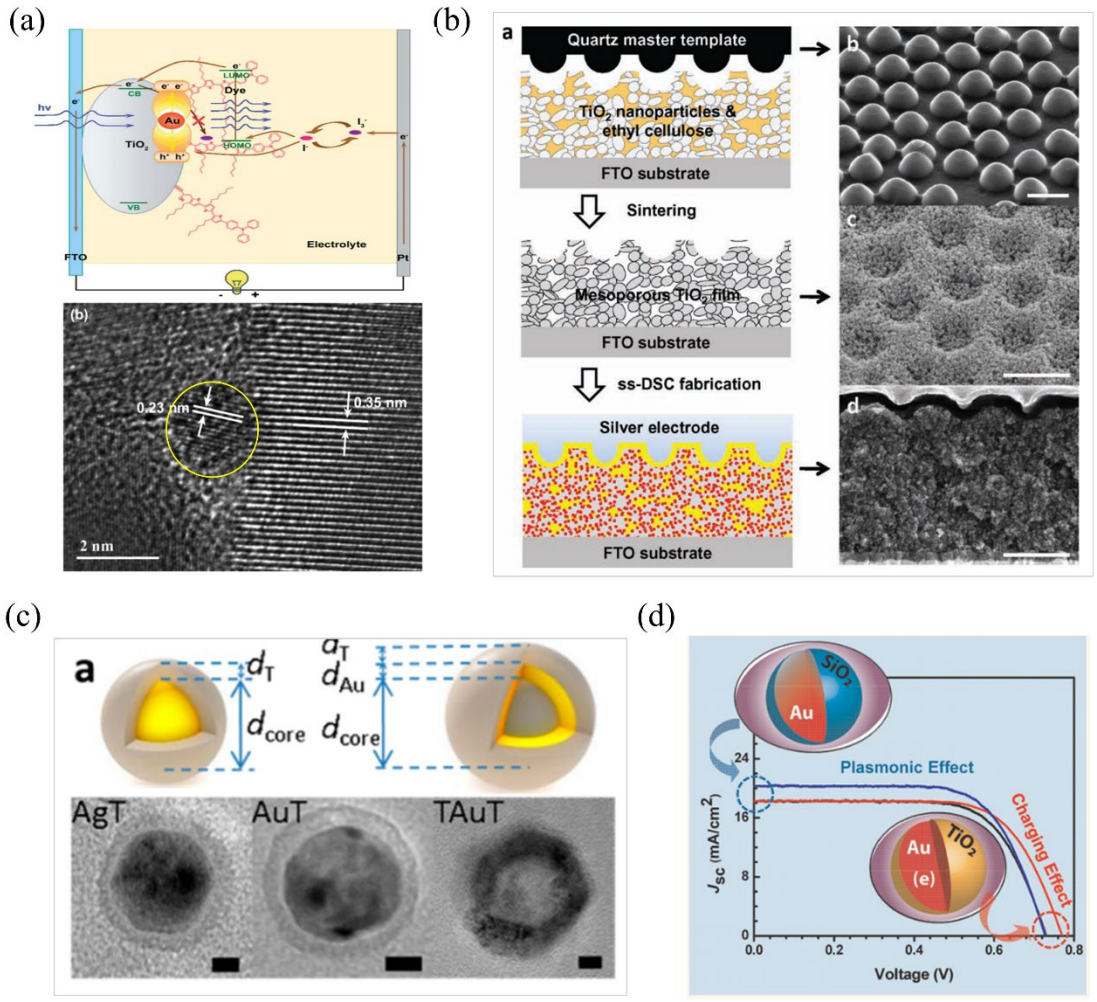

Fig. 8. (a) Schematic illustration of the charge transfer processes in the DSSC incorporating the photoanode and the HRTEM image of Au-TiO_2 nanoparticle, adopted from reference [79] with permission of © 2013 The Royal Society of Chemistry. (b) Schematic illustration of plasmonic solid-state DSSC fabrication process and the images of the nanodome array and plasmonic DSSC, adopted from reference [82] with permission of © 2010 WILEY-VCH Verlag GmbH & Co. KGaA, Weinheim. (c) Illustrations and transmission electron microscope (TEM) images of AgT, AuT, and TAuT nanoparticles, adopted from reference [84] with permission of © 2013 American Chemical Society. (d) The J-V curves of the DSSCs employing Au@SiO_2 and Au@TiO_2 photo-anode, adopted from reference [85] with permission of © 2012 American Chemical Society.

2.2 Nanostructured counter materials for DSSCs

The charge transfer process at the counter electrode/electrolyte interface has a crucial impact on the V_{OC} of the DSSCs, which significantly decreases the V_{OC} due to the overpotential of the reaction at the counter electrode. The counter electrode materials need to have high catalytic activity, high conductivity, and excellent chemical stability, *etc*. Pt is the most commonly used counter electrode material due to its outstanding catalytic performance and high chemical stability. Uniform Pt electrode can be synthesized through thermal decomposition, electrochemical

deposition, chemical reduction, and sputter deposition, *etc.*[86] In addition to the dense bulk Pt layer, nanostructured Pt electrodes and Pt-free counter electrodes will be discussed below with respect to the impact of these nanostructures on the charge transfer process at the counter electrode.

2.2.1 Nanostructured Pt counter electrodes

In comparison with planar bulk Pt electrodes, nanostructured electrodes can provide high surface area, high transmittance, and low charge transfer resistance. Jung et al. demonstrated a periodically arranged catalytic Pt nanocup array with a controlled diameter and pitch size as the counter electrode.[87] As shown in **Fig. 9a**, nanocup arrays with a diameter of 600 nm and 800 nm pitch size (PtNC-1), and a diameter of 300 nm and a 400 nm pitch size (PtNC-2) were synthesized. These nanostructures not only improve the surface area but also enable the percolation of electrolyte into the inner and outer faces of the cup to reduce charge transfer resistance. DSSCs with the nanocup array showed the conversion efficiency of 8.86 and 9.75% for the PtNC-1 and PtNC-2. This is improvement of 13% and 24%, respectively, compared to 7.87% from the DSSC with the planar Pt. 1D Pt material is promising research area for the counter electrode application. Lee et al. developed a multifunctional Pt nanofiber (PtNF) nano-network that can act as a catalyst layer in the counter electrode. PtNF showed high transmittance enabling the possibility to replace the FTO or ITO layer on the substrate to decrease the fabrication cost.[88] **Fig. 9b** shows the morphology of the as-fabricated Pt nanofiber network, which has a length of a few micrometers and a diameter range of 40~70 nm. The Pt nanofiber layer exhibited 81% transmittance and 106 Ω/sq sheet resistance, resulting in a PCE of 6%. Even though the efficiency with the nanofiber counter electrode is lower than the conventional FTO-Pt cell, it provides a promising direction for the counter electrode development with catalytic activity, conductivity, and transparency.

In addition to the morphological modulation, crystal tailoring in terms of the catalytic activity was also attempted for use in the counter electrode. The catalytic performance of Pt nanoparticles is highly dependent on the exposed facets, since the surface atomic coordination on different facets can have different efficiencies in breaking chemical bonds.[89–91] In the liquid electrolyte DSSCs, the chemical reaction occurring at the counter electrode is the reduction of I_3^- into I^-. Yang et al. theoretically calculated the adsorption energy of I atom for {100}, {111}, and {411} facets of Pt using density functional theory (DFT). They predicted that Pt {111} facet has the highest catalytic activity. Experimentally, they synthesized the Pt nanocrystals mainly bounded

by {100}, {111} and {411} facets, as shown in **Fig. 9c**, where three shapes of Pt nanoparticles with different main facets are presented. Consistent with the DFT simulation, the DSSC based on Pt {111} has the highest PCE of 6.91% due to the lowest adsorption energy of iodine atom on Pt {111}.[92]

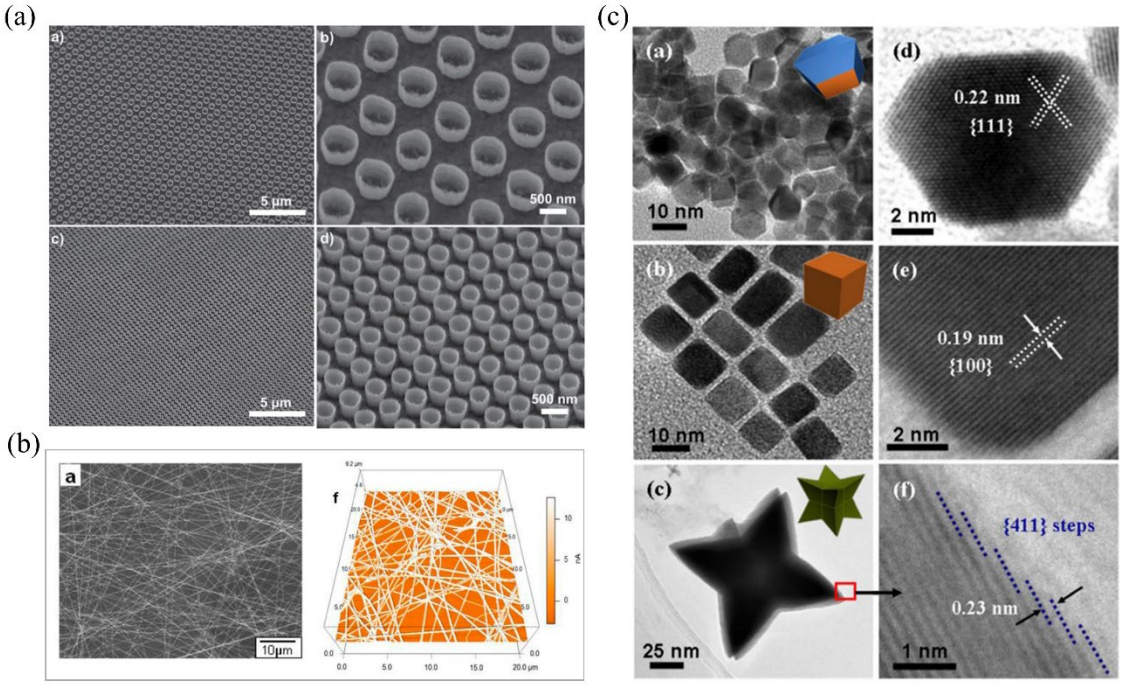

Fig. 9. (a) SEM images of the PtNC-1 (upper) and PtNC-2 (bottom), adopted from reference [87] with permission of 2012 WILEY-VCH Verlag GmbH & Co. KGaA, Weinheim. (b) SEM and conductive mode-atomic force microscopy image of the Pt nanofiber networks, adopted from reference [88], with permission of © 2013 American Chemical Society. (c) Representative morphologies and structures of Pt (111), Pt (100) and Pt (411) nanocrystals, adopted from reference [92], with permission of © 2013 Nature Publishing Group .

2.2.2 Carbon based counter electrode

In order to achieve cost-effective DSSCs, replacement of noble Pt with other more economical materials has been pursued. Carbon, due to its cost-effectiveness, environmental friendliness, easy availability, corrosion resistance and excellent catalytic activity towards the redox species, is a promising alternative to Pt.[93] Carbon materials such as carbon black, carbon nanotubes, graphene, and fullerene have been well applied in DSSCs.[94–98] In 1996, Kay and Grätzel demonstrated a monolithic DSSC based on a mixture of graphite and carbon black as a current collector, achieving a PCE of 6.67%.[99] Carbon black's low crystallinity and edges states provide sufficient active sites for the I_3^- reduction. Grätzel et al. investigated the thickness of the carbon

black film on the charge transfer resistance and found that a thick film has a lower resistance. Carbon black with a thickness of 14.47 μm showed the highest conversion efficiency of 9.1%.[94] Carbon nanotubes (CNTs) as the counter electrode in DSSCs have been investigated in an effort to use the 1D efficient electron transport. Song et al. developed a bamboolike multiwall CNT nanostructure with defect-rich edge planes, as shown in **Fig. 10a**. The CNT aggregates mainly consist of a mesoporous network with randomly oriented nanotubes. The large number of transverse walls with periodically closed compartments results in edge planes at regular intervals along the tube surface. The multiwall CNT counter-electrode DSSC showed 7.7% PCE.[98] To improve the catalytic activity of the multiwall CNT, Ho and co-workers used boron to dope the CNT, expecting the heteroatom doping to create more edge sites and oxygen-rich functional groups. The DSSC with boron doped multiwall CNT showed PCE of 7.91%, which is higher than that of the cell with non-doped CNTs (6.02%) and is comparable to that of the cell with the Pt counter electrode (8.03%).[100]

Graphene, as an important category of carbon materials. It has attracted much research attention working as the counter electrode. Aksay et al. reported a type of defective graphene, namely the functionalized graphene sheets (FGSs), through the thermal exfoliation from the graphite oxide (GO).[97] As shown in the schematics and SEM images in **Fig. 10b**, FGSs contain lattice defects and oxygen-containing functional groups, such as hydroxyls, carbonyls, and epoxides. FGS with different C/O ratio were synthesized and investigated in terms of the effect on the catalytic activity of the material. The results indicated the catalytic activity was improved by increasing the number of oxygen-containing functional groups, resulting in 5.0% PCE, which is comparable to cells with Pt counter electrode. Graphene modification has been widely investigated to improve the catalytic performance. Wang et al. reported a cationic polymer (PDDA) decorated graphene oxide (GO) thin film as the counter electrode and the PCE of 9.5% and 7.6% were achieved with low volatility and solvent-free ionic liquid electrolytes, respectively.[101] Qiu et al. synthesized a nitrogen and phosphorus dual-doped graphene (NPG) to obtain the synergistic effect, leading to a PCE of 8.57%.[102] In terms of other types of redox couple in the electrolyte, the graphene counter electrode can be more effective for the reduction of the hole transport materials. Kavan et al. used graphene nanoplatelets in coupled with a $Co(bpy)_3^{3+/2+}$ redox couple in the DSSC and demonstrated an efficiency of 9.4% which outperforms the Pt counter electrode [103].

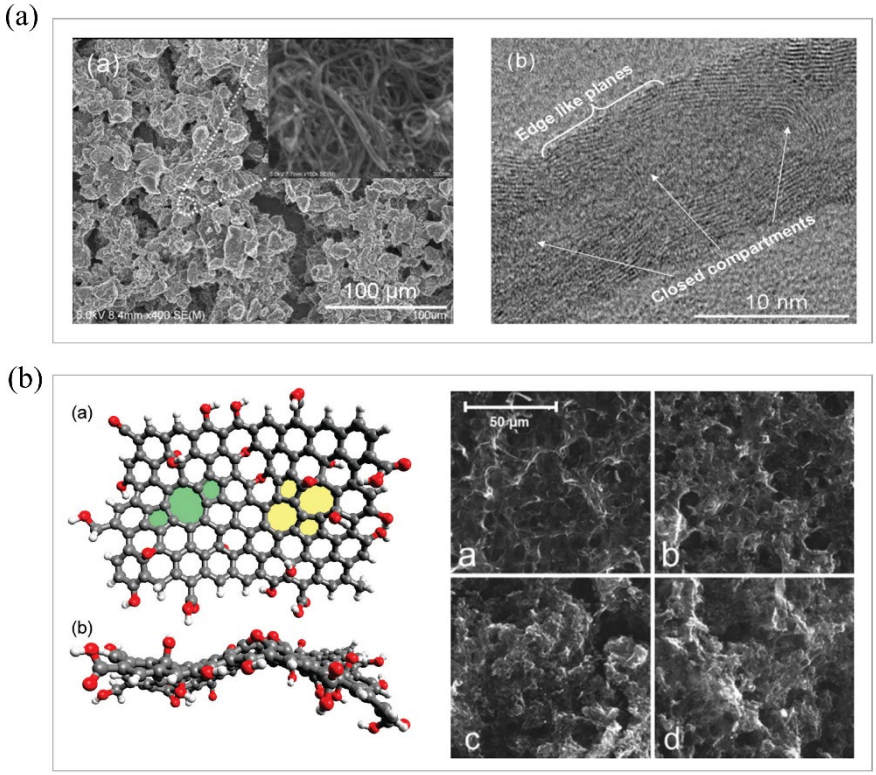

Fig. 10. (a) SEM image of a multiwall CNT and TEM image of the bamboolike structure in multiwall CNTs, adopted from reference [98], with permission of © 2009 American Chemical Society. (b) Schematic of functional groups and lattice defects on an FGS and SEM images of FGS with different C/O ratio: FGS7, FGS13, FGS48, and FGS350, adopted from reference [97], with permission of © 2010 American Chemical Society.

3. Perovskite solar cells

Among the third-generation solar cells, perovskite solar cells (PSCs) have received much attention from both scientific and industrial communities over the past few years. PSCs are a new class of PV technology and have emerged as a promising low-cost solar energy harvesting system [104–106]. This emerging PV technology, in comparison to traditional silicon solar cells, promises to be less expensive, thinner, lighter, more flexible, portable and amenable to a wide range of lighting conditions. More importantly, since 2009, the PCEs of PSCs have increased from 3.8% to over 25%, making them the fastest advancing PV technology [105,107,108]. PSCs evolved from both DSSCs and organic photovoltaics (OPVs) [109–111]. By fine tuning the functional materials and cell architectures (through change of the electron and hole transporting materials), PSCs with different structures such as mesoscopic and planar heterojunctions can be fabricated. The basic architectures of PSCs are both mesoscopic and planar structures with *n-i-p* and *p-i-n* configuration

(**Fig. 11**), where perovskite light absorber is sandwiched between electron and hole transporting materials (ETM and HTM) [109,110,112,113]. Excellent research results have been reported in all PSC architectures and many comprehensive reviews on PSCs can be found elsewhere [114–117]. Although great progress has been made in this area over the past few years, there are many challenges remaining to be addressed before potential commercialization. In particular, the major limitation of PSCs is their lack of stability which will need to be improved to compete with the mature Si solar panels [118–120]. Anomalous hysteresis observed during the current-voltage (J-V) scan of PSCs limits their stabile power output under working conditions, which could be problematic for large-scale deployment [121]. The potential environmental damage that can be caused by the presence of toxic Pb in the perovskite is another major concern [122]. These issues have led to recent advances focussed on developing new strategies to overcome these limitations using nanostructured materials. Below, after a brief overview of major advances on PSCs, we outline the recent advancements made in the integration of nanostructured functional materials in each layer of the PSCs.

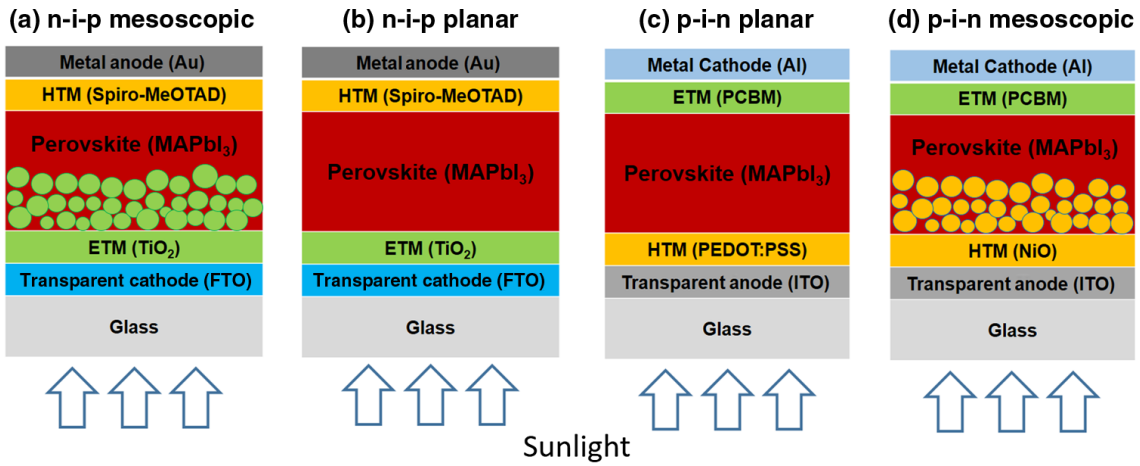

Fig. 11. Schematic illustration of the (a) n-i-p mesoscopic, (b) n-i-p planar, (c) p-i-n planar, and (d) p-i-n mesoscopic structured PSCs. The most commonly employed, representative materials are used in these cell architectures. Reproduced with permission from [123] Copyright © 2016, SPIE.

3.1. Charge transport layers

Charge transporting materials (CTMs), including electron transporting materials (ETMs) and hole transporting materials (HTMs), play very important roles in PSCs as they extract photogenerated charges from perovskite and transport them to corresponding electrodes. In the conventional *n-i-p* devices, semiconducting oxide (usually TiO_2, TiO_2 or ZnO) nanoparticles coated on transparent

conductive electrodes (FTO or ITO) act as an ETL, while organic hole conductors such as 2,2′,7,7′-tetrakis(N,N-di-p-methoxyphenylamine)-9,9′-spirobifluorene (Spiro-OMeTAD) and poly(triarylamine) (PTAA) are used as HTMs. A typical *p-i-n* PSC device is fabricated based on PEDOT:PSS or NiO_x coated ITO glass substrate as a HTM, and PCBM as an ETM.

3.1.1. Electron transporting layers

n-i-p cell structure. The mesoscopic *n-i-p* structure was the early stage architecture for PSCs, which promises to be more efficient as compared to the other types [105,108]. The "mesoscopic" term is used because this class of device relies significantly on the mesoporous semiconducting oxide layer on top of the hole blocking thin electron transport layer (known as a compact layer) [109]. Mesoporous TiO_2 nanocrystal particles with 20-30 nm diameter are used as the conventional *n*-type semiconductors in the PSC photoelectrodes [109,124]. However, the electron transport in the disordered TiO_2 nanocrystal network involves a random transit path and numerous grain boundaries, increasing the rate of charge recombination and thus limiting the device efficiency[125,126]. A range of alternative oxide semiconductors have been studied as alternatives to the traditional TiO_2 such as Al_2O_3 [106,127], ZnO [128], SnO_2 [129], Nb_2O_5 [130,131], WO_x [132] and $SrTiO_3$ [133], all of which exhibit higher electron mobility than TiO_2 while still being low cost and non-toxic. In 2012, Snaith and his colleagues made an important breakthrough in PSC research by building efficient hybrid PSCs based on a Al_2O_3 scaffold [106]. The fabricated device delivered a PCE of 10.9% under simulated AM1.5 full solar illumination. Unlike *n*-type TiO_2 semiconductor, for Al_2O_3 based cells, the electrons remained in the perovskite phase until they are collected at the planar TiO_2-coated FTO electrode (**Fig. 12a**) [106]. Despite the great progress in finding alternative oxide semiconductors, none have however replaced the nanostructured TiO_2.

A comprehensive range of strategies have been developed to enhance the PSC efficiencies such as morphology control, size effect, chemical doping, and interfacial modification. Several reviews focussing only on the ETMs of PSCs have been published [134,135]. Nanorods [136], nanofibers [137], 1D nanowires [138], 3D nanowires [139], nanotubes [140], nanocones [141] and nanohelix [142] are very promising nanostructured morphologies for PSCs due to their capability to provide a direct pathway for charge transport. However, the efficiencies of the devices based on these unique nanostructures are low. TiO_2 nanoparticles remain the material of choice for PSC

photoelectrodes. Moreover, enhancing electronic properties of the mesoporous ETMs using doping strategy is an effective approach to increase the PV efficiency of the devices [112,143–145]. The most commonly used dopant for mesoporous TiO_2 is lithium (Li). Using this dopant, Giordano et al. [143] showed an efficiency increase from 17 to >19%. Interestingly, Li-doping was also found to be effective in reducing hysteresis of the devices. Interfacial engineering of the photoelectrodes using functional nanomaterials is an effective approach to successfully improve the device performance. Many different classes of nanomaterials have been designed and used to engineer the electrode interface of the PSCs. Some of the most effective materials include carbon nanomaterials (graphene, carbon nanotubes and C_{60}), 2D materials, and conductive polymers [146–149]. Abrusci et al. [146] functionalized the TiO_2 surface using a fullerene self-assembled monolayer (C_{60}SAM) and improved the efficiency of PSC from 10.2 to 11.7% (**Fig. 12b**). Optical tuning using plasmonic nanostructures is used to enhance the efficiency of PSCs. Snaith and co-workers used core-shell metal (Au) nanoparticles to enhance the PCE of the PSCs [150]. The origin of increased photocurrent was related to the reduced exciton binding energy caused by the incorporation of the metal nanoparticles, rather than enhanced light absorption. Recently, Au and Ag nanostructures have been demonstrated to improve the efficiency of PSCs [151,152].

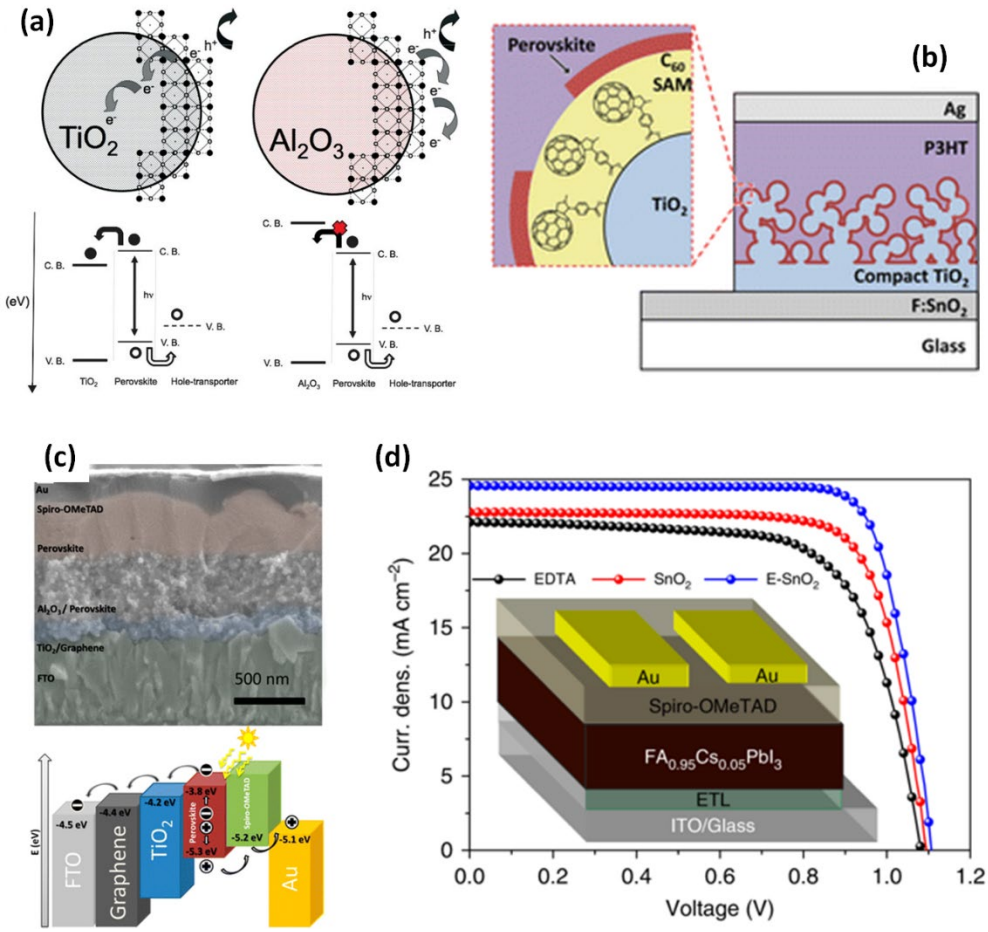

Fig. 12. (a) Schematic illustration of the charge transfer and transport in TiO_2 (left) and Al_2O_3 (right) based PSCs with the corresponding energy level diagrams, adopted from reference [106] with permission of ©2012 The American Association for the Advancement of Science. (b) Schematic of C_{60}SAM functionalized TiO_2 based PSC, adopted from reference [146] with permission of © 2013 American Chemical Society. (c) Cross-sectional SEM image and the corresponding energy level diagram of low temperature processed TiO_2-graphene ETL based PSC, adopted from reference [153] with permission of © 2014 American Chemical Society. (d) J-V curves with the inset showing device configuration of planar PSCs with various SnO_2 ETMs, adopted from reference [154] with permission of © 2018 Nature Publishing Group.

ETLs based on high surface area nanoparticles such as TiO_2 and Al_2O_3 were initially considered critical for high efficiency PSCs. Liu et al. [155] showed that efficient planar *n-i-p* PSCs can be fabricated without the use of a mesoporous layer and achieved a PCE of 15.4% using a vapour deposition method. In 2014, by using graphene, the same group was able to fabricate low-temperature processed PSC with an efficiency of 15.6% which is even higher than that of the device fabricated using high-temperature TiO_2 nanoparticles (see **Fig. 12c**) [153]. A PCE of 19.3% was achieved using Yttrium-doped planar TiO_2 photoelectrode in PSCs [112]. The advantage of

planar PSCs is that the devices can be fabricated using low-temperature TiO_2 processing method which will facilitate the commercialization [156]. Tin oxide (SnO_2) based planar PSCs are very promising as they can be fabricated using simple steps and exhibit high device performance. In 2015, Ke et al. [147] demonstrated that low-temperature solution-processed nanocrystalline SnO_2 can be an excellent alternative ETL material for efficient PSCs. The fabricated device exhibited a PCE of 17.21% with small hysteresis. Since then, excellent progress has been made in the development of SnO_2 based planar PSCs [154,157,158]. Recently, a certified efficiency of 21.52% was reported by Yang et al. [154] using EDTA-complexed SnO_2 (**Figure 12d**). A flexible device was demonstrated with 18.28% efficiency. More importantly, the unsealed PSCs with EDTA-complexed SnO_2 degraded only by 8% exposed to an ambient atmosphere for 2880 h.

p-i-n cell structure. The inverted *p-i-n* PSCs is an extension of OPVs and are usually fabricated on a 50- to 80-nm *p*-type conducting polymer such as poly(3,4-ethylenedioxythiophene) poly(styrene-sulfonate) (PEDOT:PSS) coated ITO substrates. After depositing ~ 300 nm perovskite layer on top of *p*-type HTL, the ETL is deposited and device fabrication is completed by evaporating metal electrode. [6,6]-phenyl C61 butyric acid methyl ester (PCBM), C_{60} and their derivatives are the typical ETMs used for this class of devices. Jeng et al. [111] demonstrated an inverted PSC using PEDOT:PSS as the HTL and PCBM as the ETL (**Fig. 13a** and **3b**). In this work, C_{60} or its derivatives such as PCBM was used as the electron acceptor, while $CH_3NH_3PbI_3$ ($MAPbI_3$) is the electron donor. The device fabricated in this work delivered a PCE of 3.90%. Since then, this work has inspired many studies in this area. Lam and co-workers used PEDOT:PSS and $PC_{61}BM$ as the HTL and ETL respectively, and studied the $MAPbI_3/PC_{61}BM$ bilayer solar cell interface. They demonstrated an improved FF of up to 0.76 resulting in a PCE of 7.4% [159]. Docampo et al. [110] used a thin layer of TiO_2 on top of $PC_{60}BM$ to enhance the electron transport properties of the device and achieved an efficiency of 9.80%. A flexible device based on the same ETL ($PC_{60}BM$-TiO_2) exhibited a PCE of 6.4%. Yang's group reported a low-temperature solution processed PSC (PCBM was used as an ETM) with PCEs of 11.5% (for rigid substrate) and 9.2% (for flexible substrate).

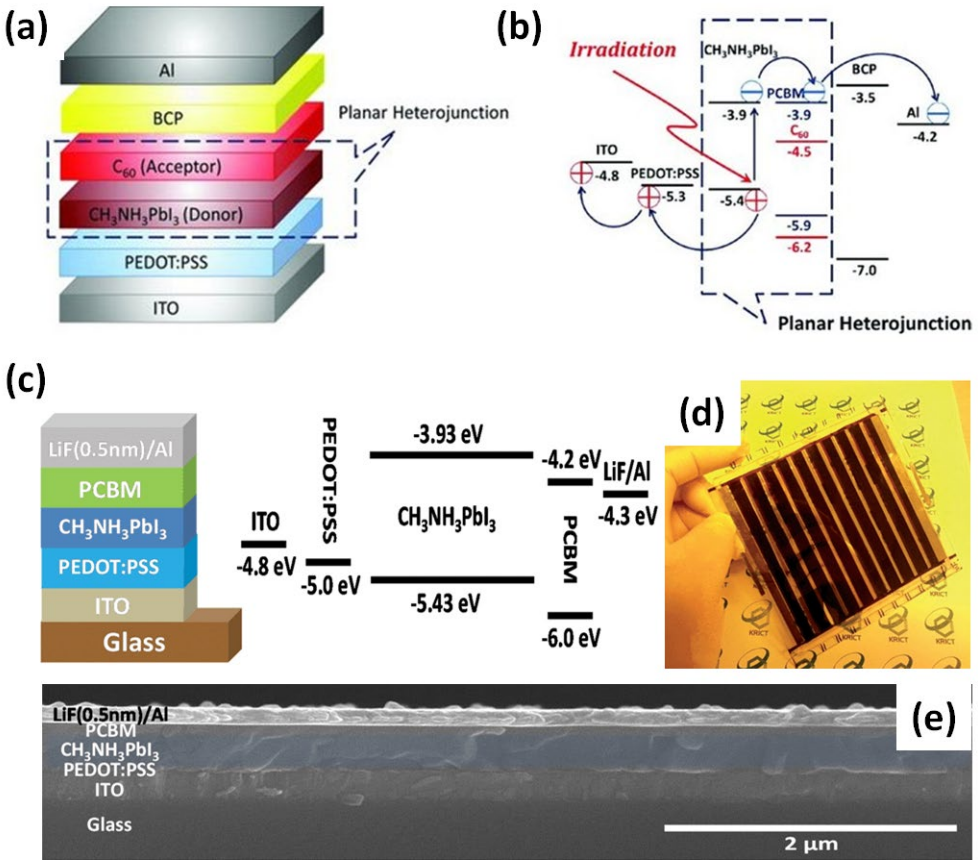

Fig. 13. (a) Layered device structure and (b) the corresponding energy level of the first inverted p-i-n PSC, adopted from reference [111] with permission of © 2013 WILEY-VCH Verlag GmbH & Co. KGaA, Weinheim. (c) Schematic illustration of the device architecture and energy level of LiF inserted inverted PSC. (d) Picture of the flexible module (size: 10 cm × 10 cm) fabricated using the cell structure depicted in (c) and (e) its cross-section SEM image, adopted from reference [160] with permission of © 2014 The Royal Society of Chemistry.

One of the major issues in using C_{60} derivatives as the ETL in PSCs is that the fullerene itself cannot fully form a perfect ohmic contact with the metal electrode. Therefore several buffer layers such as BCP [111], PFN [161], SAM [162], and LiF [160] have been reported to improve the ohmic contact and enhance the device efficiency. For instance, Seok's group used a LiF interlayer between the ETL (PCBM) and the Al electrode in an inverted PSC (**Fig. 13c**) and obtained a PCE of 14.1% [160]. The group also fabricated a large area (10 cm × 10 cm) flexible module using the same cell architecture and achieved 8.70% efficiency (**Fig. 13d**). Employing metal oxides such as SnO_2 [163], ZnO [164], and CeO_2 [165] as an electron transport layer on top of the traditional PCBM not only improved the ohmic contact but also improved device stability.

Recently, Fang et al.[165] used CeO_x as an ETM in the inverted PSC and showed an outstanding device stability in both humid and N_2 atmospheres, in addition to a high efficiency of 18.7%.

Table 1. Summary of important progress on the ETLs for PSCs.

Progress (year)	Device structure	J_{sc} (mA cm^{-2})	V_{oc} (V)	FF	PCE (%)	Ref.
Mesoporous TiO_2 (2009)	FTO/cp-TiO_2/mp-TiO_2/$CH_3NH_3PbI_3$/Liquid electrolyte/Au	11.0	0.61	0.57	3.81	[105]
Mesoporous Al_2O_3 (2012)	FTO/cp-TiO_2/mp-Al_2O_3/$CH_3NH_3Pb_2CI$/Spiro-OMeTAD/Ag	17.8	0.98	0.63	10.9	[106]
Au@SiO_2 – Al_2O_3 (2013)	FTO/cp-TiO_2/Al_2O_3-Au@SiO_2/$CH_3NH_3PbI_{3-x}Cl_x$/Spiro-OMeTAD/Ag	16.91	1.02	0.64	11.4	[150]
Mesoporous TiO_2 (2013)	FTO/cp-TiO_2/mp-TiO_2/$CH_3NH_3PbI_3$/Spiro-OMeTAD/Au	20.0	0.99	0.73	15.0	[109]
Planar TiO_2 (2013)	FTO/cp-TiO_2/$CH_3NH_3PbI_{3-x}Cl_x$/Spiro-OMeTAD/Ag	21.5	1.07	0.67	15.4	[155]
Planar ZnO (2014)	ITO/ZnO/$CH_3NH_3PbI_3$/Spiro-OMeTAD/Ag	20.4	1.03	0.75	15.7	[128]
Graphene/TiO_2 nanocomposite (2014)	FTO/cp-TiO_2-graphene/$CH_3NH_3PbI_{3-x}Cl_x$/Spiro-OMeTAD/Au	21.9	1.04	0.73	15.6	[153]
Planar SnO_2 (2015)	FTO/cp-SnO_2/ $CH_3NH_3PbI_3$/Spiro-OMeTAD/Au	23.27	1.11	0.67	17.21	[147]
Mesoporous Li-TiO_2 (2016)	FTO/cp-TiO_2/mp-TiO_2/ $(FAPbI_3)_{0.85}(MAPbBr_3)_{0.15}$ /Spiro-OMeTAD/Au	23.0	1.11	0.74	19.3	[143]
Mesoporous TiO_2-SWNTs (2017)	FTO/cp-TiO_2/mp-TiO_2-SWCNTs/$CH_3NH_3PbI_3$/Spiro-OMeTAD/Au	21.96	1.04	0.70	16.1	[148]
Planar EDTA-SnO_2 (2018)	ITO/E-SnO_2/ $FA_{0.95}Cs_{0.05}PbI_3$/Spiro-OMeTAD/Au	24.57	1.11	0.79	21.6	[154]
Inverted PCBM/BCP planar (2013)	ITO/PEDOT:PSS/ $CH_3NH_3PbI_3$/PCBM/ BCP/Al	10.32	0.60	0.63	3.90	[111]
Inverted $PC_{61}BM$ planar (2014)	ITO/PEDOT:PSS/ $CH_3NH_3PbI_3$/$PC_{61}BM$/Al	10.80	0.91	0.76	7.40	[159]
Inverted $PC_{60}BM$/TiO_2 planar (2014)	ITO/PEDOT:PSS/ $CH_3NH_3PbI_3$/$PC_{60}BM$/ TiO_2/Al	15.8	0.94	0.66	9.80	[110]
Inverted PCBM/PFN planar (2014)	ITO/PEDOT:PSS/ $CH_3NH_3PbI_{3-x}Cl_x$/PCBM/ PFN/Al	20.3	1.05	0.80	17.1	[161]
Inverted PFN-2TNDI planar (2015)	ITO/PEDOT:PSS/ $CH_3NH_3PbI_{3-x}Cl_x$/PFN-2TNDI/Ag	21.9	0.98	0.78	16.7	[166]
Inverted PCBM/LiF planar (2014)	ITO/PEDOT:PSS/ $CH_3NH_3PbI_3$/PCBM/ LiF/Al	20.7	0.87	0.78	14.1	[160]

Inverted ZnO planar (2015)	ITO/NiO_x/ $CH_3NH_3PbI_3$/ZnO/Al	21.0	1.01	0.76	16.1	[164]
Inverted C_{60}/SnO_2 planar (2016)	FTO/NiO/$CH_3NH_3PbI_3/C_{60}/SnO_2$/ Ag	21.8	1.12	0.77	18.8	[163]
Inverted PCBM/CeO_x planar (2018)	FTO/NiMgLiO/ $CH_3NH_3PbI_3$/ PCBM/CeO_x/Ag	21.8	1.11	0.77	18.7	[165]

3.1.2. Hole transporting layers

n-i-p cell structure. In order to reduce potential recombination within the cell, the holes are extracted by the HTM which provides a stepwise energy flow between the contact of active layer and the electrode. This is achieved using materials with suitable band positions and high hole selectivity so that the transport of holes is facilitated while the transport of electrons is thermodynamically unfavorable. HTMs such as spiro-OMeTAD [109], poly(triarylamine) (PTAA) [108] and poly(3-hexylthiophene) (P3HT) [167] have been proven to be the best materials for high-performance PSCs. Particularly, the spiro-OMeTAD is the most widely used HTM in solid-state solar cells including PSCs as well as DSSCs. However, the issues associated with the stability and cost in using this state-of-the-art HTM have led to recent efforts on finding alternative HTMs [168]. An ideal HTM should have *(i)* high hole selectivity and mobility to reduce losses during cell operation, *(ii)* compatible ionization potential with the perovskite, *(iii)* high thermal stability and resistance to external degradation factors such as moisture and oxygen and *(iv)* low cost. In this context, many different types of HTMs have been developed including *p*-type inorganic semiconductors (*e.g.,* CuI, CuSCN, and NiO) [169–171], polymeric HTMs (poly[2,1,3-benzothiadiazole-4,7-diyl[4,4-bis(2-ethylhexyl)-4H-cyclopenta[2,1-b:3,4-b′]dithiophene-2,6-diyl]] (PCPDTBT)) [172], and small molecular HTMs (*e.g.,* N,N-di-p-methoxyphenylamine-substituted pyrene derivatives, 4-(4-phenyl-4-a-naphthyl-butadienyl)-N,N-di(4-methoxyphenyl)-phenylamine, 2′,7′-bis(bis(4-methoxyphenyl)amino)spiro[cyclopenta[2,1-b:3,4-b′]dithiophene-4,9′-fluorene] (FDT)) [124,173]. An efficiency of 20.2% was achieved using a newly designed HTM (FDT) by Saliba et al. [124], and the showed negligible hysteresis. The energy level diagram of some of HTMs and their band alignment with perovskite absorbers is illustrated in **Fig. 14**.

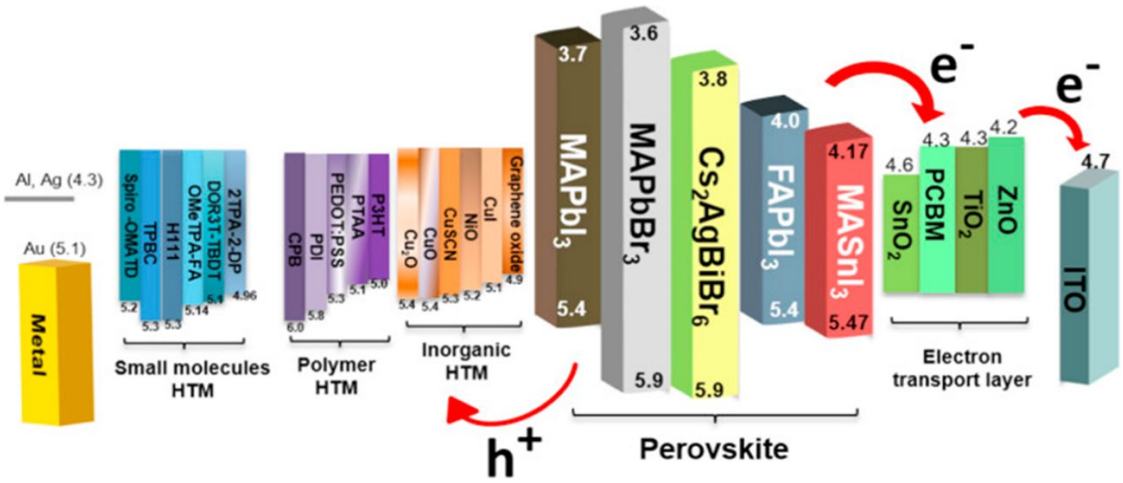

Fig. 14. Energy levels of various common HTMs together with iodide and bromide-based halide-perovskite, adopted from reference [168] with permission of © 2017 Elsevier Ltd.

P3HT is one of the widely used HTM in OPVs since it has relatively high hole mobility and good stability. In addition, P3HT is much cheaper than Spiro-OMeTAD. However, P3HT based PSCs show poor device efficiency and always require unstable and toxic doping treatment [174]. Snaith's group established a new way to fabricate stable and efficient PSCs using P3HT/SWNT(CG200)-PMMA as HTM. A PCE of 15.3% can be achieved using this HTM in addition to its excellent stability in water exposure [167]. Graphdiyne (GD) has also been used to improve the performance of P3HT HTM based PSCs[174], and the PCE was found to increase from 11.11 to 13.17% [174]. Palma et al. [175] used reduced graphene oxide as an alternative to the traditional HTMs and observed excellent device stability, although the initial efficiency was only around 5%. In addition to the efficiency enhancement, the main advantage of these nanocarbons is that their hydrophobic nature helps to improve the stability. The major limitation in using carbon nanomaterials as HTMs in PSCs is their limited hole selectivity. Therefore, future studies should focus on increasing the hole selectivity of carbon based HTMs. Heteroatomic doping using *p*-type dopants is expected to improve the hole selectivity and thus enhance the device efficiency.

NiO_x is a promising HTM for high efficiency in *p-i-n* PSCs. However, the demonstrated efficiencies of the *n-i-p* PSCs with NiO_x as HTM is less than 10% [170]. The possible reason is that the NiO_x nanoparticles are hard to disperse in perovskite-friendly solvents such as chlorobenzene, isopropanol, and toluene. Therefore, improving the dispersion of NiO_x in these solvents would be pathway towards enhancing the efficiency of this class of solar cells. You et al.

[164] fabricated inverted PSCs using solution processed *p*-type NiO_x (HTL) and *n*-type ZnO (ETL), and demonstrated 16.1% efficiency. The fabricated device showed outstanding stability for more than 60 days.

Recently, 2D materials including black phosphorus, MoS_2, and graphene have been successfully used as HTMs in PSCs [176–180]. For example, Najafi et al. [180] prepared MoS_2 quantum dot/graphene hybrids and used them as both HTM and active buffer layer in PSCs. Owing to their favourable energy level and high conductivity, a PCE of over 20% was achieved using MoS_2 quantum dot/graphene incorporated Spiro-OMeTAD based devices. The devices also showed excellent stability.

p-i-n cell structure. PEDOT:PSS is a typical HTM for inverted planar *p-i-n* PSCs and shows promising efficiencies. However, in comparison to the *n-i-p* PSC devices, the inverted PSCs suffer from relatively low V_{OC} values (0.9~1.0 V). The growth of perovskite film on PEDOT:PSS often leads to pinhole generation and incomplete surface coverage resulting in low device performance [161,181]. The growth of the perovskite film depends strongly on the bottom substrate. Wetting properties between the solvent with PEDOT:PSS is a significant issue affecting perovskite film growth. In addition to the inferior crystal film quality on PEDOT:PSS, other issues include the band alignment between perovskite and PEDOT:PSS. The work function of the PEDOT:PSS (4.9-5.1 eV) is lower than that of the valence band of perovskite (5.4 eV), which results in an imperfect ohmic contact. These issues have led to recent efforts being devoted to development of new nanostructured materials.

2D materials such as black phosphorus and carbon nanomaterials such as CNTs and graphene oxide have played an important role [178,182–184]. Recently, Chen et al. [178] introduced black phosphorus quantum dots (BPQDs) in the HTL of inverted planar PSCs (**Fig. 15a**). Due to their high carrier mobility and well-matched band alignment, the BPQD-incorporated PSC devices showed an impressive PV efficiency of 16.69%, which was significantly higher than that of the PEDOT:PSS based cell (14.10%). Lee et al. [183] investigated the effect of graphene oxide in PEDOT:PSS for inverted PSCs (**Fig. 15b**). The presence of graphene oxide in the PEDOT:PSS HTL improved the efficiency of the device from 8.24 to 9.74% (**Fig. 15c**). Interestingly, these authors showed that the graphene oxide itself can act as a HTM. The device fabricated with only a graphene oxide HTM showed an efficiency of 6.55% and promising stability

(**Fig. 15d**). Therefore, it is reasonable to expect significantly improved efficiency of inverted PSCs by employing *p*-type doped graphene as HTMs.

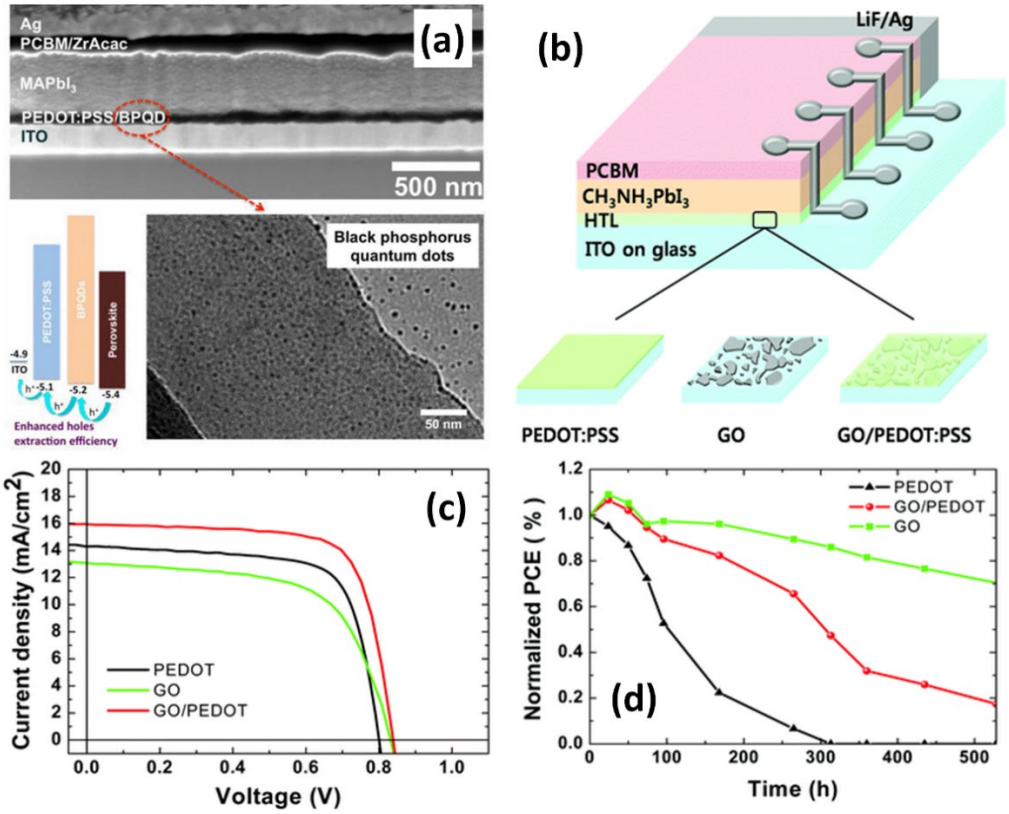

Fig. 15. (a) Cross-sectional SEM and energy diagram of BPQDs incorporated PEDOT:PSS HTM based inverted PSC device, adopted from reference [178] with permission of © 2017 American Chemical Society. (b) Device structure, (c) J-V curves and (d) stability of the inverted PSCs fabricated with GO, PEDOT:PSS, and GO/PEDOT:PSS composite, adopted from reference [183] with permission of © 2016 The Royal Society of Chemistry.

3.2. Perovskite layer

The performance of the PSCs is mainly determined by the film quality of the light absorber. High-quality perovskite films with appropriate morphology, uniformity, phase purity, and crystallinity are critically important to obtain high device efficiencies. Well-controlled crystallization and interface engineering of perovskite films are vital to meet these quality criteria. The deposition techniques of the perovskite precursors have significant roles in achieving high-quality perovskite crystals for high performance. A single-step solution deposition method was initially used to prepare the perovskite thin film owing to the ease of processing [106]. In general, organic halides such as CH_3NH_3I and lead halides (PbX_2, X = I, Br, or Cl) are mixed and dissolved in solvents

such as gamma-butyrolactone (GBL), dimethylformamide (DMF), or dimethyl sulfoxide (DMSO) to prepare the precursor solution [106]. Then the perovskite precursor solution is spin coated onto the electrodes, followed by heating at 90 to 150 ºC [105,185]. The first solid-state PSCs were fabricated based on this single-step method exhibiting efficiency up to 9.7% [185]. In 2013, Gratzel and co-workers introduced a sequential deposition method, which is a two-step deposition approach, and reported a certified efficiency of 15% [109]. In comparison to the single-step solution process, the two-step sequential deposition process results in more uniform and dense perovskite films. Moreover, the two-step sequential deposition technique is a very promising method for porous carbon based PSCs [186]. In reality, the single-step deposition method is the simplest way to prepare preparing perovskite films; but it is difficult to achieve a homogeneous composition and uniform thickness over large areas. The use of antisolvent (*e.g.,* toluene, chlorobenzene) is a very promising method to fabricate outstanding quality of dense perovskite film with excellent uniformity [124,187]. The antisolvent does not dissolve the perovskite film, ensuring high device efficiency. In addition to spin-coating, other solution-based deposition techniques such as spray, doctor-blade, inkjet printing and slot-die printing have been developed, all of which demonstrate the potential for large-scale roll-to-roll manufacturing [188–190]. However, the devices fabricated by these techniques show lower efficiencies than the cells made by spin coating. This is due to the poor film morphology and compositional uniformity [123].

The electron injection time from the perovskite to the electron acceptor has been measured to be ~ 0.3 ns, which is considered too long compared to the measurement of the hot carrier cooling (or thermalization) time (~ 0.4 ps) [191]. Zhu et al. [192] synthesized graphene quantum dots using an electrochemical method and used them to engineer the interface of the perovskite. The use of edge modified graphene quantum dots in PSCs reduced the electron injection time nearly 3 times (**Fig. 16a**) and resulted in much improved device efficiency from 8.81 to 10.15% [192]. Zuo et al. [193] developed a facile and efficient method for modifying the ZnO-coated substrates with 3-aminopropanioc acid (C3-SAM) to improve the crystallinity of $CH_3NH_3PbI_3$ perovskite film (**Fig. 16b**). As a result, highly crystalline perovskite films were formed with reduced pin-holes and trap state density (**Fig 16c**). A remarkable increase in the efficiency of the device was observed by introducing C3-SAM (from 11.96 to 15.67%).

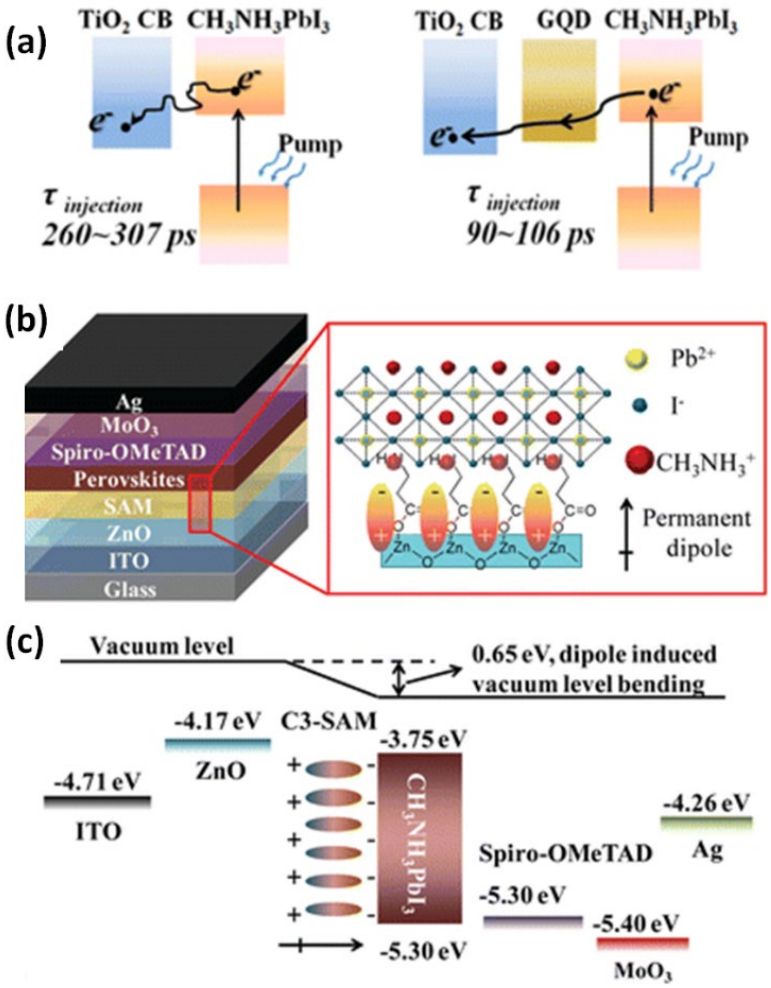

Fig. 16. (a) Schematic illustration of electron generation and extraction at PT (E) and PGT (F) interfaces, adopted from reference [192], with permission of © 2015 The Royal Society of Chemistry. (b) Schematic diagram of the device structure, SAM induced permanent dipole formation and involvement of the SAM in the crystalline structure of perovskite crystals and (c) the corresponding energy level.

Despite their high efficiencies, the traditional 3D perovskites undergo fast degradation upon exposure to moisture. This poor stability has been ascribed to the low formation energy and the pronounced hydroscopic nature. As an emerging solar cell material, 2D perovskite has attracted intensive attention from the PV community due to its large degree of freedom in tailoring chemistry and quantum mechanics in addition to the high environmental stability [194–196]. The efficiencies of 2D perovskites based solar cells are relatively low as compared to the traditional PSCs. Within the past year, high PCEs such as 13.7% and 14.1% have been achieved [197,198], which shows promise for the future development of highly stable and efficient 2D perovskite based solar cells.

3.3. Conductive electrodes

3.3.1. Transparent conductive electrodes (FTO and ITO)

For both *n-i-p* and *p-i-n* PSCs, high efficiency devices rely heavily on the transparent conductive electrode (TCEs). An ideal TCE should possess a very low sheet resistance (R_S) at high transmittance and should be synthesized using cheap and abundant materials. To date, ITO and FTO are the most widely used TCEs due to their high conductivity and optical transparency. The R_S of typical TCEs (ITO and FTO) varies from 5 to 100 Ω sq^{-1} at about 80~97% transparency depending upon the film preparation conditions [199]. However, ITO and FTO electrodes have several disadvantages including high cost and scarcity of material. Other limitations can be their lack of flexibility, high structural defects and poor stability at high temperature. Although excellent efforts have been made in the development of new TCEs, their applications in the PSCs are quite limited, especially for *n-i-p* PSCs. Han et al. [200] reported the FTO/ITO-free *n-i-p* PSCs using TCEs based on Ag nanowires/ZnO:F composite with a R_S of 19.2 Ω/sq at ~ 90% transmittance. Despite this low R_S, the fabricated device showed a PCE of only 3.29% which interestingly was higher than that of the FTO based PSC (2.95%).

In addition to metallic nanowires, graphene has attracted much attention as an emerging transparent conductive material for optoelectronic devices due to its excellent electrical and mechanical properties, potentially low cost and abundance [201]. In early-2016, solution processed transparent conductive graphene films were employed as a substitute for the electron collecting TCE in PSCs [202]. However, a PCE of only 0.62% was achieved for the *n-i-p* device fabricated with graphene film. This extremely low PCE was due to the high R_S and low transparency of the films.

Much progress has been made in the application of alternative TCEs for *p-i-n* PSCs. Sun et al. [203] reported the use of conductive polymer (PEDOT:PSS) as TCEs for inverted PSCs. The fabricated device structure based on highly conductive PEDOT:PSS is shown in **Fig. 17a**. The functionalized PEDOT:PSS film showed a conductivity of over 2000 S cm^{-1} at high transmittance. The optimized PSCs showed efficiencies of 11% and 8.6% for the glass and flexible substrates, respectively. A promising PCE of 17.1% has been achieved using transparent conductive graphene film based *p-i-n* PSC (**Fig. 17b**) [204]. However, it was found that the use of an extra ultrathin MoO_3 layer (2 nm) is necessary to achieve this high device efficiency due to a desirable energy level alignment. Moreover, acid functionalized single-walled carbon nanotubes (HNO_3-doped

SWCNTs) have been used as a TCE to fabricate flexible *p-i-n* PSCs and resulting in 5.38% efficiency [205]. Super-flexible bis(trifluoromethanesulfonyl)-amide (TFSA)-doped graphene TCE based PSC have been shown to exhibit PCEs of 18.9% (rigid device) and 18.3% (flexible device) with excellent bending stabilities [206]. Promisingly, the unencapsulated device maintained ~ 95% of its initial PCE under a continuous light soaking of one-sun at 60°C/30% relative humidity for 1000 h.

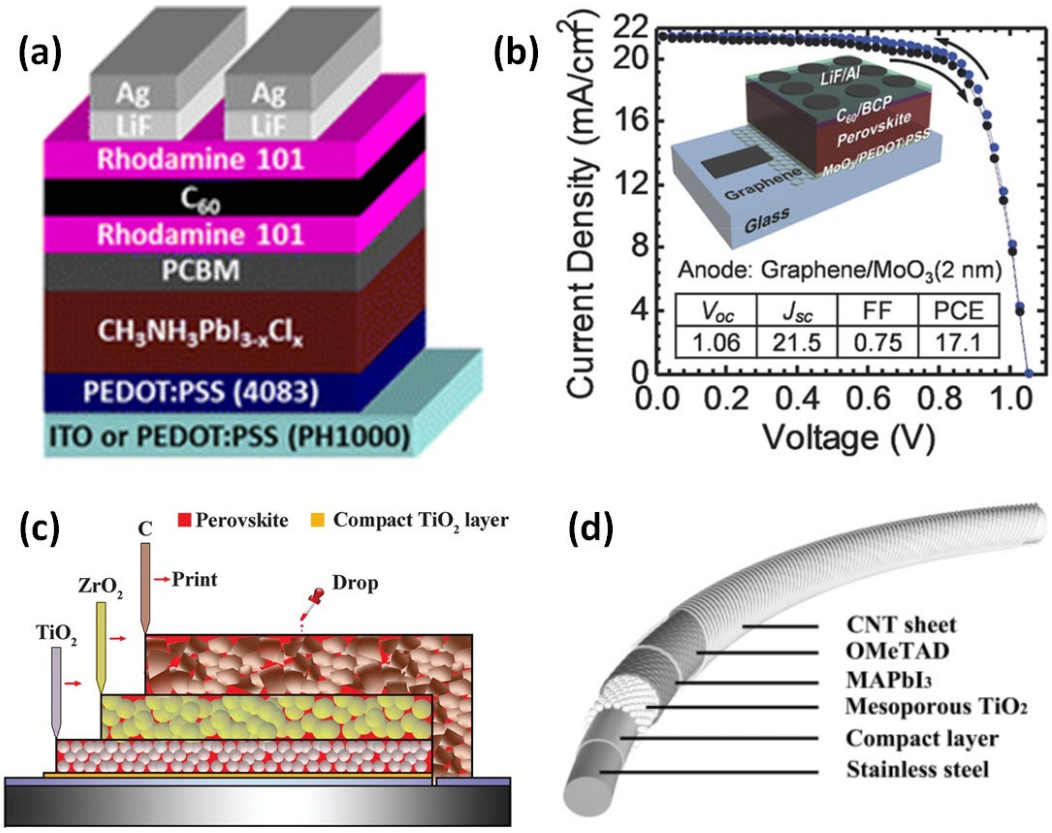

Fig. 17. (a) Schematic architecture of PSCs fabricated based on (a) ITO or conductive PEDOT:PSS electrodes, adopted from reference [203] with permission of © 2015 American Chemical Society. (b) J-V curve and parameters of p-i-n PSC fabricated with MoO_3 treated graphene TCE. Inset shows the device structure, adopted from reference [204] with permission of © 2016 WILEY-VCH Verlag GmbH & Co. KGaA, Weinheim. (c) Layered device structure of a porous carbon based HTM-free PSC, adopted from reference [186] with permission of © 2014 The American Association for the Advancement of Science. (d). Schematic illustration of the device structure of fibre-shaped PSC, adopted from reference [207] with permission of © 2014 WILEY-VCH Verlag GmbH & Co. KGaA, Weinheim.

3.3.2. Metal electrodes

The fabrication of PSCs is completed by depositing a thin layer (less than 100 nm) of noble metals such as gold (Au) or silver (Ag). This process is usually performed using thermal evaporation and

involves inherently complicated vacuum technologies. Importantly, the costs of Au, Ag and their coating techniques are expensive and would limit large-scale production of PSCs. As such, finding an alternative to these precious metal electrodes are of great interest in PCS community. In this context, nanocarbons are unique candidates that show great promise for metal-free PSCs [208]. Carbon nanomaterials such as CNTs and graphene possess good chemical stability, excellent conductivity and suitable energy levels for PSCs, while being low-cost and abundant.

Han and co-workers made excellent progress on fabricating HTM-free fully printable porous carbon based mesoscopic PSCs [186,209,210]. They employed the carbon black/spheroidal graphite to fabricate the mesoscopic PSC and achieved a PCE of 6.64% [209]. In 2014, an experimental demonstration was conducted on fabricating HTM-free, metal-free PSCs using a porous carbon film and 5-ammoniumvaleric acid (5-AVA) [186]. The fabricated cell achieved a certified PCE of 12.8% and was stable for >1000 h in ambient air under full sunlight. In this class of solar cells, a ZrO_2 spacer layer plays an important role in protecting the direct recombination between TiO_2 and carbon (**Fig. 17c**). Wei et al. [211] reported the fabrication of PSCs by clamping a mesoporous $TiO_2/CH_3NH_3PbI_3$ perovskite based photoelectrode to a candle-soot film. The candle soot films were prepared by simply holding FTO glass substrates above the candle flame. The best performing PSC fabricated with this candle-soot electrode showed a PCE of 11.02%. The simplicity of this approach coupled with the fact that two layers, the metal electrode, and the HTL, are replaced with one layer makes this work very promising in terms of future commercial production.

Li et al. [212] used CNT networks to fabricate HTM-free, metal-free PSCs. In the absence of HTMs, the PCE of CNTs electrode employed device was 6.87% while HTM-free Au-only based PSC exhibited an efficiency of 5.14%. The PCE of this device with CNT electrode was further increased to 9.90% by adding spiro-OMeTAD. Much improved efficiency can be expected by doping CNTs with *p*-type heteroatoms. Furthermore, by using CNTs, fibre shaped PSCs can be fabricated. The first fibre-shaped device showed a PCE of 3.30% (**Fig. 17d**) [207]. The main advantage of the fibre-shaped PSCs is that they are lightweight and flexible. The fabrication of semitransparent PSCs by laminating stacked multi-layer graphene prepared by the chemical vapor deposition (CVD) method as top transparent electrodes has been reported by You et al. [213] This CVD-graphene based PSC showed a maximum PCE of 11.65%. Considering the excellent properties and low-cost, graphene electrodes are expected to be used to fabricate highly efficient,

flexible PSCs with large device area by a printing or roll-to-roll process. This will enable the commercialization of the PSCs with 2D graphene nanosheets.

4. Nanomaterials in OPV

Organic photovoltaics (OPVs) have attractive features such as low-cost, mechanical flexibility, environmental friendliness and easy-processability [214,215]. The development of OPVs can be historically traced back to the initial discovery of ultrafast electron transfer between polymer and fullerene in 1992 [216,217]. This ultrafast charge transfer between a so-called "electron donor" and "electron acceptor" lays down the foundation for the bulk heterojunction (BHJ) organic solar cells, which has now become the most widely developed device design for the state-of-the-art OPVs. The BHJ OPV were demonstrated by Heeger et al. in 1995 [218,219] by using the 0D nanomaterial of fullerene derivative, PCBM as the electron acceptor, which now has not only been applied in OPVs but also in halide perovskite PVs as efficient electron extraction layer. For efficient OPVs, a nanoscopic BHJ morphology of donor-acceptor network with continuous interpenetrating phase feature is of the great importance. Because of the low dielectric constant in organic semiconducting materials, the photon generated electron-hole pair (exciton) has an extremely large exciton binding energy and a limited diffusion length (typically *ca.* 10 nm) [220]. This sets a maximum dimension of 10-20 nm for the donor-acceptor phase separation (**Fig. 18 a & b**). As displayed in **Fig. 18c & d**, the photogenerated electron-hole pair, or exciton can either be recombined for energy loss or dissociated into free carriers for energy collection. To ensure high PCE, the key is to maximize the dissociation efficiency. Since the exciton is tightly bonded, efficient separation of the electron-hole pair requires an additional "field", which can be realized by the large chemical potential difference at the donor-acceptor interface and relying on the ultrafast electron transfer. The donor-acceptor interface can function as the "*p-n* junction" analogous to that in Si solar cells. As a consequence, enlarging the donor-acceptor interfacial area can sufficiently improve the charge separation ratio *vs.* recombination. Bearing in mind the 10 nm diffusion length of the exciton, decreasing the donor-acceptor phase separation dimension at first glance seems a positive factor for charge separation. Nevertheless, for high PCE, another factor is the charge transport efficiency because recombination can also occur during the transport. As donor and acceptor materials are separate hole and electron transport pathways to deliver as-separated free charge carriers to their corresponding electrode, both donor and acceptor materials

need to be assembled into their own continuous form to achieve efficient charge transport. In order to balance the exciton dissociation with the charge transport, a specific donor-acceptor nanoscopic morphology of a bi-continuous network with 10-20 nm phase separation (**Fig. 18b**) is highly desirable. Over decades, one dominant research direction in BHJ OPVs is the nanoscopic morphological control through various methods including solvent engineering [221–225], solvent annealing [226–231], thermal annealing [232–237], post-annealing [238–242], donor-acceptor ratio manipulation [243–247], additive processing [225,232,248–251], molecular engineering for both donor and acceptor materials and developing novel multifunctional organic semiconductors [252–258]. However, the actual control of the nanoscale morphology is still the most challenging topic in OPVs, although some attempts in designing charge transport favorable nanostructures such as the vertically ordered BHJ structure [259] have been made. Regarding the nanomaterials beyond the traditional polymer: fullerene BHJ composite, novel nanomaterials as electron donor (*e.g.,* small organic molecules [258]) and electron acceptor (*e.g.,* non-fullerene organics,[260] inorganic metal oxides such as TiO_x, ZnO_x, *etc.* [231]) have also been researched. Multifunctional nanomaterials for electrode buffer layer [261], interfacial modification layer [262] as well as plasmonic additives [263,264] for enhancing PCE of OPVs are other potential research directions.

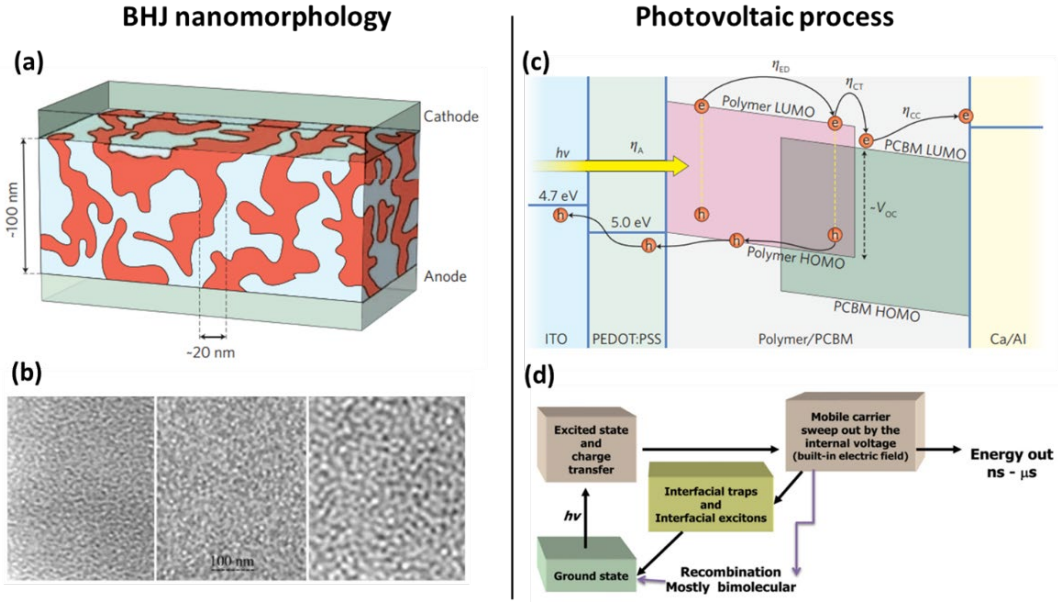

Fig. 18. Left panel: BHJ nanomorphology of bi-continuous interpenetrating donor:acceptor network. (a) Scheme showing the morphology in the device configuration, where the phase separation scale of 20 nm is depicted, reprinted from ref [231] with the permission from © 2012 Macmillan Publishers Limited and ref [265], with the permission from © 2007 American Chemical Society. **(b)** TEM images of the donor and acceptor phase separation with different separation degrees, using the defocused phase contrast mode

of operation, see reference [266] reprinted with permission from © 2005 Wiley-VCH Verlag GmbH & Co. KGaA. Right panel: basic working principle for OPVs. **(c)** The operating mechanism of a polymer solar cell, reprinted from ref [231] with the permission from © 2012 Macmillan Publishers Limited. **(d)** Schematic diagram displaying the successive steps in the operation of the BHJ solar cell, reprinted from [220] with permission from © 2013 WILEY-VCH Verlag GmbH & Co. KGaA, Weinheim.

4.1 Buffer Layer

Similar to other types of solar cells, the buffer layer has multiple functions in OPVs. In general, the functionality of the buffer layer in OPVs can be classified into *(i)* passivating surface states of organic active layer and modifying the active layer morphology, *(ii)* protecting the organic layer from being damaged by the metallic electrode and improving the interfacial stability, *(iii)* offering energetic transitional steps for charge transport from organic layer to electrode, *i.e.,* minimizing the energy barrier for interlayer charge extraction, *(iv)* selectively extracting one type of charge carrier and blocking the other to suppress charge recombination, *and (v)* acting as an optical spacer. Various nanomaterials having specific functionalities have been applied either as the charge transfer layer, or as additive to modify the optoelectronic properties of the buffer layer. Nanomaterials have also been used as functional interfacial modification layer to address interfacial issues. Here, we briefly review several representative nanomaterials in terms of their multiple functionalities when applied in buffer layer of the OPVs.

4.1.1 Nanoparticles

For charge transport layer in OPVs, there are three major types of semiconducting nanocrystals: *(i)* transition metal oxides (TMOs), *(ii)* alkali-metal compounds and *(iii)* organic monolayers. Transition metal oxide (TMO) nanoparticles (NP) represents one of the most common charge transfer layer in OPVs due to their good optical transparency and enough electrical conductivity. Based on the functionality, different TMO NPs can be used as either electron or hole transfer layer. Efficient charge transfer layers require excellent electronic properties including good electrical conductivity or low series resistance, and high charge carrier mobility to reduce energy loss during the transport within the charge transfer layer. Well-aligned energy levels of TMO with that of the active layer material are also crucial. Nanocrystals of TiO_2 and ZnO have been widely applied as ETL due to their optimal electronic properties and their wide bandgap that allows sufficient sunlight pass through in the inverted OPV structures [215]. It is worth noting that the LUMO energy levels of ZnO and TiO_2 are around -4.3 eV and -4.4 eV respectively which are well matched with that of PCBM (-4.2 eV), and their large HOMO energy level difference (*ca.* -7.5 eV of ZnO

and TiO_2 *vs.* -6.0 eV of PCBM) induces a high energy barrier blocking the back-transfer of holes. Hence, the recombination is usually reduced. There are still several limitations in TiO_2 and ZnO nanocrystal ETLs such as the lack of flexibility to tune the energy levels to match with that of novel BHJ material systems, low mobility issues (*e.g.,* TiO_2 displays a low electron mobility of 0.1-4 $cm^2V^{-1}s^{-1}$), difficulty in morphological control to get the electrically homogeneous thin film, surface defects (dangling bonds [267] and negatively charged oxygen adsorption on the surface [268,269]) which induces severe recombination. A direct example is the well-known "light-soaking" effect that occurs when ZnO is used in inverted OPVs, in which device performance increases upon prolonging the time of UV or white light exposure. To overcome these issues, attention has been shifted towards the chemical-doped metal oxides, which typically includes ZnO doped with Al^{3+} [270], Li^{+} [271], Mg^{2+} [272], Ga^{2+} [273], Sn^{4+} [274], and Cs^{2+} [275]. **Table 2** compares the device performance of OPVs using different TMO nanocrystals. Although the development of TMO nanocrystal ETLs enables PCE increases for OPVs, one major issue that remains to be solved is the strong tendency of large-scale aggregation by the polycondensation of surface hydroxyl groups of TMOs, leading to unwanted interface between the buffer layer and the photoactive layer [276]. Consequently, developing intrinsically stable and well-dispersed TMO NP ink is crucial for their application as the OPV buffer layer. In order to suppress aggregation, approaches using surface coating by surface modifier like n-propylamine [277], 2-aminoethanol [278], coupling agents [279], polyyinylpyrrolidone (PVP) surfactant [280] and cosolvent engineering [281] have been attempted. For example, the silane coupling agents with their alkoxy groups having chemical reactivity with the surface hydroxyl groups of the TMOs are excellent candidates [282]. TMO HTLs processed from nanoparticle solutions, sol-gel method or ALD techniques have also been researched for conventional structured OPVs where they are directly deposited on the transparent electrode substrates [283,284].

Table 2 OPV device performance based on different ETL TMO nanomaterials.

Device structure	EEL nanomaterials	V_{OC} (V)	J_{SC} (mA cm^{-2})	FF (%)	PCE (%)	ref
ITO/TiO_2+Au NPs/PTB7:PCBM/MoO_x/Ag	[a]s-TiO_2 NP	0.71	18.07	68.1	8.74	[285]
ITO/TiO_2+Au NPs/P3HT:PCBM/MoO_x/Ag	s-TiO_2 NP	0.64	10.15	64.8	4.20	[285]
ITO/TiO_x/C_{60}/Cy3-P/MoO_x/Ag	s-TiO_x NP	0.86	6.60	58.2	3.30	[286]
ITO/TiO_x/P3HT:PCBM/PETDOT:PSS/Ag	s-TiO_x NP	0.57	8.33	54.4	2.58	[287]
ITO/TiO_x/PCBM:P3HT/PEDOT:PSS/Au	s-TiO_x NP	0.55	7.00	60.0	2.31	[288]
FTO/TiO_x/P3HT:PCBM/PEDOT:PSS/Au	s-TiO_x NP	0.55	6.95	56.0	2.13	[289]
ITO/TiO_2/P3HT:PCBM/PEDOT:PSS/Ag	[b]sp-TiO_2 NP	0.59	7.44	55.0	2.41	[290]
ITO/TiO_x/PEI/PTB7:PCBM/MoO_3/Ag	[c]ms-TiOx NP	0.72	17.56	69.0	8.72	[291]

ITO/TiO_x/PTB7:PCBM/MoO_3/Ag	ms-TiOx NP	0.68	16.69	65.0	7.38	[291]
ITO/ZnO/P3HT:PCBM/PEDOT:PSS/Ag	s-ZnO NP	0.62	11.17	54.3	3.78	[292]
FTO/ZnO/P3HT:PCBM/Au	s-ZnO NP	0.56	8.19	43.0	2.01	[293]
ITO/ZnO/P3HT:PCBM/PETDOT:PSS/Ag	s-ZnO NP	0.57	8.41	53.9	2.56	[294]
ITO/ZnO/P3HT:PCBM/PETDOT:PSS/Ag	s-ZnO NP	0.56	8.33	56.5	2.62	[287]
ITO/ZnO/P3HT:PCBM/PEDOT:PSS/Ag	s-ZnO NP	0.54	8.85	56.0	2.67	[295]
ITO/ZnO/P3HT:PCBM/Ag	s-ZnO NP	0.55	11.22	47.5	2.97	[296]
FTO/ZnO/P3HT:PCBM/MoO_3/Ag	s-ZnO NP	0.62	8.86	57.0	3.09	[297]
ITO/ZnO NPs/P3HT:PCBM/PEDOT:PSS/Au	s-ZnO NP	0.82	9.96	38.0	3.10	[278]
ITO/ZnO/PSiF-DBT:PCBM/MoO_3/Au	s-ZnO NP	0.90	5.03	60.0	3.80	[298]
ITO/diethylzinc–ZnO/P3HT:PCBM/MoO_3/Ag	s-ZnO NP	0.57	11.26	52.5	4.03	[299]
ITO/PEN/ZnO/P3HT:PCBM/MoO_3/Ag	[d]ALD-ZnO NP	0.59	11.90	60.0	4.14	[300]
ITO/ZnO/P3HT:PCBM/PEDOT:PSS/Ag	ALD-ZnO NP	0.59	8.70	64.0	3.23	[301]
ITO/ZnO/P3HT:PCBM/PEDOT:PSS/Au	ALD-ZnO NP	0.59	11.14	61.8	4.10	[302]
ITO/ZnO/HfO2/P3HT:PCBM/PEDOT:PSS/Au	ALD-ZnO NP	0.59	11.89	64.1	4.50	[302]
ITO/AALD ZnO/P3HT:PCBM/MoO_3/Ag	ALD-ZnO NP	0.60	9.70	54.0	3.30	[303]
ITO/ZnO/P3HT:PCBM/MoO_3/Au	ALD-ZnO NP	0.47	12.60	51.0	3.62	[304]
ITO/ZnO/PBDTTPD:PCBM/MoO_3/Ag	ALD-ZnO NP	0.86	12.10	54.0	6.00	[305]
ITO/AZO/P3HT:PCBM/PETDOT:PSS/Ag	s-AZO NP	0.54	8.97	55.0	2.65	[294]
ITO/AZO/P3HT:PCBM/PETDOT:PSS/Ag	s-AZO NP	0.57	8.36	50.8	2.42	[294]
ITO/GZO/P3HT:PCBM/MoO_3/Au	s-GZO NP	0.42	11.70	39.7	1.95	[273]
ITO/ZMO/PTB7-Th:PCBM/MoO_3/Ag	s-ZMO NP	0.80	18.40	63.5	9.39	[272]
ITO/ZnO:Cs/PTB7:PCBM/MoO_3/Ag	s-ZnO:Cs NP	0.73	14.88	73.0	7.89	[306]
ITO/ZnO/PTB7:PCBM/MoO_x/Ag	s-ZnOx NP	0.73	16.10	64.0	7.50	[271]
ITO/Li-ZnO/PTB7:PCBM/MoO_x/Ag	s-ZnOx:Li NP	0.75	16.54	68.0	8.40	[271]
ITO/ZTO/P3HT:PCBM/MoO_3/Au	s-ZTO NP	0.80	17.51	66.4	9.32	[274]

[a] s- is solution processing, [b] sp- is spray pyrolysis, [c] ms- is magnetron sputtering, [d] ALD- is atomic layer deposition.

4.1.2 Ultrathin nanolayer

Another type of electrode buffer layer is the insulating alkali-metal compound including LiF, NaF, KF, CsF, Li_2O, Na_2O, Cs_2CO_3, *etc.,* which is used to establish a desired interfacial chemistry and surface charge density for assisting electron or hole extraction from the active layer to electrodes. In the field of OLED (organic light emitting diode), Al coated with LiF represents an efficient cathode for improving the electron injection efficiency [307]. For OPVs, insertion of an ultrathin LiF layer (~ 1.5 nm) at the organic/Al interface has been reported to boost PCE increase over 20% [308] by significantly reducing the serial resistivity across the contact. To date, although the true mechanism of the effect of LiF on the interface contact is still unambiguous, two explanations are given in terms of the formation of a dipole layer lowering the energy level offset between the Fermi level of the metal and the LUMO energy level of the electron acceptor [309], and the LiF diffusion induced surface doping effect on the underlying organic layer that allows reduced energy barrier formation between the organics and metals [310,311]. In addition to LiF, Cs_2CO_3 layer with thickness of several nanometers has been widely applied in OPVs as well. In 2006, Li et al. reported a 1 nm thick Cs_2CO_3 layer for OPV application [312]. By using a device structure of

ITO/Cs_2CO_3 (1 nm)/P3HT:PCBM/V_2O_5/Al, they demonstrated a PCE of 2.25% with a J_{SC} of 8.42 mA/cm^2 and V_{OC} of 0.56 V. In 2008, a low temperature annealed Cs_2CO_3 layer was reported for OPV which improved the PCE to 4.2% with significantly larger J_{SC} of 11.17 mA/cm^2 [313]. It should be noted that besides the alkali compounds, ultrathin layer of metals, small organic molecules, and conjugated polymers can serve as the efficient interfacial modification layer as well, facilitate charge extraction. In 2009, Zhao et al. reported a 1 nm-Ca modified inverted OPV using P3HT:PCBM BHJ as the active layer and demonstrated a PCE of 3.55% [314]. The low work function (2.9 eV) of Ca was pinned to that of PCBM *via* surface states and consequently improved the V_{OC}. In 2014, Qiu et al. reported a 4 nm thick ammonium heptamolybdate ultrathin films as HTL for OPVs [315]. The ammonium heptamolybdate ultrathin film modified electrode is even compatible for donor materials of very low HOMO level of -5.6 eV and efficient for a wide window of donor materials.

Another big group of efficient ultrathin electrode modifier is the conjugated polymers, where the strong dielectric group induces interfacial dipoles that substantially reduce the work function at the interface and facilitate charge carrier selectivity. Three major categories of organic polymer materials are based on polyethylene oxide [316], polyethyleneimine [317,318] and polyvinylpyrrolidone [319]. These materials have been reported as efficient nanoscopic interfacial modification layers in OPVs [320]. **Table 3** compares the device performance of OPVs using these ultrathin polymeric interfacial modification layers. The interfacial phenomena in solar cells is crucial for charge extraction, transport, and recombination. Historically, the interfacial modification layer was introduced to provide charge injection ability in OLEDs, followed by further applications in OFETs (organic field effective transistors) and photodetectors. In the past decades, tremendous progress has been made in addressing interfacial issues by using newly developed ultrathin interfacial materials. Further optimization is required in order to push the PCE of OPVs to a higher and more reliable values that can compete with commercial silicon PVs. Interfacial materials with solution-processability, low-cost, compatibility with roll-to-roll manufacturing and printing technologies are of practical importance. Additionally, excellent electrical, optical and mechanical properties as well as robust chemical stability are desired.

Table 3 Device performance of OPVs using different ultrathin polymeric interfacial modification layers with nanometer thicknesses.

Device structure	Device type	Nanolayer material	Nanolayer thickness (nm)	V_{OC} (V)	J_{SC} (mA cm^{-2})	FF (%)	PCE (%)	ref
ITO/PEDOT:PSS/PTB7:PCBM/PFN/Al	conventional	PFN	10	0.759	15.4	70.6	8.24	[114]
ITO/PEDOT/P3HT:ICBA/PFCn6:K^+/Ca/A	conventional	PFCn6:K^+	5	0.89	11.65	72.6	7.5	[115]
ITO/PEDOT:PSS/PCDTBT:PCBM/PF2/6-b-P3TMAHT/Al	conventional	PF2/6-b-P3TMAHT		0.89	10.6	67	6.5	[116]
ITO/PEDOT:PSS/PCDTBT:PCBM/P3TMAHT/Al	conventional	P3TMAHT		0.86	10.8	66	6.3	[116]
ITO/PEDOT:PSS/PECz-DTQx:PCBM/PFN/Al	conventional	PFN	5	0.81	11.4	65.8	6.07	[117]
ITO/PEDOT:PSS/P(VDF-TrFE)/PSBTBT:PCBM/P(VDF-TrFE)/Al	conventional	P(VDF-TrFE)	10	0.66	13.8	54	4.9	[118]
ITO/PEDOT:PSS/P3HT:PCBM/ZnO/BA-OCH_3/Al	conventional	BA-OCH_3		0.65	11.61	55	4.21	[119]
ITO/PEDOT:PSS/P3HT:PCBM/WPF-6-oxy-F/Al	conventional	WPF-6-oxy-F	3	0.64	10.08	60	3.89	[120]
ITO/PEDOT:PSS/P3HT:PCBM/F-PCBM/Al	conventional	F-PCBM	2	0.57	9.51	70	3.79	[121]
ITO/PEDOT:PSS/P3HT:PCBM/WPF-oxy-F/Al	conventional	WPF-oxy-F	3	0.62	9.89	59	3.67	[120]
ITO/PEDOT:PSS/P3HT:PCBM/ZnO/BA–OCH_3/Ag	conventional	BA–OCH_3		0.65	9.97	57	3.65	[119]
ITO/PEDOT:PSS/P3HT:PCBM/ZnO/BA–CH_3/A	conventional	BA–CH_3		0.64	11.63	49	3.63	[119]
ITO/PEDOT:PSS/P3HT:PCBM/ZnO/BA–CH_3/Ag	conventional	BA–CH_3		0.66	9.73	54	3.49	[119]
ITO/PEDOT:PSS/P3HT:PCBM/ZnO/BA–H/Al	conventional	BA–H		0.64	11.46	48	3.48	[119]
ITO/PEDOT/P3HT:PCBM/PF-EP/Al	conventional	PF-EP	5	0.64	9.01	59	3.38	[122]
ITO/PEDOT:PSS/PFO-TST50:PCBM/PFNBr-DBT15/Al	conventional	PFNBr-DBT15	5	0.8	8.9	36.6	2.6	[123]
ITO/PEDOT:PSS/PFO-TST50:PCBM/PFPNBr/Al	conventional	PFPNBr	5	0.8	8	39.3	2.5	[123]
ITO/PEODT:PSS/MEH-PPV:PCBM/$SnCl_2Pc$/LiF/Al	conventional	$SnCl_2Pc$	6	0.82	6.77	44.9	2.49	[124]
ITO/PEDOT:PSS/P3HT:PCBM/PEO/Al	conventional	PEO	3	0.54	9.26	48	2.41	[120]
ITO/PEDOT:PSS/P3HT:PCBM/P3HTN/Al	conventional	P3HTN	5	0.596	7.57	37.3	1.67	[125]
ITO/PEDOT:PSS/P3HT:PCBM/PFNBr-DBT15/Al	conventional	PFNBr-DBT15	3	0.586	3.96	35.7	0.824	[125]
ITO/PFN/PTB7:PCBM/MoO_3/Al	inverted	PFN	10	0.754	17.46	60.99	9.214	[114]
ITO/PFN-OX/PBDT-TZNT:PCBM/MoO_3/Al	inverted	PFN-OX		0.92	11.71	65	7.11	[126]
ITO/PC-P/PCDTBT12:PCBM/MoO_3/Al	inverted	PC-P	10	0.97	10.68	58.3	6.04	[127]
ITO/[P3(TBP)PHT+/PEDOT-]/P3HT:PCBM/V_2O_5/Al	inverted	[P3(TBP)PHT+/PEDOT-]	1.2	0.91	11.2	55	5.6	[128]
ITO/PCP-EP/PCDTBT:PCBM/MoO_3/Al	inverted	PCP-EP	10	0.88	8.76	56.9	5.48	[129]
ITO/PCP-NOH/PCDTBT:PCBM/MoO_3/Al	inverted	PCP-NOH	10	0.88	8.25	59.4	5.39	[129]
ITO/P3ImHT/PCDTBT:PCBM/MoO_3/Ag	inverted	P3ImHT	<11	0.84	11.2	51	4.8	[130]

ITO/[P3(TBP)PHT+Br-/PEDOT]/P3HT:PCBM/V_2O_5/Al	inverted	[P3(TBP)PHT+Br-/PEDOT]	1.2	0.55	9.9	60	3.8	[128]
ITO/P3ImHT/P3HT:PCBM/MoO_3/Ag	inverted	P3ImHT	<10	0.53	10.4	61	3.3	[130]
ITO/PTCDI+:PEDOT:PSS-/P3HT:PCBM/V_2O_5/Al	inverted	PTCDI+:PEDOT:PSS-	6	0.39	8.43	40	1.31	[131]

4.1.3 Graphene oxide

Graphene oxides (GOs) and their derivatives have been applied as a new class of efficient charge (*i.e.,* electron- and hole-) extraction materials in OPVs, thanks to their unique 2D structure, solution processability, and functionalization-induced flexible electronic structures. Highly efficient and stable OPVs incorporated with GO and its derivatives based ETL and HTL have been widely researched and well-reviewed elsewhere [338]. Here we briefly summarize and add the most recent progresses in this emerging field in terms of their applications in HTL and ETL.

In the case of HTL, the most widely used material is PEDOT:PSS, which suffers from its strong acidity (pH of *ca.* 1-2) and hygroscopicity that can etch the ITO electrode and induce device degradation [339]. Moreover, the diffusion of H^+ from PEDOT:PSS to the active layer further accelerate the performance degradation by affecting the complex photovoltaic process within the active layer [340,341]. In relation to this aspect of performance, GO and its derivatives with pH neutral and additional virtues such as flexible electronic tunability and processing advantages that allows for large-scale solution printing manufacturing are excellent candidates. In fact, successful applications of GO and its derivatives have been demonstrated in multiple energy conversion and storage fields of catalysts, batteries, supercapacitors, solar cells, and fuel cells [342]. The first work of GO as an efficient HEL in OPVs was reported by Li et al. [343] The GO thin film served to smooth the anode surface and offer a better contact with active layer due to the large work function of 4.9 eV of GO. By incorporating a 2 nm thick layer of GO, OPVs using P3HT:PCBM system displayed a PCE of 3.5%, comparable to those using PEDOT:PSS HTL. While increasing the thickness from 2 nm to 10 nm, the FF of OPV devices significantly decreased from 54% to 19% (rendering a PCE drop from 3.5% to 0.9%) due to the increase in serial resistance because of its insulating properties (induced by epoxy and hydroxyl groups on the GO basal plane, which disrupt its sp^2 conjugation) for thicker GO film. A direct result of the insulating properties in GO HEL is a low FF for the OPV devices, especially for the P3HT:PCBM system. One promising approach to remove these oxygen-containing groups to recover the conjugated structure of GO and thereby

improving the electrical conductivity is the *post-oxidation reduction* to achieve the reduced graphene oxide (r-GO) [344]. However, after reducing these groups, the solubility of r-GO is significantly reduced, making it difficult to process. Various approaches including development of particular reduction reagents to achieve soluble r-GO [345,346], post GO thin film treatment for reduction [347,348] and introduction of conductive filler to GO thin film [349] have been reported. Yun et al. [346] utilized p-toluenesulfonyl hydrazide to reduce the GO and obtained a pr-GO solution for HEL deposition. With a significantly improved electrical conductivity and film morphology of pr-GO HEL, the OPVs using P3HT:PCBM system displayed a PCE of 3.63% with a V_{OC} of 0.59 V, J_{SC} of 9.33 mA/cm^2 and FF of 66.7% as well as a dramatically improved device lifetime compared with that of PEDOT:PSS-based device. Liu et al. [345] reported the solution processable sulfated graphene oxide (GO-OSO_3H). The higher electrical conductivity (1.3 S m^{-1}) and surface doping effect on P3HT gave rise to a higher PCE of 4.37%. Further, post-thermal annealing can also reduce the GO *via* releasing the H_2O, CO_2 from the oxygenated functional groups in GO. Joen et al. confirmed the composition of r-GO after 250 ºC thermal annealing through XPS characterization [348]. An improved electrical conductivity from 8×10^{-6} S m^{-1} to 1.8 S m^{-1} boost the OPVs with PCE from 1.47% to 3.98% and improved lifetime.

Smart strategies of employing graphene-based HEL materials have also been attempted. Hersam and coworkers reported the electronically tuned GO thin film for HEL by density control deposition *via* Langmuir-Blodgett assembly, followed by low-level ozone exposure [350]. The controllable oxidation level of GO improved the energy level alignment and thus the charge extraction. Meanwhile, the GO can concurrently template a face-on π-π stacking of the conjugated polymer donor (PTB7) in the active layer, which further facilitates the hole extraction from PTB7 to GO HEL. As a result, a PCE of 7.39% has been achieved in the GO-based device, comparable to that (7.46%) of PEDOT:PSS-based counterpart with a 20 fold improved ambient device lifetime. Yang et al. [350] employed oxygen plasma to modify the surface of GO HEL to ensure a large work function and better hole extraction process. Consequently, a boosted PCE from 2.71% to 3.59% with simultaneously improved performance parameters (V_{OC} increased from 0.58 V to 0.60 V, J_{SC} increased from 8.42 mA/cm^2 to 9.91 mA/cm^2, and FF increased from 0.55 to 0.60) have been obtained. Kymakis and coworkers developed a facile and roll-to-roll compatible photochemical approach to simultaneously reduce and dope GO film *via* UV irradiation with the presence of Cl_2 gas [351]. The laser-induced chloride atoms substituted the defects at the GO edges

and inside the lattices, and tailored its work function to 5.23 eV, making an ohmic-like contact with HOMO levels of most polymeric donor materials in OPVs. The device using PCDTBT:PCBM system and chlorinated graphene oxide (Cl-GO) showed a PCE of 6.56% with 17.35%- and 19.48%-increase compared to those using pristine GO or PEDOT:PSS HELs, respectively, and higher device stability *versus* the PEDOT:PSS-based devices. Li and coworkers used the PBDTTT-C:PCBM system and Cl-GO HEL and obtained a PCE of 7.6% (*vs.* 6.53% from PEDOT:PSS devices) [352].

In parallel, using highly conductive fillers such as carbon nanotubes, to reduce the serial resistance of GO HEL has also been investigated. Particularly, single-walled carbon nanotubes (SWCNTs) having small diameter of 1 nm are promising as the surface roughness of GO will not be drastically increased after blending with SWCNTs. But the dispersion of the SWCNTs in the GO matrix can be challenging. Kim et al. reported a SWCNTs:GO composite HEL spin-coated from their water solution dispersed by sonication [349]. OPVs using P3HT:PCBM system and GO:SWCNT HEL exhibited a PCE of 4.10% with V_{OC} of 0.60 V, J_{SC} of 10.82 mA cm^{-2}, and FF of 0.63. In addition to SWCNT, mixture of PEDOT:PSS with GO has also attracted huge attention. Particularly, the viscosity increase in the water mixture of GO and PEDOT:PSS gives rise to a sticky film upon solution deposition, which offer the possibility for assembling of tandem PV devices by direct adhesive lamination process with the sticky film [353–355]. Additional applications of GO in HEL includes the nanoparticle-decorated GO mixed within PEDOT:PSS,[354] the GO and TMO bilayer-structured HEL,[356] graphene oxide ribbon (GOR) [338], *etc.*

For GO and its derivatives in the application of ETL, the requirement is a low work function that can align with the LUMO of electron acceptor material in the active layer. Similar to the HEL, minimized series resistance for efficient electron transport is of great importance. As an ambipolar material, GO and derivatives can thus be tuned to have suitable energy levels by functionalization for application as ETL. The first application of GO-based ETL materials in OPVs was reported by Liu et al. in 2012 [357]. By adding Cs_2CO_3 into an aqueous GO solution, the periphery -COOH groups of GO sheets were neutralized into -COOCs and a reduced work function of 4.0 eV has been achieved, which is well-matched with the LUMO of PCBM. OPVs with a device structure of ITO/GO/P3HT:PCBM/GO-Cs/Al displayed a PCE of 3.67% (with V_{OC} of 0.61 V, J_{SC} of 10.30 mA cm^{-2}, and FF of 0.59). Moreover, Qu et al. also developed a r-GO:fullerene

composite as the EEL for OPVs with a PCE of 3.89% [358]. Wang et al. reported a GO/TiO_x bilayer as the EEL in OPVs using PCDTBT:PCBM BHJ composite as the active layer and 7.5% has been achieved [359]. Overall, GO and its derivatives with flexible energy level tunability and ambipolar transport feature enables the creativity of various HEL and EEL materials for OPVs, which may find applications in other type of PV devices in the future.

4.2 Active layer

The active layer is functional for photon absorption and exciton separation into free electrons and holes, which then separately transport towards electrodes *via* electron acceptor and donor material phases separately in the BHJ mixture, respectively. Typical donor materials include conjugated polymers and small organic molecules. Typical acceptor materials include inorganic TMO nanocrystals, fullerene derivatives, and non-fullerene small organics.

4.2.1 Electron donor

Low-bandgap (LBG) conjugated polymers: To ensure sufficient photon absorption, low-bandgap (LBG) conjugated polymers that are able to exploit sun-irradiation from UV to NIR are attracting growing attention for OPV application. Design, synthesis and application of novel LBG conjugated polymers is the one of the major researches in the field of OPVs. Several design rules for LBG polymer with high molar photon absorptivity, optimal energy levels, high charge carrier mobility and good solubility in organic solvents for high performance OPVs have been demonstrated, which are *(i)* fused heterocycles to facilitate π-electron flowing along the polymer backbone, *(ii)* high planarity maintenance for high π-electron delocalization *via* groups/atoms bridging adjacent rings, *(iii)* introduction of electron-withdrawing units to reduce the bandgap (E_g), *(iv)* donor-acceptor (D-A) copolymerization strategy for narrowing E_g and *(v)* 2D conjugation across the polymer backbone for broadened absorption and higher hole mobility [214]. Rational design enables polymers with optimal E_g values identical to that of the ideal light absorber (1.34 eV) for maximum PCE (33.7%) predicted by S-Q limit.[360] However, the world PCE record of OPVs is 12.3%, far less than the S-Q limit [361] because of nanoscopic issues in the BHJ composite. The ultrafast electron transfer (50 fs) from donor polymer to fullerene acceptor after photoexcitation make the polymer:fullerene boundary function as a "field" separating the exciton into free carriers, followed by transport towards corresponding electrodes. Meanwhile, the limited

exciton diffusion length as well as the charge carrier mobility of each polymer and fullerene mono-phase as hole and electron transport channels, respectively, confine a strict requirement for nanomorphology of the polymer:fullerene BHJ composite. A bicontinuous nanonetwork of polymer:fullerene BHJ with phase separation of 10-20 nm is then the optimal morphology for the active layer film. The BHJ nanomorphology has been studied by usng a variety of experimental methods (principally by transmission electron microscopy (TEM), atomic force microscopy (AFM) and grazing-incidence wide-angle X-ray scattering (GWAX)) for a long time. Despite that, the precise control and manipulation of such an optimal nanomorphology still remains challenging. There have been various methods of controlling the liquid-liquid phase separation during the formation of the BHJ film or by subsequent treatment on the solid film to fine-tune the nanomorphology for a higher OPV performance. Several parameters have been identified as important for their effectiveness on the nanoscopic features of the BHJ morphology: *(i)* material molecular structure and polymer weight; *(ii)* molar ratio between polymer and fullerene; *(iii)* solvent form which the BHJ layer cast; *(iv)* processing additives for the BHJ solution; *(v)* solution concentration and spin dynamics parameters during the processing; *(vi)* thermal and solvent annealing for the BHJ thin film; *(vii)* BHJ film thickness. Details on these topics can be seen in separated reviews [231,237,362–365].

Small molecules electron donor: in parallel, several new classes of small molecules as electron donors in BHJ nanocomposite have been reported for the use in OPVs [366,367]. In comparison to their polymeric counterpart, small-molecule OPVs were developed quickly with a PCE leap from 6.7% [368] to 9.9% [369–371] in just two years. The intensive investigations on small molecule OPVs have led to tremendous scientific articles and several well-organized review papers [372]. Compared with conjugated polymer electron donor materials in polymer solar cells, besides their mutual favorable optical and electron properties, small molecules offer advantages over their polymeric counterparts not only because their structures are well defined and they have higher purity and lower batch-to-batch variation, but also they usually display highly ordered nanostructures that can significantly improve the charge carrier mobilities. Moreover, small molecules can be structurally flexible by intentionally design the molecular structure, which enables them to have tunable electronic energy levels, broaden the optical absorption range, and self-assemble to maximize the device performance. Similar to polymer solar cells, the small

molecules-based BHJ OPVs have the small molecules as the photogenerated electrons as the donor and fullerene as the acceptor. The vast majority of BHJ OPV device efficiency improvements has been a result from the development of new "donor" materials with well-designed optoelectronic features for maximizing the light absorption, charge transport, and the formation of ordered nanostructures when blended with fullerene derivatives. Although the most attention has been received by the π-conjugated polymers, small molecules with strategic design for effective electron donor material in the blend have also been well investigated. Similarly, molecular design with several requirements has been demonstrated, which includes *(i)* strong optical absorption extending into the near-IR region (absorption peak needs to be centered around 700 nm, where maximum solar photon flux is located) and light extinction coefficients greater than 50,000 $M^{-1}cm^{-1}$ are required to maximize the photon absorption; *(ii)* deep HOMO energy levels from -5 to -5.5 eV to maximize the V_{OC} and match well with the commonly used high work function anodes; *(iii)* sufficient structural coplanarity to foster the intermolecular π-π interactions and consequently high charge carrier mobility; *(iv)* suitable solubility in solution and sufficient viscosity to facilitate film formation through solution deposition and *(v)* simple synthetic procedures for high yield and highly tunable production of the molecular libraries.

4.2.2 Electron acceptor

In contrast to the polymer:fullerene BHJ composite based OPVs, another type of organic solar cell is the organic-inorganic BHJ nanostructured hybrid solar cells consisting of organic electron donor (either conjugated polymers or the small molecules) and inorganic nanostructures. The organic electron donor is blended with the inorganic semiconducting electron acceptor with specific nanostructures that favor the charge separation, extraction, transport and collection [373,374], or with different nanostructures intentionally manipulated to reach high PCEs. **Fig. 19** shows different nanoarchitectures of the inorganic-organic hybrid OPVs.

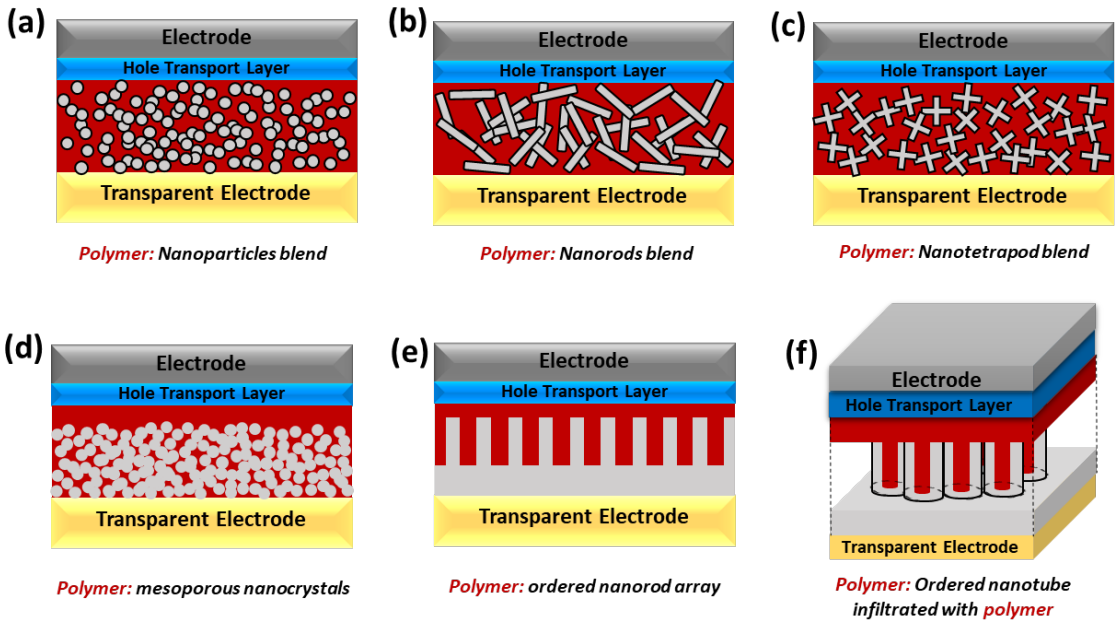

Fig. 19. Inorganic-organic hybrid OPVs with different nanoarchitectures. **(a)** Nanoblends of polymer and NPs, **(b)** nanoblends of polymer and NRs, **(c)** nanoblends of polymer and NTPs, **(d)** polymer immersed in the mesoporous structured nanocrystals, **(e)** polymer covering ordered nanocrystal arrays, **(f)** polymer infiltrated into the ordered nanotube arrays.

Inorganic electron acceptors: To date, various inorganic nanomaterials such as GaAs [375], CdSe [376], CdS [377], PbS [378] and ZnO [379,380] nanowires and nanocrystals have been investigated for the BHJ hybrid OPVs. In order to boost the PCE, several design rules need to be taken into consideration: *(i)* the domain size of the inorganic electron acceptor and organic electron donor is required to be comparable or smaller than the exciton diffusion length (<10 nm) to minimize the recombination and to increase the exciton dissociation probability across the heterojunction; *(ii)* the electron and hole mobilities in the inorganic and organic component should be large enough to maintain efficient transport; *(iii)* traps and defects should be as low as possible to minimize the trap-assisted charge carrier recombination. Thus, similar to their organic BHJ counterpart, high electron and hole mobilities, controllable nanomorphology, and a well-structured interface are critical performance factors for developing efficient hybrid solar cells [364]. Traditional *n*-type TMOs with intentionally designed nanostructures can be used as the electron acceptor in the blend. For example, the first study on BHJ interpenetrating networks of conjugated polymer and TiO_2 NP was reported in 1999, where the sintering isotropic, colloidal TiO_2 NPs was introduced into a connected thin film [381]. Further studies employed mesoporous TiO_2 with a pore size less than 10 nm in conjunction with the P3HT for the active layer in OPVs, in which the

small pore size in scale of exciton diffusion assisted the exciton dissociation and enhanced the PCE to 1.5% [382]. The interface of polymer:TiO_2 is crucial for *(i)* charge separation, *(ii)* ultrafast transfer of electron, mediation of forward charge transfer, compression, and block of back charge recombination for large J_{SC}, and *(iii)* inducing interfacial dipole moment to adjust the energy offset for higher V_{OC} [383–385]. Typical processing for nanostructured TiO_2:polymer OPVs include either infiltrating the polymer into the pores of as-prepared TiO_2 film or the single step method that direct spin-cast the film from the polymer-TiO_2 blends solution. Due to the incomplete infiltration of porous TiO_2 by polymers, the single step method guarantees an improved interface compatibility between TiO_2 and polymer. To make such a blend solution, typical coaters like trioctylphosphine oxide (TOPO) or oleic acid (OA) [386,387] used to disperse the hydrophilic NPs in typical nonpolar solvents for conjugated polymers will hinder the charge separation at the donor/acceptor interface and decrease the electron hopping rate between particles. On the other hand, the donor:acceptor BHJ nanomorphology with well-self-organized phase separation is also crucial to high PCEs. One effective method for optimizing the nanomorphology in the TiO_2:polymer BHJ OPVs is the solvent selection. For example, Kwong et al. found that lower vapor pressure solvents such as xylene worked as good solvent for sufficiently mixing the P3HT and TiO_2 into smaller domain size giving larger interfacial area for charge separation [388]. Chuang et al. utilized mixed solvents consisting of dichloromethane, pyridine and chloroform to optimize the nanomorphology and achieved uniformly dispersed TiO_2 NR (nanorod) in the BHJ hybrid film [389]. Another correlation between the nanomorphology of the hybrid BHJ composite and the nanocrystals of the inorganic acceptor is their geometric feature. Nanoparticles (e.g., TiO_2 NPs) can be more homogeneously dispersed in the polymer (e.g., P3HT) matrix, while the NRs (e.g., TiO_2 NPs) were found to induce obvious phase separation with significant NR rich clusters in separation with the P3HT domains [389]. Similar to TiO_2, ZnO has also been reported to be used as the electron acceptors in the BHJ hybrid OPVs. The application of ZnO was in the form of either blending the ZnO NPs within the polymer solution to operate a single-step method or infiltrating the ZnO NRs film with the polymer solution. Mixed solution of NPs and polymers [390,391] or the ZnO NP precursor and polymers [392] can be directly used for a single-step spin-coating process. For the infiltration of pores in ZnO NRs arrays, carefully handling the contact between polymer layer and the ZnO NRs arrays to get a sufficient but not excessive coverage of ZnO nanostructures with a satisfying infiltration is of great importance to achieve high PCE.

However, microscopically manipulating the ZnO:polymer nanostructures to reach a macroscopic homogeneous film is challenging, even with the help of advanced techniques such as self-assembly methods. In general, PCEs obtained in these hybrid devices incorporated with ZnO nanostructures are far below their purely organic counterparts, where most reports only demonstrated a low PCE less than 1% [392,393], significantly lagging behind the general 3% PCE of P3HT:PCBM BHJ based OPVs.

Besides the TiO_2 and ZnO nanostructures, extensive research efforts have enabled other inorganic electron acceptors in the hybrid OPVs. For example, a hybrid containing a LBG polymer and PbS_xSe_{1-x} nanocrystals foster the hybrid OPVs with a PCE of 5.5% [394]. In contrast to their organic counterparts, the hybrid OPVs suffering from low PCE principally have lower charge carrier mobility due to the disordered polymer domain and discontinuously dispersed inorganic nanocrystals trapping the free charges causing large internal resistance. Again, the nanomorphology in hybrid OPVs is still difficult to control. Various strategic methods such as the annealing treatment of the as-prepared hybrid films [395], molecular structural reengineering [221,396,397] and solvent modifications [398,399] have been reported.

Intentionally orientating the molecular chains to obtain an ordered packing enables higher charge carrier mobilities. Likewise, self-assembly of polymers with the formation of organic NWs has been proven to be successful in achieving enhanced charge transport efficiency and higher PCE [400,401]. Nanocomposites made from NPs and polymer usually requires sufficiently mixed phase to assist charge separation, which however, are at the cost of charge carrier transport. In this concern, modulation of the charge transport properties in the nanocomposite are extensively studied *via* orientated nanoarrays [402,403], nanorods and nanotubes [404–406], and core-shell-shaped nanocrystals [407–409]. Among them, the monodispersed nanotetrapod (NTP) offers extended charge path with its three-dimensional continuity for efficient charge transport [410,411]. Overall, inorganic nanocrystals have been widely researched for the hybrid OPVs. Nanostructures and the materials themselves are important to the photovoltaic performance of corresponding OPV performances.[412–414].

Non-fullerene acceptor: For decades, the OPVs have been dominated by donor:acceptor BHJ blends based on fullerene electron acceptors. Recently this has changed where the emerging non-fullerene (NF) OPVs are developing very quickly with a PCE over 16%, much higher than the best

fullerene-based OPVs. This is because the NF acceptors exhibit greater tunability in absorption spectra and energy levels, rendering a wider range of new opportunities. The simultaneously improved V_{OC} and J_{SC} in these sorts of devices indicate new nanoscopic device physics and photophysics. Over the years, NF based OPVs suffered from uncontrollable morphology [415] and thereby low PCE [416,417]. The PCEs of NF based OPVs have increased significantly since 2015, reaching a milestone of 13.1% [418], outperforming the other types of OPVs [419,420]. The fast development in NF based OPVs (including tremendous efforts have been paid to synthetic methods, materials design strategies and device engineering protocols as well as the development of a wide range of donor materials which provide a rich library for immediate use in NF OPVs) allows the flexibility in realizing donor:acceptor BHJ systems with optimized energy band diagram and complementary light absorption and thereby the outstanding device performance. Nevertheless, the investigations on the device physics and photophysics in NF OPVs are lagging behind the rapid developments and PCE surge. In contrast to the fullerene-based OPVs, the NF OPVs have a sufficient exciton separation process upon negligible driving energies [421–425], which is typically accompanied by high photocurrent and low voltage loss simultaneously. How the exciton split into free carriers in these NF OPVs at a low driving energy remains to be answered. From the nanoscopic view, one major difference from the fullerene is the anisotropic structures of NF. The π-π interactions between the donor and acceptor are known to be very important to electron transfer. In contrast to the isotropic ball-like (0D) feature in fullerene derivatives, the anisotropic conjugated structures of NF acceptors even make it more challenging to secure an efficient π-π interaction between polymer donor and NF acceptor [426–428].

The early application of NF electron acceptor in OPVs can be traced back to the bilayer device structure using a perylene-based acceptor [429], and later the application of electron-rich and electron-poor poly(phenylene vinylene)s [219,417]. Since 2015, OPVs based on NF electron acceptors has experienced a PCE surge from 6% to over 13%, owing to the development of a large variety of NF materials including phthalocyanines (PCE_{max}= 1.07%) [430], pentacene derivatives (PCE_{max}= 1.29%) [431], aceneimides (PCE_{max}= 5.04%) [432], rylene monoimides (PCE_{max}= 5.44%) [433], twisted polymers containing B←N moieties (PCE_{max}= 6.26%),[434] tetracyanobutadiene derivatives (PCE_{max}= 7.19%) [435] and various bis(acceptor)-terminated conjugated small molecules such as bis(phthalimide vinyl)benzothiadiazole derivative (PCE_{max}= 3.7%)[436]. It should be noted that the incorporation of NF acceptor in planar heterojunction cells

also benefits the PCE boost towards 8.4% (from subphthalocyanines and subnaphthalocyanines NF acceptors) [437]. **Table 4** summarizes the device performance (over 9%) with the newly developed NF acceptor materials used in the BHJ nanocomposite for the active layer. Despite the fact that an exciting PCE over 13% has been achieved, several factors affecting the device performance still require further investigations, especially the counterintuitive phenomena of simultaneously obtaining ultrahigh J_{SC} and V_{OC} in NF-based OPVs.

Table 4 Device performance (over 9%) with the newly developed NF acceptor materials used in the BHJ nanocomposite for the active layer.

Acceptor	E_{op} (eV)	Energy levels	μ_e (10^{-5} $cm^2V^{-1}s^{-1}$)	Device structure	V_{OC} (V)	J_{SC} (mA cm^{-2})	FF (%)	PCE (%)	Ref
SF-PDI2		[a]3.62/5.99		ITO/Zno/P3TEA:SF-PDI2/V_2O_5/Al	1.11	13.27	64.3	9.5	[240]
Ta-PDI	2.05	[a] 3.81/6.03	27[c]	ITO/ZnO/PTB7-Th:Ta-PDI/MoO_3/Ag	0.78	17.1	68.5	9.15	[241]
TPH-Se	2.17	[a] 3.80/5.97	320[d]	ITO/ PEDOT:PSS/PDBT-T1:TPH-Se/Ca/Al	1.0	12.99	71.5	9.28	[242]
N2200HW				ITO/PEDOT:PSS/PTzBI : N2200HW/PFNDI-Br/Al	0.844	15.48	70.1	9.16	[243]
IHIC	1.38	[a] 3.93/5.45	240[e]	ITO/ZnO/PTB7-Th:IHIC/MoO_3/Au/Ag	0.754	19.01	68.1	9.77	[244]
ITIC	1.73	[a] 3.78/5.51	30.7[c]	ITO/PEDOT: PSS /J71:ITIC /PDINO51/Al	0.94	17.32	69.77	11.41	[245]
ITIC	1.73	[a] 3.78/5.51	31.3[c]	ITO/ZnO/PBDB-T:ITIC/MoO_3/Al	0.899	16.81	74.2	11.21	[246]
ITIC	1.59	[b] -3.84/-5.54	16[d]	ITO/PEDOT:PSS/J61:ITIC/PDINO /Al	0.898	17.97	65.49	10.57	[247]
m-ITIC	1.58	[a] 3.82/5.52	24.5[e]	ITO/PEDOT:PSS/J61:m-ITIC/PDINO/Al	0.912	18.31	70.55	11.77	[247]
ITIC		[b] -3.83/-5.48		ITO/PEDOT:PSS/J51:ITIC/PDINO/Al	0.82	16.47	69.0	9.26	[248]
NFBDT	1.56	[a] 3.83/5.40	13.8[c]	ITO/PEDOT:PSS/PBDBT:NFBDT/PDIN/Al	0.868	17.85	67.2	10.42	[249]
ATT-1	1.54	[a] 3.63/5.50	24[c]	ITO/PEDOT:PSS/PTB7-Th:ATT-1/PFN/Al	0.87	16.48	70.0	10.07	[250]
IT-M	1.6	[a] 3.98/5.58	11[c]	ITO/ZnO/PBDB-T:IT-M/MoO_3/Al	0.94	17.44	73.5	12.05	[251]
IT-DM	1.63	[a] 3.93/5.56		ITO/ZnO/PBDB-T:IT-DM/MoO_3/Al	0.97	16.48	70.6	11.29	[251]
INIC1	1.56	[a] 3.97/5.54	10[e]	ITO/ZnO/FTAZ:INIC1/MoO_x/Ag	0.929	16.63	64.3	10.1	[252]
INIC2	1.52	[a] 3.98/5.52	12[e]	ITO/ZnO/FTAZ:INIC2/MoO_x/Ag	0.903	17.56	66.8	10.8	[252]
INIC3	1.48	[a] 4.02/5.52	17[e]	ITO/ZnO/FTAZ:INIC3/MoO_x/Ag	0.852	19.68	68.5	11.5	[252]
IT-4F		[a] 4.14/5.66	50.5[e]	ITO/ZnO/PBDB-TSF:IT-4F/MoO_3/Al	0.88	20.88	71.3	13.1	[253]
ITCC	1.67	[a] 3.76/5.47	92.6[e]	ITO/PEDOT:PSS/PBDB-T:ITCC/PFN-Br/Al	1.01	15.9	71	11.4	[254]
ITCPTC	1.58	[a] 3.96/5.62	320[e]	ITO/PEDOT:PSS/PBT1-EH:ITCPTC/Zracac/Al	0.95	16.5	75.1	11.8	[255]
ITIC-Th	1.6	[a] 3.93/5.66	61[e]	ITO/ZnO/PDBT-T1:ITIC-Th/MoO_x/Ag	0.88	16.24	67.1	9.6	[256]

ITIC-Th1	1.55	[a] 4.01/5.74	760[c]	ITO/ZnO/FTAZ:ITIC-Th1/MoO_x/Ag	0.849	19.33	73.73	12.1	[257]
ITIC2	1.53	[a] 3.80/5.43	130[e]	ITO/ZnO/FTAZ:ITIC2/MoO_x/Ag	0.925	18.88	63.0	11.0	[258]
IDIC	1.62	[a] 3.91/5.69	110[e]	ITO/ZnO/PTFBDT-BZS:IDIC/MoO_x/Ag	0.905	17.3	70.8	11.03	[259]
IEICO-4F	1.24	[a] 4.19/5.44	11.4[e]	ITO/PEDOT:PSS/PBDTS-DTBTO:IEICO-4F/PFN-Br/Al	0.731	25.3	58.9	10.9	[260]

[a] EA/IE (eV), [b]LUMO/HOMO (eV) energy levels; [c] μ_e measured from blended film by the SCLC method, [d] μ_e measured from pristine film by the SCLC method, and [e] μ_e measured in organic field-effect transistors.

4.3 Electrode

Typically for OPVs, metals of different work functions are used for the electrode, where the reflection from the metal side can further improve the photon recycling and thus give higher photocurrent. The charge carrier mobility in organic materials is rather low (10^{-4} cm^2 $V^{-1}s^{-1}$), limiting their thickness to ~ 100 nm which results in poor photon absorption. Early in 1988, Stuart and coworkers found that by introducing the Ag NPs onto the surface of the silicon-on-insulator (SOI) photodetector, the photocurrent was boosted by 20 fold, indicating the local surface plasmon resonance effect from the metallic NPs [456]. Physically, the introduction of periodic nanostructures to the interfaces within the OPVs can redistribute the optical fields and trap the incident light for improved photon absorptions by the internal scattering or near-field surface plasmonic resonance effect [457–460]. Metallic rear electrodes with plasmonic nanostructures to redistribute the optical field and scattering light waves in OPVs have been widely explored. Accordingly, a large variety of plasmonic electrodes (*e.g.,* metallic gratings) have been designed in order to improve the photon absorption in the OPVs along with different implementation strategies such as soft nanoimprint lithography (NIL) techniques [459]. Surface plasmon polaritons in the style of light waves propagating along the metal/semiconductor interface can be excited *via* using a periodically nanopatterned metallic NP array, giving rise to the near-field enhancement and improved optical absorption for the OPVs. The metallic gratings at the rear electrodes of OPVs represents the feature of most commonly used light trapping method by exciting the surface plasmon polaritons, as shown in **Fig. 20** [461]. A large scope of strategic methods employing 1D or 2D periodic gratings have been studied. You et al. employed the stamping method of 1D nanograting onto the active layer for the metallic plasmonic grating rear electrode and boosted the PCE to 7.73% (from 7.20%) [462]. Both the light diffraction and coupling with surface plasmon polaritons enable the enhancement in light absorption and thereby higher device performance. Hsiao et al. reported a 2D periodic granular-like rear electrode *via* similar pattern-transfer process

[463]. Peer et al. demonstrated a nanostructured metallic rear electrode along with an external microlens arrays for light trapping in OPVs. Such a design significantly diffracted the incident light by the excitation of both waveguiding and surface plasmon modes and boosted the photocurrent by 58% [464]. Particularly, the 2D patterns displayed advantages over the 1D design by exhibiting superior light harvesting capacity from a polarization independent plasmonic response [465].

In addition, nanostructured materials and various nonstructural designs can also be employed in OPVs to improve the light harvesting by multiple mechanisms and light trapping metallic NPs can also be employed in either function layer in OPVs such as buffer layers, active layer or interfaces. Overall, for light trapping in OPVs novel successful strategies include: *(i)* antireflection coatings by microscale textures & biomimetic nanostructures; *(ii)* substrate geometry-induced trapping; *(iii)* electrode engineering by transparent front electrodes, reflective rear electrodes and synergistic effects; *(iv)* nanostructuring of charge extraction and photoactive layers by metal NPs-mediated plasmonic enhancement & photonic structures-integrated photoactive layers.

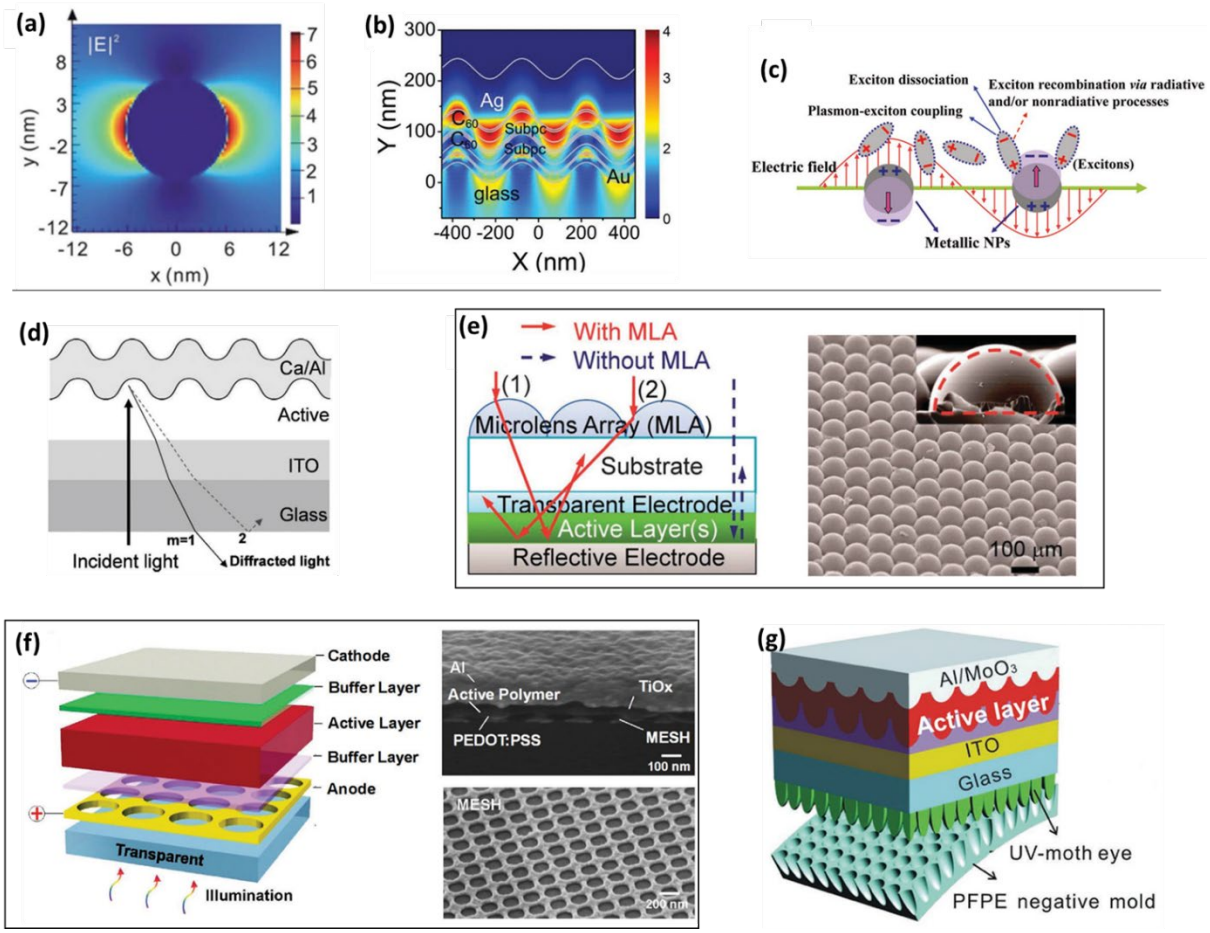

Fig. 20. Plasmonic effect on light trapping for OPVs. *Fundamentals:* **(a)** Light trapping through exciting the localized surface plasmons in metallic NPs. Adapted with permission from ref [354], Copyright 2012, Royal Society of Chemistry. **(b)** Excitation of propagating surface plasmon polaritons at metal/organic interfaces. Reproduced with permission from ref [466], © 2013 WILEY-VCH Verlag GmbH & Co. KGaA, Weinheim. **(c)** The interplay between the metal NP-induced plasmons and the exciton recombination. Reproduced with permission from ref [467], Copyright 2011, American Chemical Society. *Plasmonic nanostructures at metallic rear electrodes.* **(d)** Schematic illustration of an OPV device with periodic surface relief gratings for light trapping. Reproduced with permission from ref [461], © 2008 WILEY-VCH Verlag GmbH & Co. KGaA, Weinheim. *Geometric microstructures for plasmonic OPVs.* **(e)** Schematics of photon transmission into OPVs with an antireflection coating and the SEM image of a representative light trapping functional layer with hemispherical shape, reproduced with permission from ref [468], Copyright 2012, Royal Society of Chemistry. *Improved light harvesting via optical engineering of transparent front electrodes.* **(f)** Plasmonic cavity of subwavelength hole-array metal front electrode. Reproduced with permission from ref [469], Copyright 2013, Optical Society of America. *Biomimetic nanostructures for light trapping coatings.* **(g)** An OPV with nanoimprinted moth's eye nanostructures, and the reflectance properties of incident light. Reproduced with permission from ref [459], © 2014 WILEY-VCH Verlag GmbH & Co. KGaA, Weinheim.

Over all, development of novel functional nanomaterials enables the fast-moving OPV field of growing attention from the society, especially the development of TMO nanocrystals, new classes of electron donor and nonfullerene electron acceptor materials, as well as the rational

design of light trapping strategies, ultrahigh photocurrent over 25 mA/cm^2, voltage over 1.1 V have been realized in OPVs.

5. Conclusion and outlook

The production of electricity using photovoltaic technologies can not only help to meet the growing energy demand, but can also mitigate the global climate change by reducing dependence on fossil fuels. The levelized competitiveness of the innovative new-generation of solar cells is growing due to efforts from researchers, scientists, engineers and industrial professionals related to developing novel functional materials, particularly the nanomaterials and nanotechnologies. This review has highlighted the most recently developed functional nanomaterials for the PV application in the new-generation of solar cells *(i)* DSSC, *(ii)* Perovskite SC, *(iii)* OPV.

(i) DSSC: The very first success of nanomaterials in DSSCs was the application of a mesoporous electron-acceptor layer that can adsorb the dye sensitizer and accept the photogenerated electrons from the dye molecules. With the tremendous efforts in developing ***(a)*** nanostructured photo-anode materials including 1D nanostructure (*e.g.,* TiO_2 nanotube, ZnO and TiO_2 nanowires and nanorods), facet-dependent nanostructures (*e.g.,* orientated TiO_2 nanocrystals, yolk@shell hierarchical TiO_2 spheres), and nanocomposites (*e.g.,* ZnO nanorods coated with TiO_2 nanoparticles) and ***(b)*** nanostructured Pt and nanostructured carbon counter electrodes. The certificated record PCE of DSSC is 11.9% with a device area of 1.005 cm^2 from Sharp, which is significantly lower than that of the commercialized Si-PVs. The predicted theoretical PCE for DSSCs is around 32%, which however is not feasible as there are so many energetic losses in a practical device. In addition to low PCE, another hurdle in limiting the transition of DSSCs is the low stability of the aqueous electrolyte. Although development of ionic liquid, polymer and solid electrolyte such as Spiro-OMeTAD (which revealed its success in DSSCs and later in perovskite PVs) has attracted attention for the transition of DSSCs, the achieved PCE is lower than that of the liquid electrolyte devices. Commercial DSSCs will be required to maintain PCEs without significant degradation for over 10 years to be compatible with alternatives (*i.e.,* Si-PV) that perform at 80% of the original PCE after ~25 years. While the best DSSCs have been reported to perform for 2.5 years in outdoor aging test, they are vulnerable to various degradations in practical applications. Consequently, the DSSCs still requires tremendous improvement in both PCE and stability. The ongoing nanomaterials research is expected to provide practical solution for DSSCs.

Further, nanomaterials will provide benefit in other areas such as mesoporous structured TiO_2 in perovskite PVs.

(ii) Perovskite SC: Perovskite solar cells based on organic-inorganic hybrid perovskites have attracted significant attention due to their high PCEs that are comparable to Si-PVs. We have reviewed here the fast development of ***(a)*** charge transport layer comprising of nanoscale features (such as mesoporous TiO_2 for efficient electron extraction, strategic design of ETL consisting of different nanostructures such as nanorods, nanofibers, 1D nanowires, 3D nanowires, nanotubes, nanocones and nanohelix for efficient electron transfer across the ETL/perovskite interface, and nano-morphological control of PEDOT:PSS for efficient hole transport); ***(b)*** microscopic optimization in perovskite crystals to obtain large grain sizes and smooth surface morphology for minimizing charge recombination loss; and ***(c)*** various nanoscopic modifications and nanomaterials for transparent electrodes and back contact electrodes. Despite the success in demonstrating high PCE, serious issues regarding deployment of PSCs still needs to be addressed. Nanoscopic modification of the perovskite materials or use of multifunctional nanomaterials can be promising directions. Here we list several challenges related to PSCs and potential solutions from nanoscopic perspective: ***a)*** stability issues originating from moisture and oxygen sensitivity of perovskite materials can be mitigated through microscopic coatings such as core-shell grain structure *via* self-assembling nanomaterials and device encapsulation with ultrathin hydrophobic protection layers; ***b)*** hysteresis issues from mobile ions, trapping/detrapping and ferroelectric effect induced interfacial phenomena can be addressed by interfacial engineering at nanoscopic scale; ***c)*** lead-toxicity from the core element in perovskites can be reduced by nanoscopic molecular engineering and crystallographic B-site substitution with less toxic elements or molecules; ***d)*** further PCE boost can be realized through optimized crystallization, advanced charge extraction/transport materials, novel light-trapping or photon recycling techniques to either enhance photon absorption, suppress recombination loss and improve transport and collection efficiency. The nanomaterials previously applied in either DSSCs or OPVs can be quickly transferred to the PSCs to take advantage of the known chemistry and interactions.

(iii) OPVs: Nanoscopic engineering *via* novel nanomaterials or restructuring the morphology of active layer or using light trapping nanomaterials to extend light absorption represents some of the best approached in the OPV field. We have described a range of nanomaterials and their applications in ***(a)*** buffer layer such as the TMO nanoparticle electron or

hole transport layers, ultrathin monomolecular layer for self-assembled interfacial modification and low-dimensional carbon based (*e.g.,* graphene oxide) charge transport layers; ***(b)*** newly developed active layer materials including electron donor materials like LGB polymers, small donor molecules and electron acceptors such as nanostructured inorganics, nonfullerene acceptors for efficient photon absorption and charge separation; and ***(c)*** functional nanostructured electrodes with light trapping strategies for enhancing photon absorption and application efficiency. Incorporating these concepts, PCEs over 13% have been reported. Various fundamentals and physics related to the relatively less ordered mixture in the active layer needs further exploration. For example, in the process of light-absorption in BHJ active layer of OPVs, the photon position is uncertain due to a momentum uncertainty. Thus, the position where photoexcitation occurs is uncertain with a value of $\lambda/4\pi$, according to the Heisenberg's uncertainty principle. For visible absorption, this length scale imposed by Heisenberg's uncertainty principle is larger than the typical well-known length of optimal phase separation of 20 nm in OPVs. Then the photoexcitation generates a delocalized coherent superposition of eigenfunctions of the Schrodinger equation, which describes the nanostructured BHJ blend. More generally, when phenomena (*e.g.,* the charge transfer in nanostructured materials) occur at the same time scale as the lifetime of the coherent wavefunction, new physics may be expected.

Overall, although perovskite solar cells emerged as a star in PV community with efficiency of over 25%, high efficiency devices are only fabricated based on extremely toxic lead (Pb) based components. This issue associated with the toxicity of perovskite solar cells significantly hinders the commercialization of this promising technology. Therefore, research effort on the development of other emerging solar technologies such as DSSCs and OPVs should still be actively made due to their promising PV performances and many other attractive features. Clearly, multifunctional nanostructured materials not only boost the efficiency of these classes of solar cells, but also reduce the overall manufacturing costs. In addition to these emerging solar cells covered in this Review, recent advances in heterojunction solar cells based on n-type silicon and functional nanomaterials (graphene, CNTs, PEDOT:PSS and MXene) have shown great promises in reducing the fabrication cost of silicon based solar cells, while maintaining high cell efficiencies. Therefore combining these novel types of solar cells with emerging PVs would be of great value. Tandem structured solar cells designed based on heterojunction solar cells and emerging PVs are expected to obtain remarkably high efficiencies.

Moreover, the next advancement in solar cells is expected to be the use of stacks of materials with different bandgaps. One of the weaknesses of the current approaches using only one material is that at any wavelength except the one that matches the bandgap exactly, there are thermal losses and some of the absorbed energy is lost. The use of a stack of different materials will allow energy matching to various wavelengths minimising these losses. The tandem solar cells that have been reported is the first step on this path. The potential to use nanotubes in such devices has been discussed. 2D materials present a great opportunity to explore such devices because layered structures can be prepared easily forming heterostructures and there are many materials with many bandgaps available."

In summary, nanotechnology and newly developed multifunctional nanomaterials can help to overcome current performance barriers and substantially to improve the solar energy collection and conversion through PV techniques. At the nanoscale, numerous physical phenomena have been identified as factors for improving the solar energy collection and conversion. Nanostructures including 0D, 1D, 2D, and 3D materials have shown great effectiveness on enhancing light absorption in terms of light extinction and wide spectra absorption, exciton dissociation, charge separation/extraction/transport/collection, recombination suppression, and improved solar-electricity conversion for next-generation PV techniques. Nevertheless, challenges (*e.g.,* unpredictable micro and nanostructures during synthesis, poor control over featured size or placement, inferior interface formation, and in many cases short device lifetimes) in these technologies still have issues when incorporated with the PV manufacturing. A deeper theoretical understanding of the physical phenomena at the nanoscale during the photovoltaic process is key for technical adjustment towards higher PCE. On the other hand, ensuring device lifetime and reliability of the next-generation PV technology is also crucial to the success of the initiative. With the preliminary success achieved in past years, nanomaterials are one of the most promising technologies for future energy harvesting and are expected to reform the future energy market significantly.

Acknowledgements

C.W. acknowledges the financial support from the SBIR program through Nanosonic. K.W. would like to acknowledge the Stewardship Seed Grant Program. S.P. would like to acknowledge the financial support from Office of Naval Research (I. Perez). The support of the Australian Research

Council Discovery Program (DP150101354, DP160101301 and DP170100450) is gratefully acknowledged.

References

[1] M.I. Hoffert, K. Caldeira, A.K. Jain, E.F. Haites, L.D.D. Harvey, S.D. Potter, M.E. Schlesinger, S.H. Schneider, R.G. Watts, T.M.L. Wigley, D.J. Wuebbles, Energy implications of future stabilization of atmospheric CO2 content, Nature. 395 (1998) 881. http://dx.doi.org/10.1038/27638.

[2] L. Wang, H. Liu, R.M. Konik, J.A. Misewich, S.S. Wong, Carbon nanotube-based heterostructures for solar energy applications, Chem. Soc. Rev. 42 (2013) 8134–8156. doi:10.1039/C3CS60088B.

[3] N.S. Lewis, Toward Cost-Effective Solar Energy Use, Science 315 (2007) 798 LP-801. http://science.sciencemag.org/content/315/5813/798.abstract.

[4] N. AL-Rousan, N.A.M. Isa, M.K.M. Desa, Advances in solar photovoltaic tracking systems: A review, Renew. Sustain. Energy Rev. 82 (2018) 2548–2569. doi:https://doi.org/10.1016/j.rser.2017.09.077.

[5] D.M. Chapin, C.S. Fuller, G.L. Pearson, A New Silicon p-n Junction Photocell for Converting Solar Radiation into Electrical Power, J. Appl. Phys. 25 (1954) 676–677. doi:10.1063/1.1721711.

[6] H. nrel. gov/pv/assets/images/efficiency-char.-20180716. jpg. NREL. Efficiency chart, No Title, (n.d.).

[7] M. Bosi, C. Pelosi, The potential of III-V semiconductors as terrestrial photovoltaic devices, Prog. Photovoltaics Res. Appl. 15 (2006) 51–68. doi:10.1002/pip.715.

[8] T.W. Hamann, R.A. Jensen, A.B.F. Martinson, H. Van Ryswyk, J.T. Hupp, Advancing beyond current generation dye-sensitized solar cells, Energy Environ. Sci. 1 (2008) 66–78. doi:10.1039/B809672D.

[9] G. Conibeer, Third-generation photovoltaics, Mater. Today. 10 (2007) 42–50. doi:https://doi.org/10.1016/S1369-7021(07)70278-X.

[10] M. Grätzel, Perspectives for dye-sensitized nanocrystalline solar cells, Prog. Photovoltaics Res. Appl. 8 (2000) 171–185. doi:10.1002/(SICI)1099-159X(200001/02)8:1<171::AID-PIP300>3.0.CO;2-U.

[11] A. Hagfeldt, G. Boschloo, L. Sun, L. Kloo, H. Pettersson, Dye-Sensitized Solar Cells, Chem. Rev. 110 (2010) 6595–6663. doi:10.1021/cr900356p.

[12] B.E. Hardin, H.J. Snaith, M.D. McGehee, The renaissance of dye-sensitized solar cells, Nat. Photonics. 6 (2012) 162. http://dx.doi.org/10.1038/nphoton.2012.22.

[13] M. Grätzel, Conversion of sunlight to electric power by nanocrystalline dye-sensitized solar cells, J. Photochem. Photobiol. A Chem. 164 (2004) 3–14. doi:https://doi.org/10.1016/j.jphotochem.2004.02.023.

[14] H. Gerischer, M.E. Michel-Beyerle, F. Rebentrost, H. Tributsch, Sensitization of charge injection into semiconductors with large band gap, Electrochim. Acta. 13 (1968) 1509–1515. doi:https://doi.org/10.1016/0013-4686(68)80076-3.

[15] M. Nakao, K. Itoh, T. Watanabe, Mechanism of Electrochemical Dye Sensitization: Effects of Semiconductor Doping Level and Reducing Agent on the Photocurrent Quantum Yield, Berichte Der Bunsengesellschaft Für Phys. Chemie. 89 (1985) 134–138.

doi:10.1002/bbpc.19850890211.
[16] M. Matsumura, S. Matsudaira, H. Tsubomura, M. Takata, H. Yanagida, Dye Sensitization and Surface Structures of Semiconductor Electrodes, Ind. Eng. Chem. Prod. Res. Dev. 19 (1980) 415–421. doi:10.1021/i360075a025.
[17] H. TSUBOMURA, M. MATSUMURA, Y. NOMURA, T. AMAMIYA, Dye sensitised zinc oxide: aqueous electrolyte: platinum photocell, Nature. 261 (1976) 402. http://dx.doi.org/10.1038/261402a0.
[18] B. O'Regan, M. Grätzel, A low-cost, high-efficiency solar cell based on dye-sensitized colloidal TiO2 films, Nature. 353 (1991) 737. http://dx.doi.org/10.1038/353737a0.
[19] M. Grätzel, Solar Energy Conversion by Dye-Sensitized Photovoltaic Cells, Inorg. Chem. 44 (2005) 6841–6851. doi:10.1021/ic0508371.
[20] S. Ito, T.N. Murakami, P. Comte, P. Liska, C. Grätzel, M.K. Nazeeruddin, M. Grätzel, Fabrication of thin film dye sensitized solar cells with solar to electric power conversion efficiency over 10%, Thin Solid Films. 516 (2008) 4613–4619. doi:https://doi.org/10.1016/j.tsf.2007.05.090.
[21] J. Bisquert, A. Zaban, P. Salvador, Analysis of the Mechanisms of Electron Recombination in Nanoporous TiO2 Dye-Sensitized Solar Cells. Nonequilibrium Steady-State Statistics and Interfacial Electron Transfer via Surface States, J. Phys. Chem. B. 106 (2002) 8774–8782. doi:10.1021/jp026058c.
[22] A. Hauch, A. Georg, Diffusion in the electrolyte and charge-transfer reaction at the platinum electrode in dye-sensitized solar cells, Electrochim. Acta. 46 (2001) 3457–3466. doi:https://doi.org/10.1016/S0013-4686(01)00540-0.
[23] D. Cahen, G. Hodes, M. Grätzel, J.F. Guillemoles, I. Riess, Nature of Photovoltaic Action in Dye-Sensitized Solar Cells, J. Phys. Chem. B. 104 (2000) 2053–2059. doi:10.1021/jp993187t.
[24] R. Jose, V. Thavasi, S. Ramakrishna, Metal Oxides for Dye-Sensitized Solar Cells, J. Am. Ceram. Soc. 92 (2009) 289–301. doi:10.1111/j.1551-2916.2008.02870.x.
[25] M. Grätzel, Photoelectrochemical cells, Nature. 414 (2001) 338. http://dx.doi.org/10.1038/35104607.
[26] M. Adachi, Y. Murata, I. Okada, S. Yoshikawa, Formation of Titania Nanotubes and Applications for Dye-Sensitized Solar Cells, J. Electrochem. Soc. 150 (2003) G488. doi:10.1149/1.1589763.
[27] T. Kasuga, M. Hiramatsu, a Hoson, T. Sekino, K. Niihara, Titania Nanotubes Prepared by Chemical Processing, Adv. Mater. 11 (1999) 1307–1311. doi:10.1002/(SICI)1521-4095(199910)11:15<1307::AID-ADMA1307>3.0.CO;2-H.
[28] T. Kasuga, M. Hiramatsu, A. Hoson, T. Sekino, K. Niihara, Formation of Titanium Oxide Nanotube, Langmuir. 14 (1998) 3160–3163. doi:10.1021/la9713816.
[29] M. Wei, Y. Konishi, H. Zhou, H. Sugihara, H. Arakawa, Utilization of Titanate Nanotubes as an Electrode Material in Dye-Sensitized Solar Cells, J. Electrochem. Soc. 153 (2006) A1232. doi:10.1149/1.2194667.
[30] Y. Ohsaki, N. Masaki, T. Kitamura, Y. Wada, T. Okamoto, T. Sekino, K. Niihara, S. Yanagida, Dye-sensitized TiO 2 nanotube solar cells: fabrication and electronic characterization, Phys. Chem. Chem. Phys. 7 (2005) 4157–4163.
[31] J.M. Macák, H. Tsuchiya, A. Ghicov, P. Schmuki, Dye-sensitized anodic TiO2nanotubes, Electrochem. Commun. 7 (2005) 1133–1137. doi:10.1016/j.elecom.2005.08.013.
[32] K. Shankar, J. Bandara, M. Paulose, H. Wietasch, O.K. Varghese, G.K. Mor, T.J.

Latempa, M. Thelakkat, C.A. Grimes, Highly Efficient Solar Cells using TiO 2 Nanotube Arrays Sensitized with a Donor-Antenna Dye 2008, Nano Lett. (2008) 2–7.
[33] C. Adán, J. Marugán, E. Sánchez, C. Pablos, R. Van Grieken, Understanding the effect of morphology on the photocatalytic activity of TiO2nanotube array electrodes, Electrochim. Acta. 191 (2016) 521–529. doi:10.1016/j.electacta.2016.01.088.
[34] K. Shankar, G.K. Mor, H.E. Prakasam, S. Yoriya, M. Paulose, O.K. Varghese, C.A. Grimes, Highly-ordered TiO2 nanotube arrays up to 220 μm in length: Use in water photoelectrolysis and dye-sensitized solar cells, Nanotechnology. 18 (2007). doi:10.1088/0957-4484/18/6/065707.
[35] L.-L. Li, C.-Y. Tsai, H.-P. Wu, C.-C. Chen, E.W.-G. Diau, Fabrication of long TiO2 nanotube arrays in a short time using a hybrid anodic method for highly efficient dye-sensitized solar cells, J. Mater. Chem. 20 (2010) 2753. doi:10.1039/b922003h.
[36] J. Zhang, S. Li, H. Ding, Q. Li, B. Wang, X. Wang, H. Wang, Transfer and assembly of large area TiO2 nanotube arrays onto conductive glass for dye sensitized solar cells, J. Power Sources. 247 (2014) 807–812. doi:10.1016/j.jpowsour.2013.08.124.
[37] O.K. Varghese, M. Paulose, C.A. Grimes, Long vertically aligned titania nanotubes on transparent conducting oxide for highly efficient solar cells, Nat. Nanotechnol. 4 (2009) 592–597. doi:10.1038/nnano.2009.226.
[38] P. Roy, D. Kim, K. Lee, E. Spiecker, P. Schmuki, TiO2 nanotubes and their application in dye-sensitized solar cells, Nanoscale. 2 (2010) 45–59. doi:10.1039/B9NR00131J.
[39] M. Law, L.E. Greene, J.C. Johnson, R. Saykally, P. Yang, Nanowire dye-sensitized solar cells, Nat. Mater. 4 (2005) 455–459. doi:10.1038/nmat1387.
[40] J.B. Baxter, E.S. Aydil, Dye-sensitized solar cells based on semiconductor morphologies with ZnO nanowires, Sol. Energy Mater. Sol. Cells. 90 (2006) 607–622. doi:10.1016/j.solmat.2005.05.010.
[41] J.B. Baxter, A.M. Walker, K. Van Ommering, E.S. Aydil, Synthesis and characterization of ZnO nanowires and their integration into dye-sensitized solar cells, Nanotechnology. 17 (2006). doi:10.1088/0957-4484/17/11/S13.
[42] C. Xu, P. Shin, L. Cao, D. Gao, Preferential Growth of Long ZnO Nanowire Array and Its Application in Dye-Sensitized Solar Cells, J. Phys. Chem. C. 114 (2010) 125–129. doi:10.1021/jp9085415.
[43] C. Xu, J. Wu, U. V. Desai, D. Gao, Multilayer assembly of nanowire arrays for dye-sensitized solar cells, J. Am. Chem. Soc. 133 (2011) 8122–8125. doi:10.1021/ja202135n.
[44] E. Galoppini, J. Rochford, H. Chen, G. Saraf, Y. Lu, A. Hagfeldt, G. Boschloo, Fast electron transport in metal organic vapor deposition grown dye-sensitized ZnO nanorod solar cells, J. Phys. Chem. B. 110 (2006) 16139–16161. doi:10.1021/jp062865q.
[45] B. Liu, E.S. Aydil, Growth of Oriented Single-Crystalline Rutile TiO Nanorods on Transparent Conducting Substrates for Dye-Sensitized Solar Cells Growth of Oriented Single-Crystalline Rutile TiO 2 Nanorods on Transparent Conducting Substrates for Dye-Sensitized Solar Cells, J. Am. Chem. Soc. 131 (2009) 3985–3990. doi:10.1021/ja8078972.
[46] M. Lv, D. Zheng, M. Ye, J. Xiao, W. Guo, Y. Lai, L. Sun, C. Lin, J. Zuo, Optimized porous rutile TiO2 nanorod arrays for enhancing the efficiency of dye-sensitized solar cells, Energy Environ. Sci. 6 (2013) 1615. doi:10.1039/c3ee24125d.
[47] W.Q. Wu, Y.F. Xu, C.Y. Su, D. Bin Kuang, Ultra-long anatase TiO2 nanowire arrays with multi-layered configuration on FTO glass for high-efficiency dye-sensitized solar cells, Energy Environ. Sci. 7 (2014) 644–649. doi:10.1039/c3ee42167h.

[48] M. Lazzeri, A. Vittadini, A. Selloni, Structure and energetics of stoichiometric TiO2anatase surfaces, Phys. Rev. B - Condens. Matter Mater. Phys. 63 (2001) 1554091–1554099. doi:10.1103/PhysRevB.63.155409.
[49] X.Q. Gong, A. Selloni, Reactivity of anatase TiO 2 nanoparticles: The role of the minority (001) surface, J. Phys. Chem. B. 109 (2005) 19560–19562. doi:10.1021/jp055311g.
[50] H.G. Yang, C.H. Sun, S.Z. Qiao, J. Zou, G. Liu, S.C. Smith, H.M. Cheng, G.Q. Lu, Anatase TiO2single crystals with a large percentage of reactive facets, Nature. 453 (2008) 638–641. doi:10.1038/nature06964.
[51] X. Han, Q. Kuang, M. Jin, Z. Xie, L. Zheng, Synthesis of Titania Nanosheets with a High Percentage of Exposed (001) Facets and Related Photocatalytic Properties Synthesis of Titania Nanosheets with a High Percentage of Exposed (001), Society. (2009) 1–3. doi:10.1021/ja8092373.
[52] J. Yu, J. Fan, K. Lv, Anatase TiO2 nanosheets with exposed (001) facets: Improved photoelectric conversion efficiency in dye-sensitized solar cells, Nanoscale. 2 (2010) 2144–2149. doi:10.1039/c0nr00427h.
[53] X. Wu, Z. Chen, G.Q. Max Lu, L. Wang, Nanosized anatase TiO2 single crystals with tunable exposed (001) facets for enhanced energy conversion efficiency of dye-sensitized solar cells, Adv. Funct. Mater. 21 (2011) 4167–4172. doi:10.1002/adfm.201100828.
[54] L. Chu, Z. Qin, J. Yang, X. Li, Anatase TiO2 Nanoparticles with Exposed {001} Facets for Efficient Dye-Sensitized Solar Cells, Sci. Rep. 5 (2015) 12143. doi:10.1038/srep12143.
[55] C. Chen, L. Xu, G.A. Sewvandi, T. Kusunose, Y. Tanaka, S. Nakanishi, Q. Feng, Microwave-assisted topochemical conversion of layered titanate nanosheets to {010}-faceted anatase nanocrystals for high performance photocatalysts and dye-sensitized solar cells, Cryst. Growth Des. 14 (2014) 5801–5811. doi:10.1021/cg501062r.
[56] H. Zhang, Y. Han, X. Liu, P. Liu, H. Yu, S. Zhang, X. Yao, H. Zhao, Anatase TiO2 microspheres with exposed mirror-like plane {001} facets for high performance dye-sensitized solar cells (DSSCs), Chem. Commun. 46 (2010) 8395. doi:10.1039/c0cc03196h.
[57] W. Yang, J. Li, Y. Wang, F. Zhu, W. Shi, F. Wan, D. Xu, A facile synthesis of anatase TiO $_2$ nanosheets-based hierarchical spheres with over 90% {001} facets for dye-sensitized solar cells, Chem. Commun. 47 (2011) 1809–1811. doi:10.1039/C0CC03312J.
[58] W.Q. Fang, X.H. Yang, H. Zhu, Z. Li, H. Zhao, X. Yao, H.G. Yang, Yolk@shell anatase TiO2 hierarchical microspheres with exposed {001} facets for high-performance dye sensitized solar cells, J. Mater. Chem. 22 (2012) 22082. doi:10.1039/c2jm34787c.
[59] E. Palomares, J.N. Clifford, S. a Haque, T. Lutz, J.R. Durrant, Slow charge recombination in dye-sensitised solar cells (DSSC) using Al2O3 coated nanoporous TiO2 films, Chem. Commun. (2002) 1464–1465. doi:10.1039/b202515a.
[60] S. Chappel, S.G. Chen, A. Zaban, TiO2-coated nanoporous SnO2 electrodes for dye-sensitized solar cells, Langmuir. 18 (2002) 3336–3342. doi:10.1021/la015536s.
[61] T. Taguchi, X. Zhang, I. Sutanto, K. Tokuhiro, T.N. Rao, Improving the performance of solid-state dye-sensitized solar cell using MgO-coated TiO2 nanoporous film, Chem. 0 (2003) 2480–2481.
[62] N.G. Park, M.G. Kang, K.M. Kim, K.S. Ryu, S.H. Chang, D.K. Kim, J. Van de Lagemaat, K.D. Benkstein, A.J. Frank, Morphological and photoelectrochemical characterization of core-shell nanoparticle films for dye-sensitized solar cells: Zn-O type shell on SnO2and

TiO2cores, Langmuir. 20 (2004) 4246–4253. doi:10.1021/la036122x.
[63] B. Tan, Y. Wu, Dye-sensitized solar cells based on anatase TiO2 nanoparticle/nanowire composites, J. Phys. Chem. B. 110 (2006) 15932–15938. doi:10.1021/jp063972n.
[64] M. Law, L.E. Greene, A. Radenovic, T. Kuykendall, J. Liphardt, P. Yang, ZnO-Al2O3 and ZnO-TiO2 core-shell nanowire dye-sensitized solar cells, J. Phys. Chem. B. 110 (2006) 22652–22663. doi:10.1021/jp0648644.
[65] B. Boro, B. Gogoi, B.M. Rajbongshi, A. Ramchiary, Nano-structured TiO2/ZnO nanocomposite for dye-sensitized solar cells application: A review, Renew. Sustain. Energy Rev. 81 (2018) 2264–2270. doi:10.1016/j.rser.2017.06.035.
[66] V. Manthina, J.P. Correa Baena, G. Liu, A.G. Agrios, ZnO–TiO2 Nanocomposite Films for High Light Harvesting Efficiency and Fast Electron Transport in Dye-Sensitized Solar Cells, J. Phys. Chem. C. 116 (2012) 23864–23870. doi:10.1021/jp304622d.
[67] C. Xu, J. Wu, U. V. Desai, D. Gao, High-efficiency solid-state dye-sensitized solar cells based on TiO2-coated ZnO nanowire arrays, Nano Lett. 12 (2012) 2420–2424. doi:10.1021/nl3004144.
[68] R. Liu, W.D. Yang, L.S. Qiang, H.Y. Liu, Conveniently fabricated heterojunction ZnO/TiO2electrodes using TiO2nanotube arrays for dye-sensitized solar cells, J. Power Sources. 220 (2012) 153–159. doi:10.1016/j.jpowsour.2012.07.097.
[69] K.M. Lee, E.S. Lee, B. Yoo, D.H. Shin, Electrochimica Acta Synthesis of ZnO-decorated TiO 2 nanotubes for dye-sensitized solar cells, Electrochim. Acta. 109 (2013) 181–186. doi:10.1016/j.electacta.2013.07.055.
[70] Y. Bai, H. Yu, Z. Li, R. Amal, G.Q. Lu, L. Wang, In situ growth of a ZnO nanowire network within a TiO2 nanoparticle film for enhanced dye-sensitized solar cell performance, Adv. Mater. 24 (2012) 5850–5856. doi:10.1002/adma.201201992.
[71] A.N.M. Green, E. Palomares, S.A. Haque, J.M. Kroon, J.R. Durrant, Charge Transport versus Recombination in Dye-Sensitized Solar Cells Employing Nanocrystalline TiO2 and SnO2 Films, J. Phys. Chem. B. 109 (2005) 12525–12533. doi:10.1021/jp050145y.
[72] J. Qian, P. Liu, Y. Xiao, Y. Jiang, Y. Cao, X. Ai, H. Yang, TiO2-coated multilayered SnO2 hollow microspheres for dye-sensitized solar cells, Adv. Mater. 21 (2009) 3663–3667. doi:10.1002/adma.200900525.
[73] S.H. Ahn, D.J. Kim, W.S. Chi, J.H. Kim, One-dimensional hierarchical nanostructures of TiO2 nanosheets on SnO2 Nanotubes for high efficiency solid-state dye-sensitized solar cells, Adv. Mater. 25 (2013) 4893–4897. doi:10.1002/adma.201302226.
[74] S.H. Ahn, D.J. Kim, W.S. Chi, J.H. Kim, Hierarchical double-shell nanostructures of TiO2 nanosheets on SnO2 hollow spheres for high-efficiency, solid-state, dye-sensitized solar cells, Adv. Funct. Mater. 24 (2014) 5037–5044. doi:10.1002/adfm.201400774.
[75] K.L. Kelly, E. Coronado, L.L. Zhao, G.C. Schatz, The Optical Properties of Metal Nanoparticles: The Influence of Size, Shape, and Dielectric Environment, J. Phys. Chem. B. 107 (2003) 668–677. doi:10.1021/jp026731y.
[76] S.D. Standridge, G.C. Schatz, J.T. Hupp, Distance Dependence of Plasmon-Enhanced Photocurrent in Dye-Sensitized Solar Cells, J. Am. Chem. Soc. 131 (2009) 8407–8409. doi:10.1021/ja9022072.
[77] H.A. Atwater, A. Polman, Plasmonics for improved photovoltaic devices, Nat. Mater. 9 (2010) 205–213. doi:10.1038/nmat2629.
[78] N.C. Jeong, C. Prasittichai, J.T. Hupp, Photocurrent Enhancement by Surface Plasmon Resonance of Silver Nanoparticles in Highly Porous Dye-Sensitized Solar Cells,

Langmuir. 27 (2011) 14609–14614. doi:10.1021/la203557f.
[79] Y. Li, H. Wang, Q. Feng, G. Zhou, Z.-S. Wang, Gold nanoparticles inlaid TiO2 photoanodes: a superior candidate for high-efficiency dye-sensitized solar cells, Energy Environ. Sci. 6 (2013) 2156–2165. doi:10.1039/C3EE23971C.
[80] R.A. Naphade, M. Tathavadekar, J.P. Jog, S. Agarkar, S. Ogale, Plasmonic light harvesting of dye sensitized solar cells by Au-nanoparticle loaded TiO2 nanofibers, J. Mater. Chem. A. 2 (2014) 975–984. doi:10.1039/C3TA13246C.
[81] Y.-C. Yen, P.-H. Chen, J.-Z. Chen, J.-A. Chen, K.-J. Lin, Plasmon-Induced Efficiency Enhancement on Dye-Sensitized Solar Cell by a 3D TNW-AuNP Layer, ACS Appl. Mater. Interfaces. 7 (2015) 1892–1898. doi:10.1021/am507668j.
[82] I.-K. Ding, J. Zhu, W. Cai, S.-J. Moon, N. Cai, P. Wang, S.M. Zakeeruddin, M. Grätzel, M.L. Brongersma, Y. Cui, M.D. McGehee, Plasmonic Dye-Sensitized Solar Cells, Adv. Energy Mater. 1 (2010) 52–57. doi:10.1002/aenm.201000041.
[83] J. Qi, X. Dang, P.T. Hammond, A.M. Belcher, Highly Efficient Plasmon-Enhanced Dye-Sensitized Solar Cells through Metal@Oxide Core–Shell Nanostructure, ACS Nano. 5 (2011) 7108–7116. doi:10.1021/nn201808g.
[84] X. Dang, J. Qi, M.T. Klug, P.-Y. Chen, D.S. Yun, N.X. Fang, P.T. Hammond, A.M. Belcher, Tunable Localized Surface Plasmon-Enabled Broadband Light-Harvesting Enhancement for High-Efficiency Panchromatic Dye-Sensitized Solar Cells, Nano Lett. 13 (2013) 637–642. doi:10.1021/nl3043823.
[85] H. Choi, W.T. Chen, P. V Kamat, Know Thy Nano Neighbor. Plasmonic versus Electron Charging Effects of Metal Nanoparticles in Dye-Sensitized Solar Cells, ACS Nano. 6 (2012) 4418–4427. doi:10.1021/nn301137r.
[86] J. Wu, Z. Lan, J. Lin, M. Huang, Y. Huang, L. Fan, G. Luo, Y. Lin, Y. Xie, Y. Wei, Counter electrodes in dye-sensitized solar cells, Chem. Soc. Rev. 46 (2017) 5975–6023. doi:10.1039/c6cs00752j.
[87] H. Jeong, Y. Pak, Y. Hwang, H. Song, K.H. Lee, H.C. Ko, G.Y. Jung, Enhancing the charge transfer of the counter electrode in dye-sensitized solar cells using periodically aligned platinum nanocups, Small. 8 (2012) 3757–3761. doi:10.1002/smll.201201214.
[88] J. Kim, J. Kang, U. Jeong, H. Kim, H. Lee, Catalytic , Conductive , and Transparent Platinum Nano fiber Webs for FTO-Free Dye-Sensitized Solar Cells, ACS Appl. Mater. Interfaces. 5 (2013) 3176–3181. doi:10.1021/am400179j.
[89] N. Tian, Z.-Y. Zhou, S.-G. Sun, Y. Ding, Z.L. Wang, Synthesis of Tetrahexahedral Platinum Nanocrystals with High-Index Facets and High Electro-Oxidation Activity, Science 316 (2007) 732 LP-735. http://science.sciencemag.org/content/316/5825/732.abstract.
[90] M. Subhramannia, V.K. Pillai, Shape-dependent electrocatalytic activity of platinum nanostructures, J. Mater. Chem. 18 (2008) 5858–5870. doi:10.1039/b811149a.
[91] J. Chen, B. Lim, E.P. Lee, Y. Xia, Shape-controlled synthesis of platinum nanocrystals for catalytic and electrocatalytic applications, Nano Today. 4 (2009) 81–95. doi:10.1016/j.nantod.2008.09.002.
[92] B. Zhang, D. Wang, Y. Hou, S. Yang, X.H. Yang, J.H. Zhong, J. Liu, H.F. Wang, P. Hu, H.J. Zhao, H.G. Yang, Facet-dependent catalytic activity of platinum nanocrystals for triiodide reduction in dye-sensitized solar cells, Sci. Rep. 3 (2013) 1–7. doi:10.1038/srep01836.
[93] S. Thomas, T.G. Deepak, G.S. Anjusree, T.A. Arun, S. V. Nair, A.S. Nair, A review on

counter electrode materials in dye-sensitized solar cells, J. Mater. Chem. A. 2 (2014) 4474–4490. doi:10.1039/c3ta13374e.
[94] T.N. Murakami, S. Ito, Q. Wang, M.K. Nazeeruddin, T. Bessho, I. Cesar, P. Liska, R. Humphry-Baker, P. Comte, P. Péchy, M. Grätzel, Highly Efficient Dye-Sensitized Solar Cells Based on Carbon Black Counter Electrodes, J. Electrochem. Soc. 153 (2006) A2255. doi:10.1149/1.2358087.
[95] M. Wu, X. Lin, T. Wang, J. Qiu, T. Ma, Low-cost dye-sensitized solar cell based on nine kinds of carbon counter electrodes, Energy Environ. Sci. 4 (2011) 2308–2315. doi:10.1039/c1ee01059j.
[96] L. Kavan, J.H. Yum, M. Gratzel, Optically transparent cathode for dye-sensitized solar cells based on graphene nanoplatelets , ACS Nano. 5 (2011) 165–172. doi:10.1021/nn102353h [doi].
[97] J.D. Roy-Mayhew, D.J. Bozym, C. Punckt, I.A. Aksay, Functionalized graphene as a catalytic counter electrode in dye-sensitized solar cells, ACS Nano. 4 (2010) 6203–6211. doi:10.1021/nn1016428.
[98] W.J. Lee, E. Ramasamy, D.Y. Lee, J.S. Song, Efficient dye-sensitized solar cells with catalytic multiwall carbon nanotube counter electrodes, ACS Appl. Mater. Interfaces. 1 (2009) 1145–1149. doi:10.1021/am800249k.
[99] A. Kay, M. Grätzel, Low cost photovoltaic modules based on dye sensitized nanocrystalline titanium dioxide and carbon powder, Sol. Energy Mater. Sol. Cells. 44 (1996) 99–117. doi:10.1016/0927-0248(96)00063-3.
[100] Y.-A. Leu, M.-H. Yeh, L.-Y. Lin, T.-J. Li, L.-Y. Chang, S.-Y. Shen, Y.-S. Li, G.-L. Chen, W.-H. Chiang, J.-J. Lin, K.-C. Ho, Thermally Stable Boron-Doped Multiwalled Carbon Nanotubes as a Pt-free Counter Electrode for Dye-Sensitized Solar Cells, ACS Sustain. Chem. Eng. 5 (2017) 537–546. doi:10.1021/acssuschemeng.6b01895.
[101] X. Xu, D. Huang, K. Cao, M. Wang, S.M. Zakeeruddin, M. Grätzel, Electrochemically reduced graphene oxide multilayer films as efficient counter electrode for dye-sensitized solar cells, Sci. Rep. 3 (2013) 1–7. doi:10.1038/srep01489.
[102] C. Yu, Z. Liu, X. Meng, B. Lu, D. Cui, J. Qiu, Nitrogen and phosphorus dual-doped graphene as a metal-free high-efficiency electrocatalyst for triiodide reduction, Nanoscale. 8 (2016) 17458–17464. doi:10.1039/c6nr00839a.
[103] L. Kavan, J.H. Yum, M. Grätzel, Graphene nanoplatelets outperforming platinum as the electrocatalyst in co-bipyridine-mediated dye-sensitized solar cells, Nano Lett. 11 (2011) 5501–5506. doi:10.1021/nl203329c.
[104] M.A. Green, A. Ho-Baillie, H.J. Snaith, The emergence of perovskite solar cells, Nat Phot. 8 (2014) 506–514. http://dx.doi.org/10.1038/nphoton.2014.134.
[105] A. Kojima, K. Teshima, Y. Shirai, T. Miyasaka, Organometal Halide Perovskites as Visible-Light Sensitizers for Photovoltaic Cells, J. Am. Chem. Soc. 131 (2009) 6050–6051. doi:10.1021/ja809598r.
[106] M.M. Lee, J. Teuscher, T. Miyasaka, T.N. Murakami, H.J. Snaith, Efficient Hybrid Solar Cells Based on Meso-superstructured Organometal Halide Perovskites, Science 338 (2012) 643–647. doi:10.1126/science.1228604.
[107] NREL. Efficiency chart, https://www.nrel.gov/pv/assets/pdfs/best-research-cell-efficiencies.20190923.pdf
[108] W.S. Yang, B.-W. Park, E.H. Jung, N.J. Jeon, Y.C. Kim, D.U. Lee, S.S. Shin, J. Seo, E.K. Kim, J.H. Noh, S. Il Seok, Iodide management in formamidinium-lead-halide–based

perovskite layers for efficient solar cells, Science. 356 (2017) 1376–1379. doi:10.1126/science.aan2301.
[109] J. Burschka, N. Pellet, S.-J. Moon, R. Humphry-Baker, P. Gao, M.K. Nazeeruddin, M. Grätzel, Sequential deposition as a route to high-performance perovskite-sensitized solar cells, Nature. 499 (2013) 316. doi:10.1038/nature12340https://www.nature.com/articles/nature12340#supplementary-information.
[110] P. Docampo, J.M. Ball, M. Darwich, G.E. Eperon, H.J. Snaith, Efficient organometal trihalide perovskite planar-heterojunction solar cells on flexible polymer substrates, Nat. Commun. 4 (2013) 2761. doi:10.1038/ncomms3761https://www.nature.com/articles/ncomms3761#supplementary-information.
[111] J.-Y. Jeng, Y.-F. Chiang, M.-H. Lee, S.-R. Peng, T.-F. Guo, P. Chen, T.-C. Wen, CH3NH3PbI3 Perovskite/Fullerene Planar-Heterojunction Hybrid Solar Cells, Adv. Mater. 25 (2013) 3727–3732. doi:doi:10.1002/adma.201301327.
[112] H. Zhou, Q. Chen, G. Li, S. Luo, T. Song, H.-S. Duan, Z. Hong, J. You, Y. Liu, Y. Yang, Interface engineering of highly efficient perovskite solar cells, Science 345 (2014) 542–546. doi:10.1126/science.1254050.
[113] Z. Zhu, Y. Bai, T. Zhang, Z. Liu, X. Long, Z. Wei, Z. Wang, L. Zhang, J. Wang, F. Yan, S. Yang, High-Performance Hole-Extraction Layer of Sol–Gel-Processed NiO Nanocrystals for Inverted Planar Perovskite Solar Cells, Angew. Chem. Int. Ed. 53 (2014) 12571–12575. doi:doi:10.1002/anie.201405176.
[114] C. Zuo, H.J. Bolink, H. Han, J. Huang, D. Cahen, L. Ding, Adv. Sci., Adv. Sci. 3 (2016) 1500324. doi:doi:10.1002/advs.201500324.
[115] H.J. Snaith, Perovskites: The Emergence of a New Era for Low-Cost, High-Efficiency Solar Cells, J. Phys. Chem. Lett. 4 (2013) 3623–3630. doi:10.1021/jz4020162.
[116] Y. Zhao, K. Zhu, Organic–inorganic hybrid lead halide perovskites for optoelectronic and electronic applications, Chem. Soc. Rev. 45 (2016) 655–689. doi:10.1039/C4CS00458B.
[117] A. Rajagopal, K. Yao, A.K.-Y. Jen, Toward Perovskite Solar Cell Commercialization: A Perspective and Research Roadmap Based on Interfacial Engineering, Adv. Mater. 30 (2018) 1800455. doi:doi:10.1002/adma.201800455.
[118] Q. Fu, X. Tang, B. Huang, T. Hu, L. Tan, L. Chen, Y. Chen, Recent Progress on the Long-Term Stability of Perovskite Solar Cells, Adv. Sci. 5 (2018) 1700387. doi:doi:10.1002/advs.201700387.
[119] M. Saliba, Perovskite solar cells must come of age, Science 359 (2018) 388–389. doi:10.1126/science.aar5684.
[120] K. Domanski, E.A. Alharbi, A. Hagfeldt, M. Grätzel, W. Tress, Systematic investigation of the impact of operation conditions on the degradation behaviour of perovskite solar cells, Nat. Energy. 3 (2018) 61–67. doi:10.1038/s41560-017-0060-5.
[121] B. Chen, M. Yang, S. Priya, K. Zhu, Origin of J–V Hysteresis in Perovskite Solar Cells, J. Phys. Chem. Lett. 7 (2016) 905–917. doi:10.1021/acs.jpclett.6b00215.
[122] P. V Kamat, J. Bisquert, J. Buriak, Lead-Free Perovskite Solar Cells, ACS Energy Lett. 2 (2017) 904–905. doi:10.1021/acsenergylett.7b00246.
[123] Z. Song, S.C. Watthage, A.B. Phillips, M.J. Heben, Pathways toward high-performance perovskite solar cells: review of recent advances in organo-metal halide perovskites for photovoltaic applications, in: J. Photon. Energy, SPIE, 2016: p. 22001.

[124] M. Saliba, S. Orlandi, T. Matsui, S. Aghazada, M. Cavazzini, J.-P. Correa-Baena, P. Gao, R. Scopelliti, E. Mosconi, K.-H. Dahmen, F. De Angelis, A. Abate, A. Hagfeldt, G. Pozzi, M. Graetzel, M.K. Nazeeruddin, A molecularly engineered hole-transporting material for efficient perovskite solar cells, Nat. Energy. (2016) 15017. http://www.nature.com/articles/nenergy201517 (accessed January 18, 2016).
[125] G. Xing, N. Mathews, S. Sun, S.S. Lim, Y.M. Lam, M. Grätzel, S. Mhaisalkar, T.C. Sum, Long-Range Balanced Electron- and Hole-Transport Lengths in Organic-Inorganic $CH_3NH_3PbI_3$, Science 342 (2013) 344–347. doi:10.1126/science.1243167.
[126] M. Batmunkh, M.J. Biggs, J.G. Shapter, Carbonaceous Dye-Sensitized Solar Cell Photoelectrodes, Adv. Sci. 2 (2015) 1400025. doi:doi:10.1002/advs.201400025.
[127] J.M. Ball, M.M. Lee, A. Hey, H.J. Snaith, Low-temperature processed meso-superstructured to thin-film perovskite solar cells, Energy Environ. Sci. 6 (2013) 1739. doi:10.1039/c3ee40810h.
[128] D. Liu, T.L. Kelly, Perovskite solar cells with a planar heterojunction structure prepared using room-temperature solution processing techniques, Nat. Photonics. 8 (2013) 133. http://dx.doi.org/10.1038/nphoton.2013.342.
[129] B. Roose, J.-P.C. Baena, K.C. Gödel, M. Graetzel, A. Hagfeldt, U. Steiner, A. Abate, Mesoporous SnO2 electron selective contact enables UV-stable perovskite solar cells, Nano Energy. 30 (2016) 517–522. doi:https://doi.org/10.1016/j.nanoen.2016.10.055.
[130] X. Ling, J. Yuan, D. Liu, Y. Wang, Y. Zhang, S. Chen, H. Wu, F. Jin, F. Wu, G. Shi, X. Tang, J. Zheng, S. Liu, Z. Liu, W. Ma, Room-Temperature Processed Nb2O5 as the Electron-Transporting Layer for Efficient Planar Perovskite Solar Cells, ACS Appl. Mater. Interfaces. 9 (2017) 23181–23188. doi:10.1021/acsami.7b05113.
[131] J. Feng, X. Zhu, Z. Yang, X. Zhang, J. Niu, Z. Wang, S. Zuo, S. Priya, S. Liu, D. Yang, Record Efficiency Stable Flexible Perovskite Solar Cell Using Effective Additive Assistant Strategy, Adv. Mater. 30 (2018) 1801418. doi:doi:10.1002/adma.201801418.
[132] Y. Hou, C.O.R. Quiroz, S. Scheiner, W. Chen, T. Stubhan, A. Hirsch, M. Halik, C.J. Brabec, Low-Temperature and Hysteresis-Free Electron-Transporting Layers for Efficient, Regular, and Planar Structure Perovskite Solar Cells, Adv. Energy. Mater. 5 (2015) 1501056. doi:doi:10.1002/aenm.201501056.
[133] A. Bera, K. Wu, A. Sheikh, E. Alarousu, O.F. Mohammed, T. Wu, Perovskite Oxide SrTiO3 as an Efficient Electron Transporter for Hybrid Perovskite Solar Cells, J. Phys. Chem. C. 118 (2014) 28494–28501. doi:10.1021/jp509753p.
[134] J. Lian, B. Lu, F. Niu, P. Zeng, X. Zhan, Electron-Transport Materials in Perovskite Solar Cells, Small Methods. 0 (n.d.) 1800082. doi:doi:10.1002/smtd.201800082.
[135] H. Liu, Z. Huang, S. Wei, L. Zheng, L. Xiao, Q. Gong, Nano-structured electron transporting materials for perovskite solar cells, Nanoscale. 8 (2016) 6209–6221. doi:10.1039/C5NR05207F.
[136] M. Yang, R. Guo, K. Kadel, Y. Liu, K. O'Shea, R. Bone, X. Wang, J. He, W. Li, Improved charge transport of Nb-doped TiO2 nanorods in methylammonium lead iodide bromide perovskite solar cells, J. Mater. Chem. A. 2 (2014) 19616–19622. doi:10.1039/C4TA02635G.
[137] M. Batmunkh, T.J. Macdonald, C.J. Shearer, M. Bat-Erdene, Y. Wang, M.J. Biggs, I.P. Parkin, T. Nann, J.G. Shapter, Carbon Nanotubes in TiO2 Nanofiber Photoelectrodes for High-Performance Perovskite Solar Cells, Adv. Sci. 4 (2017) 1600504. doi:doi:10.1002/advs.201600504.

[138] Q. Jiang, X. Sheng, Y. Li, X. Feng, T. Xu, Rutile TiO2 nanowire-based perovskite solar cells, Chem. Commun. 50 (2014) 14720–14723. doi:10.1039/C4CC07367C.
[139] Y. Yu, J. Li, D. Geng, J. Wang, L. Zhang, T.L. Andrew, M.S. Arnold, X. Wang, Development of Lead Iodide Perovskite Solar Cells Using Three-Dimensional Titanium Dioxide Nanowire Architectures., ACS Nano. 9 (2015) 564–572. http://dx.doi.org/10.1021/nn5058672 (accessed December 31, 2014).
[140] X. Wang, Z. Li, W. Xu, S.A. Kulkarni, S.K. Batabyal, S. Zhang, A. Cao, L.H. Wong, TiO2 nanotube arrays based flexible perovskite solar cells with transparent carbon nanotube electrode, Nano Energy. 11 (2015) 728–735. doi:https://doi.org/10.1016/j.nanoen.2014.11.042.
[141] D. Zhong, B. Cai, X. Wang, Z. Yang, Y. Xing, S. Miao, W.-H. Zhang, C. Li, Synthesis of oriented TiO2 nanocones with fast charge transfer for perovskite solar cells, Nano Energy. 11 (2015) 409–418. doi:https://doi.org/10.1016/j.nanoen.2014.11.014.
[142] J.-W. Lee, S.H. Lee, H.-S. Ko, J. Kwon, J.H. Park, S.M. Kang, N. Ahn, M. Choi, J.K. Kim, N.-G. Park, Opto-electronic properties of TiO2 nanohelices with embedded HC(NH2)2PbI3 perovskite solar cells, J. Mater. Chem. A. 3 (2015) 9179–9186. doi:10.1039/C4TA04988H.
[143] F. Giordano, A. Abate, J.P. Correa Baena, M. Saliba, T. Matsui, S.H. Im, S.M. Zakeeruddin, M.K. Nazeeruddin, A. Hagfeldt, M. Graetzel, Enhanced electronic properties in mesoporous TiO2 via lithium doping for high-efficiency perovskite solar cells, Nat. Commun. 7 (2016) 10379. doi:10.1038/ncomms10379https://www.nature.com/articles/ncomms10379#supplementary-information.
[144] D. Liu, S. Li, P. Zhang, Y. Wang, R. Zhang, H. Sarvari, F. Wang, J. Wu, Z. Wang, Z.D. Chen, Efficient planar heterojunction perovskite solar cells with Li-doped compact TiO2 layer, Nano Energy. 31 (2017) 462–468. doi:https://doi.org/10.1016/j.nanoen.2016.11.028.
[145] H. Zhang, J. Shi, X. Xu, L. Zhu, Y. Luo, D. Li, Q. Meng, Mg-doped TiO2 boosts the efficiency of planar perovskite solar cells to exceed 19%, J. Mater. Chem. A. 4 (2016) 15383–15389. doi:10.1039/C6TA06879K.
[146] A. Abrusci, S.D. Stranks, P. Docampo, H.-L.L. Yip, A.K.-Y.Y. Jen, H.J. Snaith, High-performance perovskite-polymer hybrid solar cells via electronic coupling with fullerene monolayers, Nano Lett. 13 (2013) 3124–3128. doi:10.1021/nl401044q.
[147] W. Ke, G. Fang, Q. Liu, L. Xiong, P. Qin, H. Tao, J. Wang, H. Lei, B. Li, J. Wan, G. Yang, Y. Yan, Low-Temperature Solution-Processed Tin Oxide as an Alternative Electron Transporting Layer for Efficient Perovskite Solar Cells, J. Am. Chem. Soc. 137 (2015) 6730–6733. doi:10.1021/jacs.5b01994.
[148] M. Batmunkh, C.J. Shearer, M. Bat-Erdene, M.J. Biggs, J.G. Shapter, Single-Walled Carbon Nanotubes Enhance the Efficiency and Stability of Mesoscopic Perovskite Solar Cells, ACS Appl. Mater. Interfaces. 9 (2017) 19945–19954. doi:10.1021/acsami.7b04894.
[149] N. Fu, C. Huang, P. Lin, M. Zhu, T. Li, M. Ye, S. Lin, G. Zhang, J. Du, C. Liu, B. Xu, D. Wang, S. Ke, Black phosphorus quantum dots as dual-functional electron-selective materials for efficient plastic perovskite solar cells, J. Mater. Chem. A. 6 (2018) 8886–8894. doi:10.1039/C8TA01408F.
[150] W. Zhang, M. Saliba, S.D. Stranks, Y. Sun, X. Shi, U. Wiesner, H.J. Snaith, Enhancement of Perovskite-Based Solar Cells Employing Core–Shell Metal Nanoparticles, Nano Lett.

13 (2013) 4505–4510. doi:10.1021/nl4024287.
[151] M. Batmunkh, T.J. Macdonald, W.J. Peveler, A.S.R. Bati, C.J. Carmalt, I.P. Parkin, J.G. Shapter, Plasmonic Gold Nanostars Incorporated into High-Efficiency Perovskite Solar Cells, ChemSusChem. 10 (2017) 3750–3753. doi:doi:10.1002/cssc.201701056.
[152] J. Cui, C. Chen, J. Han, K. Cao, W. Zhang, Y. Shen, M. Wang, Surface Plasmon Resonance Effect in Inverted Perovskite Solar Cells, Adv. Sci. 3 (2016) 1500312. doi:doi:10.1002/advs.201500312.
[153] J.T.-W. Wang, J.M. Ball, E.M. Barea, A. Abate, J.A. Alexander-Webber, J. Huang, M. Saliba, I. Mora-Sero, J. Bisquert, H.J. Snaith, R.J. Nicholas, Low-Temperature Processed Electron Collection Layers of Graphene/TiO2 Nanocomposites in Thin Film Perovskite Solar Cells, Nano Lett. 14 (2014) 724–730. doi:10.1021/nl403997a.
[154] D. Yang, R. Yang, K. Wang, C. Wu, X. Zhu, J. Feng, X. Ren, G. Fang, S. Priya, S. (Frank) Liu, High efficiency planar-type perovskite solar cells with negligible hysteresis using EDTA-complexed SnO2, Nat. Commun. 9 (2018) 3239. doi:10.1038/s41467-018-05760-x.
[155] M. Liu, M.B. Johnston, H.J. Snaith, Efficient planar heterojunction perovskite solar cells by vapour deposition, Nature. 501 (2013) 395. http://dx.doi.org/10.1038/nature12509.
[156] C. Wu, H. Li, Y. Yan, B. Chi, J. Pu, J. Li, M. Sanghadasa, S. Priya, Cost-effective sustainable-engineering of CH3NH3PbI3 perovskite solar cells through slicing and restacking of 2D layers, Nano Energy. 36 (2017) 295–302. doi:https://doi.org/10.1016/j.nanoen.2017.04.034.
[157] Q. Jiang, L. Zhang, H. Wang, X. Yang, J. Meng, H. Liu, Z. Yin, J. Wu, X. Zhang, J. You, Enhanced electron extraction using SnO2 for high-efficiency planar-structure HC(NH2)2PbI3-based perovskite solar cells, Nat. Energy. 2 (2016) 16177. doi:10.1038/nenergy.2016.177https://www.nature.com/articles/nenergy2016177#supplementary-information.
[158] J.P. Correa Baena, L. Steier, W. Tress, M. Saliba, S. Neutzner, T. Matsui, F. Giordano, T.J. Jacobsson, A.R. Srimath Kandada, S.M. Zakeeruddin, A. Petrozza, A. Abate, M.K. Nazeeruddin, M. Grätzel, A. Hagfeldt, Highly efficient planar perovskite solar cells through band alignment engineering, Energy Environ. Sci. 8 (2015) 2928–2934. doi:10.1039/C5EE02608C.
[159] S. Sun, T. Salim, N. Mathews, M. Duchamp, C. Boothroyd, G. Xing, T.C. Sum, Y.M. Lam, The origin of high efficiency in low-temperature solution-processable bilayer organometal halide hybrid solar cells, Energy Environ. Sci. 7 (2014) 399–407. doi:10.1039/C3EE43161D.
[160] J. Seo, S. Park, Y. Chan Kim, N.J. Jeon, J.H. Noh, S.C. Yoon, S. Il Seok, Benefits of very thin PCBM and LiF layers for solution-processed p–i–n perovskite solar cells, Energy Environ. Sci. 7 (2014) 2642–2646. doi:10.1039/C4EE01216J.
[161] J. You, Y. Yang, Z. Hong, T.-B. Song, L. Meng, Y. Liu, C. Jiang, H. Zhou, W.-H. Chang, G. Li, Y. Yang, Moisture assisted perovskite film growth for high performance solar cells, Appl. Phys. Lett. 105 (2014) 183902. doi:10.1063/1.4901510.
[162] J.H. Kim, P.W. Liang, S.T. Williams, N. Cho, C.C. Chueh, M.S. Glaz, D.S. Ginger, A.K.Y. Jen, High-performance and environmentally stable planar heterojunction perovskite solar cells based on a solution-processed copper-doped nickel oxide hole-transporting layer, Adv. Mater. 27 (2015) 695–701. doi:10.1002/adma.201404189.
[163] Z. Zhu, Y. Bai, X. Liu, C.-C. Chueh, S. Yang, A.K.-Y. Jen, Enhanced Efficiency and

Stability of Inverted Perovskite Solar Cells Using Highly Crystalline SnO2 Nanocrystals as the Robust Electron-Transporting Layer, Adv. Mater. 28 (2016) 6478–6484. doi:doi:10.1002/adma.201600619.
[164] J. You, L. Meng, T.-B. Song, T.-F. Guo, Y. (Michael) Yang, W.-H. Chang, Z. Hong, H. Chen, H. Zhou, Q. Chen, Y. Liu, N. De Marco, Y. Yang, Improved air stability of perovskite solar cells via solution-processed metal oxide transport layers, Nat. Nanotechnol. 11 (2015) 75–81. doi:10.1038/nnano.2015.230.
[165] R. Fang, S. Wu, W. Chen, Z. Liu, S. Zhang, R. Chen, Y. Yue, L. Deng, Y.-B. Cheng, L. Han, W. Chen, [6,6]-Phenyl-C61-Butyric Acid Methyl Ester/Cerium Oxide Bilayer Structure as Efficient and Stable Electron Transport Layer for Inverted Perovskite Solar Cells, ACS Nano. 12 (2018) 2403–2414. doi:10.1021/acsnano.7b07754.
[166] C. Sun, Z. Wu, H.-L. Yip, H. Zhang, X.-F. Jiang, Q. Xue, Z. Hu, Z. Hu, Y. Shen, M. Wang, F. Huang, Y. Cao, Amino-Functionalized Conjugated Polymer as an Efficient Electron Transport Layer for High-Performance Planar-Heterojunction Perovskite Solar Cells, Adv. Energy. Mater. 6 (2016) 1501534. doi:doi:10.1002/aenm.201501534.
[167] S.N. Habisreutinger, T. Leijtens, G.E. Eperon, S.D. Stranks, R.J. Nicholas, H.J. Snaith, Carbon Nanotube/Polymer Composites as a Highly Stable Hole Collection Layer in Perovskite Solar Cells, Nano Lett. 14 (2014) 5561–5568. doi:10.1021/nl501982b.
[168] Z.H. Bakr, Q. Wali, A. Fakharuddin, L. Schmidt-Mende, T.M. Brown, R. Jose, Advances in hole transport materials engineering for stable and efficient perovskite solar cells, Nano Energy. 34 (2017) 271–305. doi:https://doi.org/10.1016/j.nanoen.2017.02.025.
[169] J.A. Christians, R.C.M. Fung, P. V Kamat, An Inorganic Hole Conductor for Organo-Lead Halide Perovskite Solar Cells. Improved Hole Conductivity with Copper Iodide, J. Am. Chem. Soc. 136 (2014) 758–764. doi:10.1021/ja411014k.
[170] Z. Liu, A. Zhu, F. Cai, L. Tao, Y. Zhou, Z. Zhao, Q. Chen, Y.-B. Cheng, H. Zhou, Nickel oxide nanoparticles for efficient hole transport in p-i-n and n-i-p perovskite solar cells, J. Mater. Chem. A. 5 (2017) 6597–6605. doi:10.1039/C7TA01593C.
[171] P. Qin, S. Tanaka, S. Ito, N. Tetreault, K. Manabe, H. Nishino, M.K. Nazeeruddin, M. Grätzel, Inorganic hole conductor-based lead halide perovskite solar cells with 12.4% conversion efficiency, Nat. Commun. 5 (2014) 3834. doi:10.1038/ncomms4834.
[172] J.H. Heo, S.H. Im, J.H. Noh, T.N. Mandal, C.-S. Lim, J.A. Chang, Y.H. Lee, H. Kim, A. Sarkar, M.K. Nazeeruddin, M. Grätzel, S. Il Seok, Efficient inorganic–organic hybrid heterojunction solar cells containing perovskite compound and polymeric hole conductors, Nat. Photonics. 7 (2013) 486. http://dx.doi.org/10.1038/nphoton.2013.80.
[173] N.J. Jeon, J. Lee, J.H. Noh, M.K. Nazeeruddin, M. Grätzel, S. Il Seok, Efficient Inorganic–Organic Hybrid Perovskite Solar Cells Based on Pyrene Arylamine Derivatives as Hole-Transporting Materials, J. Am. Chem. Soc. 135 (2013) 19087–19090. doi:10.1021/ja410659k.
[174] J. Xiao, J. Shi, H. Liu, Y. Xu, S. Lv, Y. Luo, D. Li, Q. Meng, Y. Li, Efficient CH3NH3PbI3 Perovskite Solar Cells Based on Graphdiyne (GD)-Modified P3HT Hole-Transporting Material, Adv. Energy. Mater. 5 (2015) 1401943. doi:doi:10.1002/aenm.201401943.
[175] A.L. Palma, L. Cinà, S. Pescetelli, A. Agresti, M. Raggio, R. Paolesse, F. Bonaccorso, A. Di Carlo, Reduced graphene oxide as efficient and stable hole transporting material in mesoscopic perovskite solar cells, Nano Energy. 22 (2016) 349–360. doi:https://doi.org/10.1016/j.nanoen.2016.02.027.

[176] A. Capasso, F. Matteocci, L. Najafi, M. Prato, J. Buha, L. Cinà, V. Pellegrini, A. Di Carlo, F. Bonaccorso, Few-Layer MoS2 Flakes as Active Buffer Layer for Stable Perovskite Solar Cells, Adv. Energy. Mater. 6 (2016) 1600920. doi:doi:10.1002/aenm.201600920.
[177] S.K. Muduli, E. Varrla, S.A. Kulkarni, G. Han, K. Thirumal, O. Lev, S. Mhaisalkar, N. Mathews, 2D black phosphorous nanosheets as a hole transporting material in perovskite solar cells, J. Power Sources. 371 (2017) 156–161. doi:https://doi.org/10.1016/j.jpowsour.2017.10.018.
[178] W. Chen, K. Li, Y. Wang, X. Feng, Z. Liao, Q. Su, X. Lin, Z. He, Black Phosphorus Quantum Dots for Hole Extraction of Typical Planar Hybrid Perovskite Solar Cells, J. Phys. Chem. Lett. 8 (2017) 591–598. doi:10.1021/acs.jpclett.6b02843.
[179] M. Batmunkh, M. Bat-Erdene, J.G. Shapter, Black Phosphorus: Synthesis and Application for Solar Cells, Adv. Energy. Mater. 8 (2018) 1701832. doi:doi:10.1002/aenm.201701832.
[180] L. Najafi, B. Taheri, B. Martín-García, S. Bellani, D. Di Girolamo, A. Agresti, R. Oropesa-Nuñez, S. Pescetelli, L. Vesce, E. Calabrò, M. Prato, A.E. Del Rio Castillo, A. Di Carlo, F. Bonaccorso, MoS2 Quantum Dot/Graphene Hybrids for Advanced Interface Engineering of a CH3NH3PbI3 Perovskite Solar Cell with an Efficiency of over 20%, ACS Nano. (2018) DOI: 10.1021/acsnano.8b05514. doi:10.1021/acsnano.8b05514.
[181] L. Meng, J. You, T.-F. Guo, Y. Yang, Recent Advances in the Inverted Planar Structure of Perovskite Solar Cells, Acc. Chem. Res. 49 (2016) 155–165. doi:10.1021/acs.accounts.5b00404.
[182] I. Jeon, S. Seo, Y. Sato, C. Delacou, A. Anisimov, K. Suenaga, E.I. Kauppinen, S. Maruyama, Y. Matsuo, Perovskite Solar Cells Using Carbon Nanotubes Both as Cathode and as Anode, J. Phys. Chem. C. 121 (2017) 25743–25749. doi:10.1021/acs.jpcc.7b10334.
[183] D.-Y. Lee, S.-I. Na, S.-S. Kim, Graphene oxide/PEDOT:PSS composite hole transport layer for efficient and stable planar heterojunction perovskite solar cells, Nanoscale. 8 (2016) 1513–1522. doi:10.1039/C5NR05271H.
[184] Q.-D. Yang‡, J. Li, Y. Cheng, H.-W. Li, Z. Guan, B. Yu, S.-W. Tsang, Graphene oxide as an efficient hole-transporting material for high-performance perovskite solar cells with enhanced stability, J. Mater. Chem. A. 5 (2017) 9852–9858. doi:10.1039/C7TA01752A.
[185] H.-S. Kim, C.-R. Lee, J.-H. Im, K.-B. Lee, T. Moehl, A. Marchioro, S.-J. Moon, R. Humphry-Baker, J.-H. Yum, J.E. Moser, M. Grätzel, N.-G. Park, Lead Iodide Perovskite Sensitized All-Solid-State Submicron Thin Film Mesoscopic Solar Cell with Efficiency Exceeding 9%, Sci. Rep. 2 (2012) 591. doi:10.1038/srep00591.
[186] A. Mei, X. Li, L. Liu, Z. Ku, T. Liu, Y. Rong, M. Xu, M. Hu, J. Chen, Y. Yang, M. Grätzel, H. Han, A hole-conductor–free, fully printable mesoscopic perovskite solar cell with high stability, Science 345 (2014) 295–298. doi:10.1126/science.1254763.
[187] N. Ahn, D.-Y. Son, I.-H. Jang, S.M. Kang, M. Choi, N.-G. Park, Highly Reproducible Perovskite Solar Cells with Average Efficiency of 18.3% and Best Efficiency of 19.7% Fabricated via Lewis Base Adduct of Lead(II) Iodide, J. Am. Chem. Soc. 137 (2015) 8696–8699. http://dx.doi.org/10.1021/jacs.5b04930 (accessed July 3, 2015).
[188] A.T. Barrows, A.J. Pearson, C.K. Kwak, A.D.F. Dunbar, A.R. Buckley, D.G. Lidzey, Efficient planar heterojunction mixed-halide perovskite solar cells deposited via spray-deposition, Energy Environ. Sci. 7 (2014) 2944–2950. doi:10.1039/C4EE01546K.
[189] Y. Deng, E. Peng, Y. Shao, Z. Xiao, Q. Dong, J. Huang, Scalable fabrication of efficient organolead trihalide perovskite solar cells with doctor-bladed active layers, Energy Environ. Sci. 8 (2015) 1544–1550. doi:10.1039/C4EE03907F.

[190] K. Hwang, Y.-S. Jung, Y.-J. Heo, F.H. Scholes, S.E. Watkins, J. Subbiah, D.J. Jones, D.-Y. Kim, D. Vak, Toward Large Scale Roll-to-Roll Production of Fully Printed Perovskite Solar Cells, Adv. Mater. 27 (2015) 1241–1247. doi:doi:10.1002/adma.201404598.
[191] M. Batmunkh, C.J. Shearer, M.J. Biggs, J.G. Shapter, Nanocarbons for mesoscopic perovskite solar cells, J. Mater. Chem. A. 3 (2015) 9020–9031. doi:10.1039/C5TA00873E.
[192] Z. Zhu, J. Ma, Z. Wang, C. Mu, Z. Fan, L. Du, Y. Bai, L. Fan, H. Yan, D.L. Phillips, S. Yang, Efficiency Enhancement of Perovskite Solar Cells through Fast Electron Extraction: The Role of Graphene Quantum Dots, J. Am. Chem. Soc. 136 (2014) 3760–3763. doi:10.1021/ja4132246.
[193] L. Zuo, Z. Gu, T. Ye, W. Fu, G. Wu, H. Li, H. Chen, Enhanced Photovoltaic Performance of CH3NH3PbI3 Perovskite Solar Cells through Interfacial Engineering Using Self-Assembling Monolayer, J. Am. Chem. Soc. 137 (2015) 2674–2679. doi:10.1021/ja512518r.
[194] H. Tsai, W. Nie, J.-C. Blancon, C.C. Stoumpos, R. Asadpour, B. Harutyunyan, A.J. Neukirch, R. Verduzco, J.J. Crochet, S. Tretiak, L. Pedesseau, J. Even, M.A. Alam, G. Gupta, J. Lou, P.M. Ajayan, M.J. Bedzyk, M.G. Kanatzidis, A.D. Mohite, High-efficiency two-dimensional Ruddlesden–Popper perovskite solar cells, Nature. 536 (2016) 312–316. doi:10.1038/nature18306.
[195] J. Yan, W. Qiu, G. Wu, P. Heremans, H. Chen, Recent progress in 2D/quasi-2D layered metal halide perovskites for solar cells, J. Mater. Chem. A. 6 (2018) 11063–11077. doi:10.1039/C8TA02288G.
[196] K. Wang, C. Wu, D. Yang, Y. Jiang, S. Priya, Quasi-Two-Dimensional Halide Perovskite Single Crystal Photodetector, ACS Nano. 12 (2018) 4919–4929. doi:10.1021/acsnano.8b01999.
[197] X. Zhang, X. Ren, B. Liu, R. Munir, X. Zhu, D. Yang, J. Li, Y. Liu, D.-M. Smilgies, R. Li, Z. Yang, T. Niu, X. Wang, A. Amassian, K. Zhao, S. (Frank) Liu, Stable high efficiency two-dimensional perovskite solar cells via cesium doping, Energy Environ. Sci. 10 (2017) 2095–2102. doi:10.1039/C7EE01145H.
[198] W. Fu, J. Wang, L. Zuo, K. Gao, F. Liu, D.S. Ginger, A.K.Y. Jen, Two-Dimensional Perovskite Solar Cells with 14.1% Power Conversion Efficiency and 0.68% External Radiative Efficiency, ACS Energy Lett. 3 (2018) 2086–2093. doi:10.1021/acsenergylett.8b01181.
[199] T.M. Barnes, M.O. Reese, J.D. Bergeson, B.A. Larsen, J.L. Blackburn, M.C. Beard, J. Bult, J. van de Lagemaat, Comparing the Fundamental Physics and Device Performance of Transparent, Conductive Nanostructured Networks with Conventional Transparent Conducting Oxides, Adv. Energy. Mater. 2 (2012) 353–360. doi:doi:10.1002/aenm.201100608.
[200] J. Han, S. Yuan, L. Liu, X. Qiu, H. Gong, X. Yang, C. Li, Y. Hao, B. Cao, Fully indium-free flexible Ag nanowires/ZnO:F composite transparent conductive electrodes with high haze, J. Mater. Chem. A. 3 (2015) 5375–5384. doi:10.1039/C4TA05728G.
[201] X. Huang, Z. Zeng, Z. Fan, J. Liu, H. Zhang, Graphene-Based Electrodes, Adv. Mater. 24 (2012) 5979–6004. doi:doi:10.1002/adma.201201587.
[202] M. Batmunkh, C.J. Shearer, M.J. Biggs, J.G. Shapter, Solution processed graphene structures for perovskite solar cells, J. Mater. Chem. A. 4 (2016) 2605–2616. doi:10.1039/C5TA08996D.

[203] K. Sun, P. Li, Y. Xia, J. Chang, J. Ouyang, Transparent conductive oxide-free perovskite solar cells with PEDOT:PSS as transparent electrode., ACS Appl. Mater. Interfaces. (2015). http://dx.doi.org/10.1021/acsami.5b03171 (accessed July 3, 2015).
[204] H. Sung, N. Ahn, M.S. Jang, J.-K. Lee, H. Yoon, N.-G. Park, M. Choi, Transparent Conductive Oxide-Free Graphene-Based Perovskite Solar Cells with over 17% Efficiency, Adv. Energy. Mater. 6 (2016) 1501873. doi:doi:10.1002/aenm.201501873.
[205] I. Jeon, T. Chiba, C. Delacou, Y. Guo, A. Kaskela, O. Reynaud, E.I. Kauppinen, S. Maruyama, Y. Matsuo, Single-Walled Carbon Nanotube Film as Electrode in Indium-Free Planar Heterojunction Perovskite Solar Cells: Investigation of Electron-Blocking Layers and Dopants, Nano Lett. 15 (2015) 6665–6671. doi:10.1021/acs.nanolett.5b02490.
[206] J.H. Heo, D.H. Shin, D.H. Song, D.H. Kim, S.J. Lee, S.H. Im, Super-flexible bis(trifluoromethanesulfonyl)-amide doped graphene transparent conductive electrodes for photo-stable perovskite solar cells, J. Mater. Chem. A. 6 (2018) 8251–8258. doi:10.1039/C8TA02672F.
[207] L. Qiu, J. Deng, X. Lu, Z. Yang, H. Peng, Integrating Perovskite Solar Cells into a Flexible Fiber, Angew. Chem. Int. Ed. 53 (2014) 10425–10428. doi:doi:10.1002/anie.201404973.
[208] S.N. Habisreutinger, R.J. Nicholas, H.J. Snaith, Carbon Nanotubes in Perovskite Solar Cells, Adv. Energy. Mater. 7 (2017) 1601839. doi:doi:10.1002/aenm.201601839.
[209] Z. Ku, Y. Rong, M. Xu, T. Liu, H. Han, Full Printable Processed Mesoscopic CH3NH3PbI3/TiO2 Heterojunction Solar Cells with Carbon Counter Electrode, Sci. Rep. 3 (2013) 3132. doi:10.1038/srep03132https://www.nature.com/articles/srep03132#supplementary-information.
[210] Y. Rong, Z. Ku, A. Mei, T. Liu, M. Xu, S. Ko, X. Li, H. Han, Hole-Conductor-Free Mesoscopic TiO2/CH3NH3PbI3 Heterojunction Solar Cells Based on Anatase Nanosheets and Carbon Counter Electrodes, J. Phys. Chem. Lett. 5 (2014) 2160–2164. doi:10.1021/jz500833z.
[211] Z. Wei, K. Yan, H. Chen, Y. Yi, T. Zhang, X. Long, J. Li, L. Zhang, J. Wang, S. Yang, Cost-efficient clamping solar cells using candle soot for hole extraction from ambipolar perovskites, Energy Environ. Sci. 7 (2014) 3326–3333. doi:10.1039/C4EE01983K.
[212] Z. Li, S.A. Kulkarni, P.P. Boix, E. Shi, A. Cao, K. Fu, S.K. Batabyal, J. Zhang, Q. Xiong, L.H. Wong, N. Mathews, S.G. Mhaisalkar, Laminated Carbon Nanotube Networks for Metal Electrode-Free Efficient Perovskite Solar Cells, ACS Nano. 8 (2014) 6797–6804. doi:10.1021/nn501096h.
[213] P. You, Z. Liu, Q. Tai, S. Liu, F. Yan, Efficient Semitransparent Perovskite Solar Cells with Graphene Electrodes, Adv. Mater. (2015) n/a-n/a. http://www.ncbi.nlm.nih.gov/pubmed/25969400 (accessed May 12, 2015).
[214] C. Liu, K. Wang, X. Gong, A.J. Heeger, Low bandgap semiconducting polymers for polymeric photovoltaics, Chem. Soc. Rev. 45 (2016) 4825–4846. doi:10.1039/C5CS00650C.
[215] K. Wang, C. Liu, T. Meng, C. Yi, X. Gong, Inverted organic photovoltaic cells, Chem. Soc. Rev. 45 (2016) 2937–2975. doi:10.1039/C5CS00831J.
[216] N.S. Sariciftci, L. Smilowitz, A.J. Heeger, F. Wudl, Photoinduced electron transfer from a conducting polymer to buckminsterfullerene., Science. 258 (1992) 1474–6. doi:10.1126/science.258.5087.1474.

[217] B. Kraabel, C.H. Lee, D. McBranch, D. Moses, N.S. Sariciftci, A.J. Heeger, Ultrafast photoinduced electron transfer in conducting polymer—buckminsterfullerene composites, Chem. Phys. Lett. 213 (1993) 389–394. doi:10.1016/0009-2614(93)85151-D.
[218] G. Yu, J. Gao, J.C. Hummelen, F. Wudl, A.J. Heeger, Polymer Photovoltaic Cells: Enhanced Efficiencies via a Network of Internal Donor-Acceptor Heterojunctions, Science (80-.). 270 (1995).
[219] G. Yu, A.J. Heeger, Charge separation and photovoltaic conversion in polymer composites with internal donor/acceptor heterojunctions, J. Appl. Phys. 78 (1995) 4510–4515. doi:10.1063/1.359792.
[220] A.J. Heeger, 25th Anniversary Article: Bulk Heterojunction Solar Cells: Understanding the Mechanism of Operation, Adv. Mater. 26 (2014) 10–28. doi:10.1002/adma.201304373.
[221] H.-Y. Chen, J. Hou, S. Zhang, Y. Liang, G. Yang, Y. Yang, L. Yu, Y. Wu, G. Li, Polymer solar cells with enhanced open-circuit voltage and efficiency, Nat. Photonics. 3 (2009) 649–653. doi:10.1038/nphoton.2009.192.
[222] M.-S. Su, C.-Y. Kuo, M.-C. Yuan, U.-S. Jeng, C.-J. Su, K.-H. Wei, Improving Device Efficiency of Polymer/Fullerene Bulk Heterojunction Solar Cells Through Enhanced Crystallinity and Reduced Grain Boundaries Induced by Solvent Additives, Adv. Mater. 23 (2011) 3315–3319. doi:10.1002/adma.201101274.
[223] G. Li, Y. Yao, H. Yang, V. Shrotriya, G. Yang, Y. Yang, "Solvent Annealing" Effect in Polymer Solar Cells Based on Poly(3-hexylthiophene) and Methanofullerenes, Adv. Funct. Mater. 17 (2007) 1636–1644. doi:10.1002/adfm.200600624.
[224] H. Zhou, Y. Zhang, J. Seifter, S.D. Collins, C. Luo, G.C. Bazan, T.-Q. Nguyen, A.J. Heeger, High-Efficiency Polymer Solar Cells Enhanced by Solvent Treatment, Adv. Mater. 25 (2013) 1646–1652. doi:10.1002/adma.201204306.
[225] Y. Yao, J. Hou, Z. Xu, G. Li, Y. Yang, Effects of Solvent Mixtures on the Nanoscale Phase Separation in Polymer Solar Cells, Adv. Funct. Mater. 18 (2008) 1783–1789. doi:10.1002/adfm.200701459.
[226] M. Al-Ibrahim, O. Ambacher, S. Sensfuss, G. Gobsch, Effects of solvent and annealing on the improved performance of solar cells based on poly(3-hexylthiophene): Fullerene, Appl. Phys. Lett. 86 (2005) 201120. doi:10.1063/1.1929875.
[227] X. Zhengguo, D. Qingfeng, B. Cheng, S. Yuchuan, Y. Yongbo, H. Jinsong, Solvent Annealing of Perovskite-Induced Crystal Growth for Photovoltaic-Device Efficiency Enhancement, Adv. Mater. 26 (2014) 6503–6509. doi:10.1002/adma.201401685.
[228] Z. Li, X. Xu, W. Zhang, X. Meng, W. Ma, A. Yartsev, O. Inganäs, M.R. Andersson, R.A.J. Janssen, E. Wang, High Performance All-Polymer Solar Cells by Synergistic Effects of Fine-Tuned Crystallinity and Solvent Annealing, J. Am. Chem. Soc. 138 (2016) 10935–10944. doi:10.1021/jacs.6b04822.
[229] Y. Kim, S.A. Choulis, J. Nelson, D.D.C. Bradley, S. Cook, J.R. Durrant, Device annealing effect in organic solar cells with blends of regioregular poly(3-hexylthiophene) and soluble fullerene, Appl. Phys. Lett. 86 (2005) 063502. doi:10.1063/1.1861123.
[230] G. Li, V. Shrotriya, Y. Yao, Y. Yang, Investigation of annealing effects and film thickness dependence of polymer solar cells based on poly(3-hexylthiophene), J. Appl. Phys. 98 (2005) 043704. doi:10.1063/1.2008386.
[231] G. Li, R. Zhu, Y. Yang, Polymer solar cells, Nat. Photonics. 6 (2012) 153–161. doi:10.1038/nphoton.2012.11.

[232] J. Peet, J.Y. Kim, N.E. Coates, W.L. Ma, D. Moses, A.J. Heeger, G.C. Bazan, Efficiency enhancement in low-bandgap polymer solar cells by processing with alkane dithiols, Nat. Mater. 6 (2007) 497–500. doi:10.1038/nmat1928.
[233] Y. KIM, S. COOK, S.M. TULADHAR, S.A. CHOULIS, J. NELSON, J.R. DURRANT, D.D.C. BRADLEY, M. GILES, I. MCCULLOCH, C.-S. HA, M. REE, A strong regioregularity effect in self-organizing conjugated polymer films and high-efficiency polythiophene: fullerene solar cells, in: Mater. Sustain. Energy, Co-Published with Macmillan Publishers Ltd, UK, 2010: pp. 63–69. doi:10.1142/9789814317665_0009.
[234] V. Dusastre, Materials for Sustainable Energy, Co-Published with Macmillan Publishers Ltd, UK, 2010. doi:10.1142/7848.
[235] F.C. Krebs, Fabrication and processing of polymer solar cells: A review of printing and coating techniques, Sol. Energy Mater. Sol. Cells. 93 (2009) 394–412. doi:10.1016/J.SOLMAT.2008.10.004.
[236] G. Zhao, Y. He, Y. Li, 6.5% Efficiency of Polymer Solar Cells Based on poly(3-hexylthiophene) and Indene-C60 Bisadduct by Device Optimization, Adv. Mater. 22 (2010) 4355–4358. doi:10.1002/adma.201001339.
[237] †,# Xiaoniu Yang, *,‡,§,# Joachim Loos, ⊥,# Sjoerd C. Veenstra, ⊥,# Wiljan J. H. Verhees, ∥,# Martijn M. Wienk, ⊥,# Jan M. Kroon, †,# and Matthias A. J. Michels, # René A. J. Janssen∥, Nanoscale Morphology of High-Performance Polymer Solar Cells, (2005). doi:10.1021/NL048120I.
[238] Y. Zheng, R. Wu, W. Shi, Z. Guan, J. Yu, Effect of in situ annealing on the performance of spray coated polymer solar cells, Sol. Energy Mater. Sol. Cells. 111 (2013) 200–205. doi:10.1016/J.SOLMAT.2013.01.011.
[239] K.-H. Ong, S.-L. Lim, H.-S. Tan, H.-K. Wong, J. Li, Z. Ma, L.C.H. Moh, S.-H. Lim, J.C. de Mello, Z.-K. Chen, A Versatile Low Bandgap Polymer for Air-Stable, High-Mobility Field-Effect Transistors and Efficient Polymer Solar Cells, Adv. Mater. 23 (2011) 1409–1413. doi:10.1002/adma.201003903.
[240] Y. Zhou, M. Eck, C. Veit, B. Zimmermann, F. Rauscher, P. Niyamakom, S. Yilmaz, I. Dumsch, S. Allard, U. Scherf, M. Krüger, Efficiency enhancement for bulk-heterojunction hybrid solar cells based on acid treated CdSe quantum dots and low bandgap polymer PCPDTBT, Sol. Energy Mater. Sol. Cells. 95 (2011) 1232–1237. doi:10.1016/J.SOLMAT.2010.12.041.
[241] J.-H. Im, C.-R. Lee, J.-W. Lee, S.-W. Park, N.-G. Park, 6.5% efficient perovskite quantum-dot-sensitized solar cell, Nanoscale. 3 (2011) 4088. doi:10.1039/c1nr10867k.
[242] H. Kim, W.-W. So, S.-J. Moon, The importance of post-annealing process in the device performance of poly(3-hexylthiophene): Methanofullerene polymer solar cell, Sol. Energy Mater. Sol. Cells. 91 (2007) 581–587. doi:10.1016/J.SOLMAT.2006.11.010.
[243] D. Chirvase, J. Parisi, J.C. Hummelen, V. Dyakonov, Influence of nanomorphology on the photovoltaic action of polymer–fullerene composites, Nanotechnology. 15 (2004) 1317–1323. doi:10.1088/0957-4484/15/9/035.
[244] S.S. van Bavel, M. Bärenklau, G. de With, H. Hoppe, J. Loos, P3HT/PCBM Bulk Heterojunction Solar Cells: Impact of Blend Composition and 3D Morphology on Device Performance, Adv. Funct. Mater. 20 (2010) 1458–1463. doi:10.1002/adfm.200902247.
[245] O. Inganäs, F. Zhang, K. Tvingstedt, L.M. Andersson, S. Hellström, M.R. Andersson, Polymer Photovoltaics with Alternating Copolymer/Fullerene Blends and Novel Device Architectures, Adv. Mater. 22 (2010) E100–E116. doi:10.1002/adma.200904407.

[246] Y. Huang, X. Guo, F. Liu, L. Huo, Y. Chen, T.P. Russell, C.C. Han, Y. Li, J. Hou, Improving the Ordering and Photovoltaic Properties by Extending π-Conjugated Area of Electron-Donating Units in Polymers with D-A Structure, Adv. Mater. 24 (2012) 3383–3389. doi:10.1002/adma.201200995.
[247] Y. Huang, L. Huo, S. Zhang, X. Guo, C.C. Han, Y. Li, J. Hou, Sulfonyl: a new application of electron-withdrawing substituent in highly efficient photovoltaic polymer, Chem. Commun. 47 (2011) 8904. doi:10.1039/c1cc12575c.
[248] H.-Y. Chen, S.-H. Lin, J.-Y. Sun, C.-H. Hsu, S. Lan, C.-F. Lin, Morphologic improvement of the PBDTTT-C and PC 71 BM blend film with mixed solvent for high-performance inverted polymer solar cells, Nanotechnology. 24 (2013) 484009. doi:10.1088/0957-4484/24/48/484009.
[249] C. Liu, X. Hu, C. Zhong, M. Huang, K. Wang, Z. Zhang, X. Gong, Y. Cao, A.J. Heeger, The influence of binary processing additives on the performance of polymer solar cells, Nanoscale. 6 (2014) 14297–14304. doi:10.1039/C4NR04958F.
[250] F. Wolfart, B.M. Hryniewicz, M.S. Góes, C.M. Corrêa, R. Torresi, M.A.O.S. Minadeo, S.I. Córdoba de Torresi, R.D. Oliveira, L.F. Marchesi, M. Vidotti, Conducting polymers revisited: applications in energy, electrochromism and molecular recognition, J. Solid State Electrochem. 21 (2017) 2489–2515. doi:10.1007/s10008-017-3556-9.
[251] J.T. Rogers, K. Schmidt, M.F. Toney, E.J. Kramer, G.C. Bazan, Structural Order in Bulk Heterojunction Films Prepared with Solvent Additives, Adv. Mater. 23 (2011) 2284–2288. doi:10.1002/adma.201003690.
[252] J. Hou, H.-Y. Chen, S. Zhang, G. Li, Y. Yang, Synthesis, Characterization, and Photovoltaic Properties of a Low Band Gap Polymer Based on Silole-Containing Polythiophenes and 2,1,3-Benzothiadiazole, J. Am. Chem. Soc. 130 (2008) 16144–16145. doi:10.1021/ja806687u.
[253] X. Guo, N. Zhou, S.J. Lou, J.W. Hennek, R. Ponce Ortiz, M.R. Butler, P.-L.T. Boudreault, J. Strzalka, P.-O. Morin, M. Leclerc, J.T. López Navarrete, M.A. Ratner, L.X. Chen, R.P.H. Chang, A. Facchetti, T.J. Marks, Bithiopheneimide–Dithienosilole/Dithienogermole Copolymers for Efficient Solar Cells: Information from Structure–Property–Device Performance Correlations and Comparison to Thieno[3,4-*c*]pyrrole-4,6-dione Analogues, J. Am. Chem. Soc. 134 (2012) 18427–18439. doi:10.1021/ja3081583.
[254] M. Morana, H. Azimi, G. Dennler, H.-J. Egelhaaf, M. Scharber, K. Forberich, J. Hauch, R. Gaudiana, D. Waller, Z. Zhu, K. Hingerl, S.S. van Bavel, J. Loos, C.J. Brabec, Nanomorphology and Charge Generation in Bulk Heterojunctions Based on Low-Bandgap Dithiophene Polymers with Different Bridging Atoms, Adv. Funct. Mater. 20 (2010) 1180–1188. doi:10.1002/adfm.200900931.
[255] H.-Y. Chen, J. Hou, A.E. Hayden, H. Yang, K.N. Houk, Y. Yang, Silicon Atom Substitution Enhances Interchain Packing in a Thiophene-Based Polymer System, Adv. Mater. 22 (2010) 371–375. doi:10.1002/adma.200902469.
[256] L. Dou, W.-H. Chang, J. Gao, C.-C. Chen, J. You, Y. Yang, A Selenium-Substituted Low-Bandgap Polymer with Versatile Photovoltaic Applications, Adv. Mater. 25 (2013) 825–831. doi:10.1002/adma.201203827.
[257] L. Huo, J. Hou, Benzo[1,2-b:4,5-b′]dithiophene-based conjugated polymers: band gap and energy level control and their application in polymer solar cells, Polym. Chem. 2 (2011) 2453. doi:10.1039/c1py00197c.

[258] Y. Lin, Y. Li, X. Zhan, Small molecule semiconductors for high-efficiency organic photovoltaics, Chem. Soc. Rev. 41 (2012) 4245. doi:10.1039/c2cs15313k.
[259] K.M. Coakley, M.D. Mcgehee, Conjugated Polymer Photovoltaic Cells, (2004). doi:10.1021/cm049654n.
[260] C. Yan, S. Barlow, Z. Wang, H. Yan, A.K.-Y. Jen, S.R. Marder, X. Zhan, Non-fullerene acceptors for organic solar cells, Nat. Rev. Mater. 3 (2018) 18003. doi:10.1038/natrevmats.2018.3.
[261] O.A. Abdulrazzaq, V. Saini, S. Bourdo, E. Dervishi, A.S. Biris, Organic Solar Cells: A Review of Materials, Limitations, and Possibilities for Improvement, Part. Sci. Technol. 31 (2013) 427–442. doi:10.1080/02726351.2013.769470.
[262] T.-H. Lai, S.-W. Tsang, J.R. Manders, S. Chen, F. So, Properties of interlayer for organic photovoltaics, Mater. Today. 16 (2013) 424–432. doi:10.1016/J.MATTOD.2013.10.001.
[263] L. Feng, M. Niu, Z. Wen, X. Hao, L. Feng, M. Niu, Z. Wen, X. Hao, Recent Advances of Plasmonic Organic Solar Cells: Photophysical Investigations, Polymers (Basel). 10 (2018) 123. doi:10.3390/polym10020123.
[264] I. Vangelidis, A. Theodosi, M.J. Beliatis, K.K. Gandhi, A. Laskarakis, P. Patsalas, S. Logothetidis, S.R.P. Silva, E. Lidorikis, Plasmonic Organic Photovoltaics: Unraveling Plasmonic Enhancement for Realistic Cell Geometries, ACS Photonics. 5 (2018) 1440–1452. doi:10.1021/acsphotonics.7b01390.
[265] X.Y. and, ‡ Joachim Loos*, Toward High-Performance Polymer Solar Cells: The Importance of Morphology Control, (2007). doi:10.1021/MA0618732.
[266] W. Ma, C. Yang, X. Gong, K. Lee, A.J. Heeger, Thermally Stable, Efficient Polymer Solar Cells with Nanoscale Control of the Interpenetrating Network Morphology, Adv. Funct. Mater. 15 (2005) 1617–1622. doi:10.1002/adfm.200500211.
[267] M. Krzywiecki, L. Grządziel, A. Sarfraz, D. Iqbal, A. Szwajca, A. Erbe, Zinc oxide as a defect-dominated material in thin films for photovoltaic applications – experimental determination of defect levels, quantification of composition, and construction of band diagram, Phys. Chem. Chem. Phys. 17 (2015) 10004–10013. doi:10.1039/C5CP00112A.
[268] S. Chen, C.E. Small, C.M. Amb, J. Subbiah, T. Lai, S.-W. Tsang, J.R. Manders, J.R. Reynolds, F. So, Inverted Polymer Solar Cells with Reduced Interface Recombination, Adv. Energy Mater. 2 (2012) 1333–1337. doi:10.1002/aenm.201200184.
[269] M. Hartel, S. Chen, B. Swerdlow, H.-Y. Hsu, J. Manders, K. Schanze, F. So, Defect-Induced Loss Mechanisms in Polymer–Inorganic Planar Heterojunction Solar Cells, ACS Appl. Mater. Interfaces. 5 (2013) 7215–7218. doi:10.1021/am4015605.
[270] T. Stubhan, M. Salinas, A. Ebel, F.C. Krebs, A. Hirsch, M. Halik, C.J. Brabec, Increasing the Fill Factor of Inverted P3HT:PCBM Solar Cells Through Surface Modification of Al-Doped ZnO via Phosphonic Acid-Anchored C60 SAMs, Adv. Energy Mater. 2 (2012) 532–535. doi:10.1002/aenm.201100668.
[271] Z. Lin, J. Chang, C. Zhang, J. Zhang, J. Wu, Y. Hao, Low temperature aqueous solution-processed Li doped ZnO buffer layers for high performance inverted organic solar cells, J. Mater. Chem. C. 4 (2016) 6169–6175. doi:10.1039/C6TC00760K.
[272] Z. Yin, Q. Zheng, S.-C. Chen, D. Cai, Y. Ma, Controllable ZnMgO Electron-Transporting Layers for Long-Term Stable Organic Solar Cells with 8.06% Efficiency after One-Year Storage, Adv. Energy Mater. 6 (2016) 1501493. doi:10.1002/aenm.201501493.
[273] K.-S. Shin, K.-H. Lee, H.H. Lee, D. Choi, S.-W. Kim, Enhanced Power Conversion Efficiency of Inverted Organic Solar Cells with a Ga-Doped ZnO Nanostructured Thin

Film Prepared Using Aqueous Solution, J. Phys. Chem. C. 114 (2010) 15782–15785. doi:10.1021/jp1013658.
[274] J. Wei, Z. Yin, S.-C. Chen, Q. Zheng, Low-Temperature Solution-Processed Zinc Tin Oxide Film as a Cathode Interlayer for Organic Solar Cells, ACS Appl. Mater. Interfaces. 9 (2017) 6186–6193. doi:10.1021/acsami.6b13724.
[275] X. Zhou, X. Fan, X. Sun, Y. Zhang, Z. Zhu, Enhanced efficiency of inverted polymer solar cells by using solution-processed TiOx/CsOx cathode buffer layer, Nanoscale Res. Lett. 10 (2015) 29. doi:10.1186/s11671-015-0754-1.
[276] Z. Ma, Z. Tang, E. Wang, M.R. Andersson, O. Inganäs, F. Zhang, Influences of Surface Roughness of ZnO Electron Transport Layer on the Photovoltaic Performance of Organic Inverted Solar Cells, J. Phys. Chem. C. 116 (2012) 24462–24468. doi:10.1021/jp308480u.
[277] Frank Verbakel, * and Stefan C. J. Meskers, R.A.J. Janssen, Surface Modification of Zinc Oxide Nanoparticles Influences the Electronic Memory Effects in ZnO−Polystyrene Diodes, (2007). doi:10.1021/JP072999J.
[278] I. Jeon, J.W. Ryan, T. Nakazaki, K.S. Yeo, Y. Negishi, Y. Matsuo, Air-processed inverted organic solar cells utilizing a 2-aminoethanol-stabilized ZnO nanoparticle electron transport layer that requires no thermal annealing, J. Mater. Chem. A. 2 (2014) 18754–18760. doi:10.1039/C4TA04595E.
[279] S. Suresh, P. Saravanan, K. Jayamoorthy, S. Ananda Kumar, S. Karthikeyan, Development of silane grafted ZnO core shell nanoparticles loaded diglycidyl epoxy nanocomposites film for antimicrobial applications, Mater. Sci. Eng. C. 64 (2016) 286–292. doi:10.1016/J.MSEC.2016.03.096.
[280] C.E. Small, S. Chen, J. Subbiah, C.M. Amb, S.-W. Tsang, T.-H. Lai, J.R. Reynolds, F. So, High-efficiency inverted dithienogermole–thienopyrrolodione-based polymer solar cells, Nat. Photonics. 6 (2012) 115–120. doi:10.1038/nphoton.2011.317.
[281] P. Li, T. Jiu, G. Tang, G. Wang, J. Li, X. Li, J. Fang, Solvents Induced ZnO Nanoparticles Aggregation Associated with Their Interfacial Effect on Organic Solar Cells, ACS Appl. Mater. Interfaces. 6 (2014) 18172–18179. doi:10.1021/am5051789.
[282] H.-Q. Shi, W.-N. Li, L.-W. Sun, Y. Liu, H.-M. Xiao, S.-Y. Fu, Synthesis of silane surface modified ZnO quantum dots with ultrastable, strong and tunable luminescence, Chem. Commun. 47 (2011) 11921. doi:10.1039/c1cc15411g.
[283] K. Wang, C. Liu, T. Meng, C. Yi, X. Gong, Inverted organic photovoltaic cells, Chem. Soc. Rev. 45 (2016) 2937. doi:10.1039/c5cs00831j.
[284] I. Litzov, C.J. Brabec, Development of Efficient and Stable Inverted Bulk Heterojunction (BHJ) Solar Cells Using Different Metal Oxide Interfaces, Materials (Basel). 6 (2013) 5796–5820. doi:10.3390/ma6125796.
[285] D. Zhang, W.C.H. Choy, F. Xie, W.E.I. Sha, X. Li, B. Ding, K. Zhang, F. Huang, Y. Cao, Plasmonic Electrically Functionalized TiO 2 for High-Performance Organic Solar Cells, Adv. Funct. Mater. 23 (2013) 4255–4261. doi:10.1002/adfm.201203776.
[286] E. Berner, T. Jäger, T. Lanz, F. Nüesch, J.-N. Tisserant, G. Wicht, H. Zhang, R. Hany, Influence of crystalline titanium oxide layer smoothness on the performance of inverted organic bilayer solar cells, Appl. Phys. Lett. 102 (2013) 183903. doi:10.1063/1.4804599.
[287] H. Oh, J. Krantz, I. Litzov, T. Stubhan, L. Pinna, C.J. Brabec, Comparison of various sol–gel derived metal oxide layers for inverted organic solar cells, Sol. Energy Mater. Sol. Cells. 95 (2011) 2194–2199. doi:10.1016/J.SOLMAT.2011.03.023.
[288] T. Kuwabara, T. Nakayama, K. Uozumi, T. Yamaguchi, K. Takahashi, Highly durable

inverted-type organic solar cell using amorphous titanium oxide as electron collection electrode inserted between ITO and organic layer, Sol. Energy Mater. Sol. Cells. 92 (2008) 1476–1482. doi:10.1016/J.SOLMAT.2008.06.012.
[289] T. Kuwabara, H. Sugiyama, T. Yamaguchi, K. Takahashi, Inverted type bulk-heterojunction organic solar cell using electrodeposited titanium oxide thin films as electron collector electrode, Thin Solid Films. 517 (2009) 3766–3769. doi:10.1016/J.TSF.2008.12.039.
[290] H. Sun, J. Weickert, H.C. Hesse, L. Schmidt-Mende, UV light protection through TiO2 blocking layers for inverted organic solar cells, Sol. Energy Mater. Sol. Cells. 95 (2011) 3450–3454. doi:10.1016/J.SOLMAT.2011.08.004.
[291] D. Yang, P. Fu, F. Zhang, N. Wang, J. Zhang, C. Li, High efficiency inverted polymer solar cells with room-temperature titanium oxide/polyethylenimine films as electron transport layers, J. Mater. Chem. A. 2 (2014) 17281–17285. doi:10.1039/C4TA03838J.
[292] S.K. Hau, H.-L. Yip, N.S. Baek, J. Zou, K. O'Malley, A.K.-Y. Jen, Air-stable inverted flexible polymer solar cells using zinc oxide nanoparticles as an electron selective layer, Appl. Phys. Lett. 92 (2008) 253301. doi:10.1063/1.2945281.
[293] A.K.K. Kyaw, X.W. Sun, C.Y. Jiang, Efficient charge collection with sol–gel derived colloidal ZnO thin film in photovoltaic devices, J. Sol-Gel Sci. Technol. 52 (2009) 348–355. doi:10.1007/s10971-009-2048-5.
[294] T. Stubhan, H. Oh, L. Pinna, J. Krantz, I. Litzov, C.J. Brabec, Inverted organic solar cells using a solution processed aluminum-doped zinc oxide buffer layer, Org. Electron. 12 (2011) 1539–1543. doi:10.1016/J.ORGEL.2011.05.027.
[295] F.C. Krebs, S.A. Gevorgyan, J. Alstrup, A roll-to-roll process to flexible polymer solar cells: model studies, manufacture and operational stability studies, J. Mater. Chem. 19 (2009) 5442. doi:10.1039/b823001c.
[296] M.S. White, D.C. Olson, S.E. Shaheen, N. Kopidakis, D.S. Ginley, Inverted bulk-heterojunction organic photovoltaic device using a solution-derived ZnO underlayer, Appl. Phys. Lett. 89 (2006) 143517. doi:10.1063/1.2359579.
[297] A.K.K. Kyaw, X.W. Sun, C.Y. Jiang, G.Q. Lo, D.W. Zhao, D.L. Kwong, An inverted organic solar cell employing a sol-gel derived ZnO electron selective layer and thermal evaporated MoO3 hole selective layer, Appl. Phys. Lett. 93 (2008) 221107. doi:10.1063/1.3039076.
[298] X. Gong, Toward high performance inverted polymer solar cells, Polymer (Guildf). 53 (2012) 5437–5448. doi:10.1016/J.POLYMER.2012.09.023.
[299] B. Pradhan, S. Albrecht, B. Stiller, D. Neher, Inverted organic solar cells comprising low-temperature-processed ZnO films, Appl. Phys. A. 115 (2014) 365–369. doi:10.1007/s00339-014-8373-8.
[300] J.-C. Wang, W.-T. Weng, M.-Y. Tsai, M.-K. Lee, S.-F. Horng, T.-P. Perng, C.-C. Kei, C.-C. Yu, H.-F. Meng, Highly efficient flexible inverted organic solar cells using atomic layer deposited ZnO as electron selective layer, J. Mater. Chem. 20 (2010) 862–866. doi:10.1039/B921396A.
[301] H. Cheun, C. Fuentes-Hernandez, Y. Zhou, W.J. Potscavage, S.-J. Kim, J. Shim, A. Dindar, B. Kippelen, Electrical and Optical Properties of ZnO Processed by Atomic Layer Deposition in Inverted Polymer Solar Cells, J. Phys. Chem. C. 114 (2010) 20713–20718. doi:10.1021/jp106641j.
[302] C.-Y. Chang, F.-Y. Tsai, Efficient and air-stable plastics-based polymer solar cells

enabled by atomic layer deposition, J. Mater. Chem. 21 (2011) 5710. doi:10.1039/c0jm04066e.
[303] R.L.Z. Hoye, D. Muñoz-Rojas, D.C. Iza, K.P. Musselman, J.L. MacManus-Driscoll, High performance inverted bulk heterojunction solar cells by incorporation of dense, thin ZnO layers made using atmospheric atomic layer deposition, Sol. Energy Mater. Sol. Cells. 116 (2013) 197–202. doi:10.1016/J.SOLMAT.2013.04.020.
[304] M. Scharrer, X. Wu, A. Yamilov, H. Cao, R.P.H. Chang, Fabrication of inverted opal ZnO photonic crystals by atomic layer deposition, Appl. Phys. Lett. 86 (2005) 151113. doi:10.1063/1.1900957.
[305] M. Eita, A. El Labban, F. Cruciani, A. Usman, P.M. Beaujuge, O.F. Mohammed, Ambient Layer-by-Layer ZnO Assembly for Highly Efficient Polymer Bulk Heterojunction Solar Cells, Adv. Funct. Mater. 25 (2015) 1558–1564. doi:10.1002/adfm.201402637.
[306] L. Zuo, S. Zhang, S. Dai, H. Chen, Versatility and robustness of ZnO:Cs electron transporting layer for printable organic solar cells, RSC Adv. 5 (2015) 49369–49375. doi:10.1039/C5RA08441E.
[307] T.M. Brown, R.H. Friend, I.S. Millard, D.J. Lacey, J.H. Burroughes, F. Cacialli, LiF/Al cathodes and the effect of LiF thickness on the device characteristics and built-in potential of polymer light-emitting diodes, Appl. Phys. Lett. 77 (2000) 3096. doi:10.1063/1.1323741.
[308] C.J. Brabec, S.E. Shaheen, C. Winder, N.S. Sariciftci, P. Denk, Effect of LiF/metal electrodes on the performance of plastic solar cells, Appl. Phys. Lett. 80 (2002) 1288–1290. doi:10.1063/1.1446988.
[309] Y.D. Jin, X.B. Ding, J. Reynaert, V.I. Arkhipov, G. Borghs, P.L. Heremans, M. Van der Auweraer, Role of LiF in polymer light-emitting diodes with LiF-modified cathodes, Org. Electron. 5 (2004) 271–281. doi:10.1016/J.ORGEL.2004.08.001.
[310] F. Bruder, R. Brenn, Photoelectron Spectroscopy of the Contact between the Cathode and the Active Layers in Plastic Solar Cells: The Role of LiF Related content Surface Phase Transition in a Polymer Blend, Japanese J. Appl. Phys. To. 44 (2005) 3695. doi:10.1143/JJAP.44.3695.
[311] B.N. Limketkai, M.A. Baldo, Charge injection into cathode-doped amorphous organic semiconductors, (n.d.). doi:10.1103/PhysRevB.71.085207.
[312] G. Li, C.-W. Chu, V. Shrotriya, J. Huang, Y. Yang, Efficient inverted polymer solar cells, Appl. Phys. Lett. 88 (2006) 253503. doi:10.1063/1.2212270.
[313] H.-H. Liao, L.-M. Chen, Z. Xu, G. Li, Y. Yang, Highly efficient inverted polymer solar cell by low temperature annealing of Cs2CO3 interlayer, Appl. Phys. Lett. 92 (2008) 173303. doi:10.1063/1.2918983.
[314] D.W. Zhao, P. Liu, X.W. Sun, S.T. Tan, L. Ke, A.K.K. Kyaw, An inverted organic solar cell with an ultrathin Ca electron-transporting layer and MoO3 hole-transporting layer, Appl. Phys. Lett. 95 (2009) 153304. doi:10.1063/1.3250176.
[315] W. Qiu, A. Hadipour, R. Müller, B. Conings, H.-G. Boyen, P. Heremans, L. Froyen, Ultrathin Ammonium Heptamolybdate Films as Efficient Room-Temperature Hole Transport Layers for Organic Solar Cells, ACS Appl. Mater. Interfaces. 6 (2014) 16335–16343. doi:10.1021/am504606u.
[316] Z. Liu, X. Ouyang, R. Peng, Y. Bai, D. Mi, W. Jiang, A. Facchetti, Z. Ge, Efficient polymer solar cells based on the synergy effect of a novel non-conjugated small-molecule electrolyte and polar solvent, J. Mater. Chem. A. 4 (2016) 2530–2536.

doi:10.1039/C5TA10083F.
[317] Y. Zhou, C. Fuentes-Hernandez, J. Shim, J. Meyer, A.J. Giordano, H. Li, P. Winget, T. Papadopoulos, H. Cheun, J. Kim, M. Fenoll, A. Dindar, W. Haske, E. Najafabadi, T.M. Khan, H. Sojoudi, S. Barlow, S. Graham, J.-L. Brédas, S.R. Marder, A. Kahn, B. Kippelen, A universal method to produce low-work function electrodes for organic electronics., Science. 336 (2012) 327–32. doi:10.1126/science.1218829.
[318] H. Kang, S. Hong, J. Lee, K. Lee, Electrostatically Self-Assembled Nonconjugated Polyelectrolytes as an Ideal Interfacial Layer for Inverted Polymer Solar Cells, Adv. Mater. 24 (2012) 3005–3009. doi:10.1002/adma.201200594.
[319] J.W. Shim, H. Cheun, J. Meyer, C. Fuentes-Hernandez, A. Dindar, Y.H. Zhou, D.K. Hwang, A. Kahn, B. Kippelen, Polyvinylpyrrolidone-modified indium tin oxide as an electron-collecting electrode for inverted polymer solar cells, Appl. Phys. Lett. 101 (2012) 073303. doi:10.1063/1.4745772.
[320] B. Xiao, H. Wu, Y. Cao, Solution-processed cathode interfacial layer materials for high-efficiency polymer solar cells, Mater. Today. 18 (2015) 385–394. doi:10.1016/J.MATTOD.2015.02.016.
[321] S.-H. Liao, Y.-L. Li, T.-H. Jen, Y.-S. Cheng, S.-A. Chen, Multiple Functionalities of Polyfluorene Grafted with Metal Ion-Intercalated Crown Ether as an Electron Transport Layer for Bulk-Heterojunction Polymer Solar Cells: Optical Interference, Hole Blocking, Interfacial Dipole, and Electron Conduction, J. Am. Chem. Soc. 134 (2012) 14271–14274. doi:10.1021/ja303813s.
[322] J.H. Seo, A. Gutacker, Y. Sun, H. Wu, F. Huang, Y. Cao, U. Scherf, A.J. Heeger, G.C. Bazan, Improved High-Efficiency Organic Solar Cells via Incorporation of a Conjugated Polyelectrolyte Interlayer, J. Am. Chem. Soc. 133 (2011) 8416–8419. doi:10.1021/ja2037673.
[323] Z. He, C. Zhang, X. Xu, L. Zhang, L. Huang, J. Chen, H. Wu, Y. Cao, Largely Enhanced Efficiency with a PFN/Al Bilayer Cathode in High Efficiency Bulk Heterojunction Photovoltaic Cells with a Low Bandgap Polycarbazole Donor, Adv. Mater. 23 (2011) 3086–3089. doi:10.1002/adma.201101319.
[324] Y. Yuan, T.J. Reece, P. Sharma, S. Poddar, S. Ducharme, A. Gruverman, Y. Yang, J. Huang, Efficiency enhancement in organic solar cells with ferroelectric polymers, Nat. Mater. 10 (2011) 296–302. doi:10.1038/nmat2951.
[325] H.-L. Yip, S.K. Hau, N.S. Baek, H. Ma, A.K.-Y. Jen, Polymer Solar Cells That Use Self-Assembled-Monolayer- Modified ZnO/Metals as Cathodes, Adv. Mater. 20 (2008) 2376–2382. doi:10.1002/adma.200703050.
[326] S.-H. Oh, S.-I. Na, J. Jo, B. Lim, D. Vak, D.-Y. Kim, Water-Soluble Polyfluorenes as an Interfacial Layer Leading to Cathode-Independent High Performance of Organic Solar Cells, Adv. Funct. Mater. 20 (2010) 1977–1983. doi:10.1002/adfm.200902386.
[327] Q. Wei, T. Nishizawa, K. Tajima, K. Hashimoto, Self-Organized Buffer Layers in Organic Solar Cells, Adv. Mater. 20 (2008) 2211–2216. doi:10.1002/adma.200792876.
[328] Y. Zhao, Z. Xie, C. Qin, Y. Qu, Y. Geng, L. Wang, Enhanced charge collection in polymer photovoltaic cells by using an ethanol-soluble conjugated polyfluorene as cathode buffer layer, Sol. Energy Mater. Sol. Cells. 93 (2009) 604–608. doi:10.1016/J.SOLMAT.2008.12.007.
[329] Enhanced open-circuit voltage in polymer solar cells, Appl. Phys. Lett. 95 (2009) 043301. doi:10.1063/1.3157278.

[330] L. Zuo, X. Jiang, M. Xu, L. Yang, Y. Nan, Q. Yan, H. Chen, Enhancement of short current density in polymer solar cells with phthalocyanine tin (IV) dichloride as interfacial layer, Sol. Energy Mater. Sol. Cells. 95 (2011) 2664–2669. doi:10.1016/J.SOLMAT.2011.05.038.
[331] K. Yao, L. Chen, Y. Chen, F. Li, P. Wang, Influence of water-soluble polythiophene as an interfacial layer on the P3HT/PCBM bulk heterojunction organic photovoltaics, J. Mater. Chem. 21 (2011) 13780. doi:10.1039/c1jm12016f.
[332] Y. Dong, X. Hu, C. Duan, P. Liu, S. Liu, L. Lan, D. Chen, L. Ying, S. Su, X. Gong, F. Huang, Y. Cao, A Series of New Medium-Bandgap Conjugated Polymers Based on Naphtho[1,2-c:5,6-c]bis(2-octyl-[1,2,3]triazole) for High-Performance Polymer Solar Cells, Adv. Mater. 25 (2013) 3683–3688. doi:10.1002/adma.201301547.
[333] J. Sun, Y. Zhu, X. Xu, L. Lan, L. Zhang, P. Cai, J. Chen, J. Peng, Y. Cao, High Efficiency and High V_{oc} Inverted Polymer Solar Cells Based on a Low-Lying HOMO Polycarbazole Donor and a Hydrophilic Polycarbazole Interlayer on ITO Cathode, J. Phys. Chem. C. 116 (2012) 14188–14198. doi:10.1021/jp3009546.
[334] B.J. Worfolk, T.C. Hauger, K.D. Harris, D.A. Rider, J.A.M. Fordyce, S. Beaupré, M. Leclerc, J.M. Buriak, Work Function Control of Interfacial Buffer Layers for Efficient and Air-Stable Inverted Low-Bandgap Organic Photovoltaics, Adv. Energy Mater. 2 (2012) 361–368. doi:10.1002/aenm.201100714.
[335] Y. Zhu, X. Xu, L. Zhang, J. Chen, Y. Cao, High efficiency inverted polymeric bulk-heterojunction solar cells with hydrophilic conjugated polymers as cathode interlayer on ITO, Sol. Energy Mater. Sol. Cells. 97 (2012) 83–88. doi:10.1016/J.SOLMAT.2011.09.030.
[336] K. Zilberberg, A. Behrendt, M. Kraft, U. Scherf, T. Riedl, Ultrathin interlayers of a conjugated polyelectrolyte for low work-function cathodes in efficient inverted organic solar cells, Org. Electron. 14 (2013) 951–957. doi:10.1016/J.ORGEL.2013.01.018.
[337] Q. Chen, B.J. Worfolk, T.C. Hauger, U. Al-Atar, K.D. Harris, J.M. Buriak, Finely Tailored Performance of Inverted Organic Photovoltaics through Layer-by-Layer Interfacial Engineering, ACS Appl. Mater. Interfaces. 3 (2011) 3962–3970. doi:10.1021/am200849r.
[338] J. Liu, M. Durstock, L. Dai, Graphene oxide derivatives as hole- and electron-extraction layers for high-performance polymer solar cells, Energy Environ. Sci. 7 (2014) 1297–1306. doi:10.1039/C3EE42963F.
[339] M. Jørgensen, K. Norrman, F.C. Krebs, Stability/degradation of polymer solar cells, Sol. Energy Mater. Sol. Cells. 92 (2008) 686–714. doi:10.1016/J.SOLMAT.2008.01.005.
[340] K. Wang, C. Yi, X. Hu, C. Liu, Y. Sun, J. Hou, Y. Li, J. Zheng, S. Chuang, A. Karim, X. Gong, Enhanced Performance of Polymer Solar Cells using PEDOT:PSS Doped with Fe_3O_4 Magnetic Nanoparticles Aligned by an External Magnetostatic Field as an Anode Buffer Layer, ACS Appl. Mater. Interfaces. 6 (2014) 13201–13208. doi:10.1021/am503041g.
[341] K. Wang, H. Ren, C. Yi, C. Liu, H. Wang, L. Huang, H. Zhang, A. Karim, X. Gong, Solution-Processed Fe_3O_4 Magnetic Nanoparticle Thin Film Aligned by an External Magnetostatic Field as a Hole Extraction Layer for Polymer Solar Cells, ACS Appl. Mater. Interfaces. 5 (2013) 10325–10330. doi:10.1021/am4033179.
[342] L. Dai, Functionalization of Graphene for Efficient Energy Conversion and Storage, Acc. Chem. Res. 46 (2013) 31–42. doi:10.1021/ar300122m.

[343] S.-S. Li, K.-H. Tu, C.-C. Lin, C.-W. Chen, M. Chhowalla, Solution-Processable Graphene Oxide as an Efficient Hole Transport Layer in Polymer Solar Cells, ACS Nano. 4 (2010) 3169–3174. doi:10.1021/nn100551j.
[344] M. Jørgensen, K. Norrman, S.A. Gevorgyan, T. Tromholt, B. Andreasen, F.C. Krebs, Stability of Polymer Solar Cells, Adv. Mater. 24 (2012) 580–612. doi:10.1002/adma.201104187.
[345] J. Liu, Y. Xue, L. Dai, Sulfated Graphene Oxide as a Hole-Extraction Layer in High-Performance Polymer Solar Cells, J. Phys. Chem. Lett. 3 (2012) 1928–1933. doi:10.1021/jz300723h.
[346] J.-M. Yun, J.-S. Yeo, J. Kim, H.-G. Jeong, D.-Y. Kim, Y.-J. Noh, S.-S. Kim, B.-C. Ku, S.-I. Na, Solution-Processable Reduced Graphene Oxide as a Novel Alternative to PEDOT:PSS Hole Transport Layers for Highly Efficient and Stable Polymer Solar Cells, Adv. Mater. 23 (2011) 4923–4928. doi:10.1002/adma.201102207.
[347] X. Liu, H. Kim, L.J. Guo, Optimization of thermally reduced graphene oxide for an efficient hole transport layer in polymer solar cells, Org. Electron. 14 (2013) 591–598. doi:10.1016/J.ORGEL.2012.11.020.
[348] Y.-J. Jeon, J.-M. Yun, D.-Y. Kim, S.-I. Na, S.-S. Kim, High-performance polymer solar cells with moderately reduced graphene oxide as an efficient hole transporting layer, Sol. Energy Mater. Sol. Cells. 105 (2012) 96–102. doi:10.1016/J.SOLMAT.2012.05.024.
[349] J. Kim, V.C. Tung, J. Huang, Water Processable Graphene Oxide:Single Walled Carbon Nanotube Composite as Anode Modifier for Polymer Solar Cells, Adv. Energy Mater. 1 (2011) 1052–1057. doi:10.1002/aenm.201100466.
[350] I.P. Murray, S.J. Lou, L.J. Cote, S. Loser, C.J. Kadleck, T. Xu, J.M. Szarko, B.S. Rolczynski, J.E. Johns, J. Huang, L. Yu, L.X. Chen, T.J. Marks, M.C. Hersam, Graphene Oxide Interlayers for Robust, High-Efficiency Organic Photovoltaics, J. Phys. Chem. Lett. 2 (2011) 3006–3012. doi:10.1021/jz201493d.
[351] E. Stratakis, K. Savva, D. Konios, C. Petridis, E. Kymakis, Improving the efficiency of organic photovoltaics by tuning the work function of graphene oxide hole transporting layers, Nanoscale. 6 (2014) 6925–6931. doi:10.1039/C4NR01539H.
[352] D. Yang, L. Zhou, W. Yu, J. Zhang, C. Li, Work-Function-Tunable Chlorinated Graphene Oxide as an Anode Interface Layer in High-Efficiency Polymer Solar Cells, Adv. Energy Mater. 4 (2014) 1400591. doi:10.1002/aenm.201400591.
[353] V.C. Tung, J. Kim, L.J. Cote, J. Huang, Sticky Interconnect for Solution-Processed Tandem Solar Cells, J. Am. Chem. Soc. 133 (2011) 9262–9265. doi:10.1021/ja203464n.
[354] G.-Q. Fan, Q.-Q. Zhuo, J.-J. Zhu, Z.-Q. Xu, P.-P. Cheng, Y.-Q. Li, X.-H. Sun, S.-T. Lee, J.-X. Tang, Plasmonic-enhanced polymer solar cells incorporating solution-processable Au nanoparticle-adhered graphene oxide, J. Mater. Chem. 22 (2012) 15614. doi:10.1039/c2jm31878d.
[355] B. Yin, Q. Liu, L. Yang, X. Wu, Z. Liu, Y. Hua, S. Yin, Y. Chen, Buffer Layer of PEDOT:PSS/Graphene Composite for Polymer Solar Cells, J. Nanosci. Nanotechnol. 10 (2010) 1934–1938. doi:10.1166/jnn.2010.2107.
[356] Y.-H. Chao, J.-S. Wu, C.-E. Wu, J.-F. Jheng, C.-L. Wang, C.-S. Hsu, Solution-Processed (Graphene Oxide)-(d^0 Transition Metal Oxide) Composite Anodic Buffer Layers toward High-Performance and Durable Inverted Polymer Solar Cells, Adv. Energy Mater. 3 (2013) 1279–1285. doi:10.1002/aenm.201300430.
[357] J. Liu, Y. Xue, Y. Gao, D. Yu, M. Durstock, L. Dai, Hole and Electron Extraction Layers

Based on Graphene Oxide Derivatives for High-Performance Bulk Heterojunction Solar Cells, Adv. Mater. 24 (2012) 2228–2233. doi:10.1002/adma.201104945.
[358] S. Qu, M. Li, L. Xie, X. Huang, J. Yang, N. Wang, S. Yang, Noncovalent Functionalization of Graphene Attaching [6,6]-Phenyl-C61-butyric Acid Methyl Ester (PCBM) and Application as Electron Extraction Layer of Polymer Solar Cells, ACS Nano. 7 (2013) 4070–4081. doi:10.1021/nn4001963.
[359] D.H. Wang, J.K. Kim, J.H. Seo, I. Park, B.H. Hong, J.H. Park, A.J. Heeger, Transferable Graphene Oxide by Stamping Nanotechnology: Electron-Transport Layer for Efficient Bulk-Heterojunction Solar Cells, Angew. Chemie. 125 (2013) 2946–2952. doi:10.1002/ange.201209999.
[360] S. Rühle, Tabulated values of the Shockley–Queisser limit for single junction solar cells, Sol. Energy. 130 (2016) 139–147. doi:10.1016/J.SOLENER.2016.02.015.
[361] M.A. Green, Y. Hishikawa, E.D. Dunlop, D.H. Levi, J. Hohl-Ebinger, A.W.Y. Ho-Baillie, Solar cell efficiency tables (version 51), Prog. Photovoltaics Res. Appl. 26 (2018) 3–12. doi:10.1002/pip.2978.
[362] S.K. Hau, H.-L. Yip, A.K.-Y. Jen, A Review on the Development of the Inverted Polymer Solar Cell Architecture, Polym. Rev. 50 (2010) 474–510. doi:10.1080/15583724.2010.515764.
[363] Y. Liu, J. Zhao, Z. Li, C. Mu, W. Ma, H. Hu, K. Jiang, H. Lin, H. Ade, H. Yan, Aggregation and morphology control enables multiple cases of high-efficiency polymer solar cells, Nat. Commun. 5 (2014) 5293. doi:10.1038/ncomms6293.
[364] L.-M. Chen, Z. Hong, G. Li, Y. Yang, Recent Progress in Polymer Solar Cells: Manipulation of Polymer:Fullerene Morphology and the Formation of Efficient Inverted Polymer Solar Cells, Adv. Mater. 21 (2009) 1434–1449. doi:10.1002/adma.200802854.
[365] M.A. Green, Y. Hishikawa, E.D. Dunlop, D.H. Levi, J. Hohl-Ebinger, A.W.Y. Ho-Baillie, Solar cell efficiency tables (version 52), Prog. Photovoltaics Res. Appl. 26 (2018) 427–436. doi:10.1002/pip.3040.
[366] Y. Chen, X. Wan, G. Long, High Performance Photovoltaic Applications Using Solution-Processed Small Molecules, Acc. Chem. Res. 46 (2013) 2645–2655. doi:10.1021/ar400088c.
[367] J.E. Coughlin, Z.B. Henson, G.C. Welch, G.C. Bazan, Design and Synthesis of Molecular Donors for Solution-Processed High-Efficiency Organic Solar Cells, Acc. Chem. Res. 47 (2014) 257–270. doi:10.1021/ar400136b.
[368] Y. Sun, G.C. Welch, W.L. Leong, C.J. Takacs, G.C. Bazan, A.J. Heeger, Solution-processed small-molecule solar cells with 6.7% efficiency, Nat. Mater. 11 (2012) 44–48. doi:10.1038/nmat3160.
[369] K. Sun, Z. Xiao, S. Lu, W. Zajaczkowski, W. Pisula, E. Hanssen, J.M. White, R.M. Williamson, J. Subbiah, J. Ouyang, A.B. Holmes, W.W.H. Wong, D.J. Jones, A molecular nematic liquid crystalline material for high-performance organic photovoltaics, Nat. Commun. 6 (2015) 6013. doi:10.1038/ncomms7013.
[370] Q. Zhang, B. Kan, F. Liu, G. Long, X. Wan, X. Chen, Y. Zuo, W. Ni, H. Zhang, M. Li, Z. Hu, F. Huang, Y. Cao, Z. Liang, M. Zhang, T.P. Russell, Y. Chen, Small-molecule solar cells with efficiency over 9%, Nat. Photonics. 9 (2015) 35–41. doi:10.1038/nphoton.2014.269.
[371] B. Kan, Q. Zhang, M. Li, X. Wan, W. Ni, G. Long, Y. Wang, X. Yang, H. Feng, Y. Chen, Solution-Processed Organic Solar Cells Based on Dialkylthiol-Substituted

Benzodithiophene Unit with Efficiency near 10%, J. Am. Chem. Soc. 136 (2014) 15529–15532. doi:10.1021/ja509703k.
[372] H. Fan, X. Zhu, Development of small-molecule materials for high-performance organic solar cells, Sci. China Chem. 58 (2015) 922–936. doi:10.1007/s11426-015-5418-6.
[373] Y. Zhou, F.S. Riehle, Y. Yuan, H.-F. Schleiermacher, M. Niggemann, G.A. Urban, M. Krüger, Improved efficiency of hybrid solar cells based on non-ligand-exchanged CdSe quantum dots and poly(3-hexylthiophene), Appl. Phys. Lett. 96 (2010) 013304. doi:10.1063/1.3280370.
[374] N.C. Greenham, X. Peng, A.P. Alivisatos, Charge separation and transport in conjugated-polymer/semiconductor-nanocrystal composites studied by photoluminescence quenching and photoconductivity, Phys. Rev. B. 54 (1996) 17628–17637. doi:10.1103/PhysRevB.54.17628.
[375] S. Ren, N. Zhao, S.C. Crawford, M. Tambe, V. Bulović, S. Gradečak, Heterojunction Photovoltaics Using GaAs Nanowires and Conjugated Polymers, Nano Lett. 11 (2011) 408–413. doi:10.1021/nl1030166.
[376] *,† Peng Wang, † Agnese Abrusci, † Henry M. P. Wong, ‡ Mattias Svensson, ‡ and Mats R. Andersson, † Neil C. Greenham*, Photoinduced Charge Transfer and Efficient Solar Energy Conversion in a Blend of a Red Polyfluorene Copolymer with CdSe Nanoparticles, (2006). doi:10.1021/NL061085Q.
[377] S. Ren, L.-Y. Chang, S.-K. Lim, J. Zhao, M. Smith, N. Zhao, V. Bulović, M. Bawendi, S. Gradečak, Inorganic–Organic Hybrid Solar Cell: Bridging Quantum Dots to Conjugated Polymer Nanowires, Nano Lett. 11 (2011) 3998–4002. doi:10.1021/nl202435t.
[378] N. Zhao, T.P. Osedach, L.-Y. Chang, S.M. Geyer, D. Wanger, M.T. Binda, A.C. Arango, M.G. Bawendi, V. Bulovic, Colloidal PbS Quantum Dot Solar Cells with High Fill Factor, ACS Nano. 4 (2010) 3743–3752. doi:10.1021/nn100129j.
[379] W.J.E. Beek, M.M. Wienk, R.A.J. Janssen, Hybrid Solar Cells from Regioregular Polythiophene and ZnO Nanoparticles, Adv. Funct. Mater. 16 (2006) 1112–1116. doi:10.1002/adfm.200500573.
[380] M.S. and, P. Guyot-Sionnest*, Organic-Capped ZnO Nanocrystals: Synthesis and n-Type Character, (2001). doi:10.1021/JA0163321.
[381] A.C. Arango, S.A. Carter, P.J. Brock, Charge transfer in photovoltaics consisting of interpenetrating networks of conjugated polymer and TiO2 nanoparticles, Appl. Phys. Lett. 74 (1999) 1698. doi:10.1063/1.123659.
[382] K.M. Coakley, M.D. McGehee, Photovoltaic cells made from conjugated polymers infiltrated into mesoporous titania, Appl. Phys. Lett. 83 (2003) 3380–3382. doi:10.1063/1.1616197.
[383] C. Goh, S.R. Scully, M.D. McGehee, Effects of molecular interface modification in hybrid organic-inorganic photovoltaic cells, J. Appl. Phys. 101 (2007) 114503. doi:10.1063/1.2737977.
[384] † Yuxiang Liu, ‡ Shawn R. Scully, *,‡ Michael D. McGehee, § Jinsong Liu, §,∥ Christine K. Luscombe, §,∥ Jean M. J. Fréchet, ⊥ and Sean E. Shaheen, D.S. Ginley⊥, Dependence of Band Offset and Open-Circuit Voltage on the Interfacial Interaction between TiO2 and Carboxylated Polythiophenes, (2006). doi:10.1021/JP056576Y.
[385] J. Yu, T.-L. Shen, W.-H. Weng, Y.-C. Huang, C.-I. Huang, W.-F. Su, S.-P. Rwei, K.-C. Ho, L. Wang, Molecular Design of Interfacial Modifiers for Polymer-Inorganic Hybrid Solar Cells, Adv. Energy Mater. 2 (2012) 245–252. doi:10.1002/aenm.201100581.

[386] J. Bouclé, S. Chyla, M.S.P. Shaffer, J.R. Durrant, D.D.C. Bradley, J. Nelson, Hybrid Solar Cells from a Blend of Poly(3-hexylthiophene) and Ligand-Capped TiO2 Nanorods, Adv. Funct. Mater. 18 (2008) 622–633. doi:10.1002/adfm.200700280.
[387] Y.-Y. Lin, T.-H. Chu, C.-W. Chen, W.-F. Su, Improved performance of polymer/TiO2 nanorod bulk heterojunction photovoltaic devices by interface modification, Appl. Phys. Lett. 92 (2008) 053312. doi:10.1063/1.2839405.
[388] C.Y. Kwong, A.B. Djurišić, P.C. Chui, K.W. Cheng, W.K. Chan, Influence of solvent on film morphology and device performance of poly(3-hexylthiophene):TiO2 nanocomposite solar cells, Chem. Phys. Lett. 384 (2004) 372–375. doi:10.1016/J.CPLETT.2003.12.045.
[389] C.-H. Chuang, Y.-Y. Lin, Y.-H. Tseng, T.-H. Chu, C.-C. Lin, W.-F. Su, C.-W. Chen, Nanoscale Morphology Control of Polymer/TiO $_2$ Nanocrystal Hybrids: Photophysics, Charge Generation, Charge Transport, and Photovoltaic Properties, J. Phys. Chem. C. 114 (2010) 18717–18724. doi:10.1021/jp1075516.
[390] W.J.E. Beek, M.M. Wienk, R.A.J. Janssen, Hybrid polymer solar cells based on zinc oxide, J. Mater. Chem. 15 (2005) 2985. doi:10.1039/b501979f.
[391] W.J.E. Beek, M.M. Wienk, R.A.J. Janssen, Efficient Hybrid Solar Cells from Zinc Oxide Nanoparticles and a Conjugated Polymer, Adv. Mater. 16 (2004) 1009–1013. doi:10.1002/adma.200306659.
[392] S.D. Oosterhout, M.M. Wienk, S.S. van Bavel, R. Thiedmann, L. Jan Anton Koster, J. Gilot, J. Loos, V. Schmidt, R.A.J. Janssen, The effect of three-dimensional morphology on the efficiency of hybrid polymer solar cells, Nat. Mater. 8 (2009) 818–824. doi:10.1038/nmat2533.
[393] D. Bi, F. Wu, W. Yue, Y. Guo, W. Shen, R. Peng, H. Wu, X. Wang, M. Wang, Device Performance Correlated with Structural Properties of Vertically Aligned Nanorod Arrays in Polymer/ZnO Solar Cells, J. Phys. Chem. C. 114 (2010) 13846–13852. doi:10.1021/jp103587y.
[394] Z. Liu, Y. Sun, J. Yuan, H. Wei, X. Huang, L. Han, W. Wang, H. Wang, W. Ma, High-Efficiency Hybrid Solar Cells Based on Polymer/PbS $_x$ Se $_{1-x}$ Nanocrystals Benefiting from Vertical Phase Segregation, Adv. Mater. 25 (2013) 5772–5778. doi:10.1002/adma.201302340.
[395] Y. Xie, W. Zhou, J. Yin, X. Hu, L. Zhang, X. Meng, Q. Ai, Y. Chen, Post-annealing to recover the reduced open-circuit voltage caused by solvent annealing in organic solar cells, J. Mater. Chem. A. 4 (2016) 6158–6166. doi:10.1039/C6TA00835F.
[396] Y. Shi, F. Li, L. Tan, Y. Chen, Hybrid Bulk Heterojunction Solar Cells Based on the Cooperative Interaction of Liquid Crystals within Quantum Dots and Diblock Copolymers, ACS Appl. Mater. Interfaces. 5 (2013) 11692–11702. doi:10.1021/am4033263.
[397] T. Wang, L. Han, H. Wei, D. Zhu, X. Bao, S. Qiao, W. Sun, W. Chen, R. Yang, Influence of a π-bridge dependent molecular configuration on the optical and electrical characteristics of organic solar cells, J. Mater. Chem. A. 4 (2016) 8784–8792. doi:10.1039/C6TA02977A.
[398] J. Miao, H. Chen, F. Liu, B. Zhao, L. Hu, Z. He, H. Wu, Efficiency enhancement in solution-processed organic small molecule: Fullerene solar cells via solvent vapor annealing, Appl. Phys. Lett. 106 (2015) 183302. doi:10.1063/1.4919707.
[399] J.-L. Wang, Z. Wu, J.-S. Miao, K.-K. Liu, Z.-F. Chang, R.-B. Zhang, H.-B. Wu, Y. Cao, Solution-Processed Diketopyrrolopyrrole-Containing Small-Molecule Organic Solar Cells

with 7.0% Efficiency: In-Depth Investigation on the Effects of Structure Modification and Solvent Vapor Annealing, Chem. Mater. 27 (2015) 4338–4348. doi:10.1021/acs.chemmater.5b00848.
[400] R.A. Nawrocki, E. Pavlica, N. Ćelić, D. Orlov, M. Valant, D. Mihailović, G. Bratina, Fabrication of poly(3-hexylthiophene) nanowires for high-mobility transistors, Org. Electron. 30 (2016) 92–98. doi:10.1016/J.ORGEL.2015.11.038.
[401] H. Xin, G. Ren, F.S. Kim, S.A. Jenekhe, Bulk Heterojunction Solar Cells from Poly(3-butylthiophene)/Fullerene Blends: In Situ Self-Assembly of Nanowires, Morphology, Charge Transport, and Photovoltaic Properties, Chem. Mater. 20 (2008) 6199–6207. doi:10.1021/cm801324m.
[402] L. Baeten, B. Conings, H.-G. Boyen, J. D'Haen, A. Hardy, M. D'Olieslaeger, J. V. Manca, M.K. Van Bael, Towards Efficient Hybrid Solar Cells Based on Fully Polymer Infiltrated ZnO Nanorod Arrays, Adv. Mater. 23 (2011) 2802–2805. doi:10.1002/adma.201100414.
[403] W.-P. Liao, J.-J. Wu, Efficient Electron Collection in Hybrid Polymer Solar Cells: In-Situ-Generated ZnO/Poly(3-hexylthiophene) Scaffolded by a TiO 2 Nanorod Array, J. Phys. Chem. Lett. 4 (2013) 1983–1988. doi:10.1021/jz400996d.
[404] K.F. Jeltsch, M. Schädel, J.-B. Bonekamp, P. Niyamakom, F. Rauscher, H.W.A. Lademann, I. Dumsch, S. Allard, U. Scherf, K. Meerholz, Efficiency Enhanced Hybrid Solar Cells Using a Blend of Quantum Dots and Nanorods, Adv. Funct. Mater. 22 (2012) 397–404. doi:10.1002/adfm.201101809.
[405] K.-C. Choi, E.-J. Lee, Y.-K. Baek, D.-C. Lim, Y.-C. Kang, Y.-D. Kim, K.H. Kim, J.P. Kim, Y.-K. Kim, Morphologically controlled ZnO nanostructures as electron transport materials in polymer-based organic solar cells, Electrochim. Acta. 180 (2015) 435–441. doi:10.1016/J.ELECTACTA.2015.08.151.
[406] C.-H. Chang, T.-K. Huang, Y.-T. Lin, Y.-Y. Lin, C.-W. Chen, T.-H. Chu, W.-F. Su, Improved charge separation and transport efficiency in poly(3-hexylthiophene)–TiO2 nanorod bulk heterojunction solar cells, J. Mater. Chem. 18 (2008) 2201. doi:10.1039/b800071a.
[407] F. Tan, S. Qu, L. Wang, Q. Jiang, W. Zhang, Z. Wang, Core/shell-shaped CdSe/PbS nanotetrapods for efficient organic–inorganic hybrid solar cells, J. Mater. Chem. A. 2 (2014) 14502. doi:10.1039/C4TA02469A.
[408] Q. Cui, C. Liu, F. Wu, W. Yue, Z. Qiu, H. Zhang, F. Gao, W. Shen, M. Wang, Performance Improvement in Polymer/ZnO Nanoarray Hybrid Solar Cells by Formation of ZnO/CdS-Core/Shell Heterostructures, J. Phys. Chem. C. 117 (2013) 5626–5637. doi:10.1021/jp312728t.
[409] Lori E. Greene, Matt Law, and Benjamin D. Yuhas, P. Yang*, ZnO−TiO2 Core−Shell Nanorod/P3HT Solar Cells, (2007). doi:10.1021/JP077593L.
[410] F. Tan, S. Qu, W. Zhang, Z. Wang, Hybrid morphology dependence of CdTe:CdSe bulk-heterojunction solar cells, Nanoscale Res. Lett. 9 (2014) 593. doi:10.1186/1556-276X-9-593.
[411] Baoquan Sun, and Eike Marx, N.C. Greenham*, Photovoltaic Devices Using Blends of Branched CdSe Nanoparticles and Conjugated Polymers, (2003). doi:10.1021/NL0342895.
[412] M. Wright, A. Uddin, Organic—inorganic hybrid solar cells: A comparative review, Sol. Energy Mater. Sol. Cells. 107 (2012) 87–111. doi:10.1016/J.SOLMAT.2012.07.006.

[413] X. Fan, M. Zhang, X. Wang, F. Yang, X. Meng, Recent progress in organic–inorganic hybrid solar cells, J. Mater. Chem. A. 1 (2013) 8694. doi:10.1039/c3ta11200d.
[414] J.N. de Freitas, J.P. de Carvalho Alves, A.F. Nogueira, Hybrid Solar Cells: Effects of the Incorporation of Inorganic Nanoparticles into Bulk Heterojunction Organic Solar Cells, in: Nanoenergy, Springer International Publishing, Cham, 2018: pp. 1–68. doi:10.1007/978-3-319-62800-4_1.
[415] C.R. McNeill, N.C. Greenham, Conjugated-Polymer Blends for Optoelectronics, Adv. Mater. 21 (2009) 3840–3850. doi:10.1002/adma.200900783.
[416] L. Schmidt-Mende, A. Fechtenkötter, K. Müllen, E. Moons, R.H. Friend, J.D. MacKenzie, Self-organized discotic liquid crystals for high-efficiency organic photovoltaics., Science. 293 (2001) 1119–22. doi:10.1126/science.293.5532.1119.
[417] J.J.M. Halls, C.A. Walsh, N.C. Greenham, E.A. Marseglia, R.H. Friend, S.C. Moratti, A.B. Holmes, Efficient photodiodes from interpenetrating polymer networks, Nature. 376 (1995) 498–500. doi:10.1038/376498a0.
[418] W. Zhao, S. Li, H. Yao, S. Zhang, Y. Zhang, B. Yang, J. Hou, Molecular Optimization Enables over 13% Efficiency in Organic Solar Cells, J. Am. Chem. Soc. 139 (2017) 7148–7151. doi:10.1021/jacs.7b02677.
[419] S. Zhang, L. Ye, J. Hou, Breaking the 10% Efficiency Barrier in Organic Photovoltaics: Morphology and Device Optimization of Well-Known PBDTTT Polymers, Adv. Energy Mater. 6 (2016) 1502529. doi:10.1002/aenm.201502529.
[420] J. Zhao, Y. Li, G. Yang, K. Jiang, H. Lin, H. Ade, W. Ma, H. Yan, Efficient organic solar cells processed from hydrocarbon solvents, Nat. Energy. 1 (2016) 15027. doi:10.1038/nenergy.2015.27.
[421] Y. Li, X. Liu, F.-P. Wu, Y. Zhou, Z.-Q. Jiang, B. Song, Y. Xia, Z.-G. Zhang, F. Gao, O. Inganäs, Y. Li, L.-S. Liao, Non-fullerene acceptor with low energy loss and high external quantum efficiency: towards high performance polymer solar cells, J. Mater. Chem. A. 4 (2016) 5890–5897. doi:10.1039/C6TA00612D.
[422] H. Bin, L. Gao, Z.-G. Zhang, Y. Yang, Y. Zhang, C. Zhang, S. Chen, L. Xue, C. Yang, M. Xiao, Y. Li, 11.4% Efficiency non-fullerene polymer solar cells with trialkylsilyl substituted 2D-conjugated polymer as donor, Nat. Commun. 7 (2016) 13651. doi:10.1038/ncomms13651.
[423] D. Baran, T. Kirchartz, S. Wheeler, S. Dimitrov, M. Abdelsamie, J. Gorman, R.S. Ashraf, S. Holliday, A. Wadsworth, N. Gasparini, P. Kaienburg, H. Yan, A. Amassian, C.J. Brabec, J.R. Durrant, I. McCulloch, Reduced voltage losses yield 10% efficient fullerene free organic solar cells with >1 V open circuit voltages, Energy Environ. Sci. 9 (2016) 3783–3793. doi:10.1039/C6EE02598F.
[424] P. Cheng, M. Zhang, T.-K. Lau, Y. Wu, B. Jia, J. Wang, C. Yan, M. Qin, X. Lu, X. Zhan, Realizing Small Energy Loss of 0.55 eV, High Open-Circuit Voltage >1 V and High Efficiency >10% in Fullerene-Free Polymer Solar Cells via Energy Driver, Adv. Mater. 29 (2017) 1605216. doi:10.1002/adma.201605216.
[425] J. Liu, S. Chen, D. Qian, B. Gautam, G. Yang, J. Zhao, J. Bergqvist, F. Zhang, W. Ma, H. Ade, O. Inganäs, K. Gundogdu, F. Gao, H. Yan, Fast charge separation in a non-fullerene organic solar cell with a small driving force, Nat. Energy. 1 (2016) 16089. doi:10.1038/nenergy.2016.89.
[426] J. Lee, R. Singh, D.H. Sin, H.G. Kim, K.C. Song, K. Cho, A Nonfullerene Small Molecule Acceptor with 3D Interlocking Geometry Enabling Efficient Organic Solar Cells, Adv.

Mater. 28 (2016) 69–76. doi:10.1002/adma.201504010.
[427] J.W. Jung, J.W. Jo, C.-C. Chueh, F. Liu, W.H. Jo, T.P. Russell, A.K.-Y. Jen, Fluoro-Substituted n-Type Conjugated Polymers for Additive-Free All-Polymer Bulk Heterojunction Solar Cells with High Power Conversion Efficiency of 6.71%, Adv. Mater. 27 (2015) 3310–3317. doi:10.1002/adma.201501214.
[428] L. Ye, X. Jiao, M. Zhou, S. Zhang, H. Yao, W. Zhao, A. Xia, H. Ade, J. Hou, Manipulating Aggregation and Molecular Orientation in All-Polymer Photovoltaic Cells, Adv. Mater. 27 (2015) 6046–6054. doi:10.1002/adma.201503218.
[429] C.W. Tang, Two-layer organic photovoltaic cell, Appl. Phys. Lett. 48 (1986) 183–185. doi:10.1063/1.96937.
[430] M.-T. Dang, T.M. Grant, H. Yan, D.S. Seferos, B.H. Lessard, T.P. Bender, Bis(tri-n-alkylsilyl oxide) silicon phthalocyanines: a start to establishing a structure property relationship as both ternary additives and non-fullerene electron acceptors in bulk heterojunction organic photovoltaic devices, J. Mater. Chem. A. 5 (2017) 12168–12182. doi:10.1039/C6TA10739G.
[431] Y. Shu, Y.-F. Lim, Z. Li, B. Purushothaman, R. Hallani, J.E. Kim, S.R. Parkin, G.G. Malliaras, J.E. Anthony, A survey of electron-deficient pentacenes as acceptors in polymer bulk heterojunction solar cells, Chem. Sci. 2 (2011) 363–368. doi:10.1039/C0SC00433B.
[432] H. Li, T. Earmme, G. Ren, A. Saeki, S. Yoshikawa, N.M. Murari, S. Subramaniyan, M.J. Crane, S. Seki, S.A. Jenekhe, Beyond Fullerenes: Design of Nonfullerene Acceptors for Efficient Organic Photovoltaics, J. Am. Chem. Soc. 136 (2014) 14589–14597. doi:10.1021/ja508472j.
[433] O.K. Kwon, J.-H. Park, D.W. Kim, S.K. Park, S.Y. Park, An All-Small-Molecule Organic Solar Cell with High Efficiency Nonfullerene Acceptor, Adv. Mater. 27 (2015) 1951–1956. doi:10.1002/adma.201405429.
[434] X. Long, Z. Ding, C. Dou, J. Zhang, J. Liu, L. Wang, Polymer Acceptor Based on Double B←N Bridged Bipyridine (BNBP) Unit for High-Efficiency All-Polymer Solar Cells, Adv. Mater. 28 (2016) 6504–6508. doi:10.1002/adma.201601205.
[435] Y. Patil, R. Misra, M.L. Keshtov, G.D. Sharma, Small molecule carbazole-based diketopyrrolopyrroles with tetracyanobutadiene acceptor unit as a non-fullerene acceptor for bulk heterojunction organic solar cells, J. Mater. Chem. A. 5 (2017) 3311–3319. doi:10.1039/C6TA09607G.
[436] J.T. Bloking, T. Giovenzana, A.T. Higgs, A.J. Ponec, E.T. Hoke, K. Vandewal, S. Ko, Z. Bao, A. Sellinger, M.D. McGehee, Comparing the Device Physics and Morphology of Polymer Solar Cells Employing Fullerenes and Non-Fullerene Acceptors, Adv. Energy Mater. 4 (2014) 1301426. doi:10.1002/aenm.201301426.
[437] K. Cnops, B.P. Rand, D. Cheyns, B. Verreet, M.A. Empl, P. Heremans, 8.4% efficient fullerene-free organic solar cells exploiting long-range exciton energy transfer, Nat. Commun. 5 (2014). doi:10.1038/ncomms4406.
[438] Y. Duan, X. Xu, H. Yan, W. Wu, Z. Li, Q. Peng, Pronounced Effects of a Triazine Core on Photovoltaic Performance-Efficient Organic Solar Cells Enabled by a PDI Trimer-Based Small Molecular Acceptor, Adv. Mater. 29 (2017) 1605115. doi:10.1002/adma.201605115.
[439] D. Meng, H. Fu, C. Xiao, X. Meng, T. Winands, W. Ma, W. Wei, B. Fan, L. Huo, N.L. Doltsinis, Y. Li, Y. Sun, Z. Wang, Three-Bladed Rylene Propellers with Three-

Dimensional Network Assembly for Organic Electronics, J. Am. Chem. Soc. 138 (2016) 10184–10190. doi:10.1021/jacs.6b04368.
[440] B. Fan, L. Ying, Z. Wang, B. He, X.-F. Jiang, F. Huang, Y. Cao, Optimisation of processing solvent and molecular weight for the production of green-solvent-processed all-polymer solar cells with a power conversion efficiency over 9%, Energy Environ. Sci. 10 (2017) 1243–1251. doi:10.1039/C7EE00619E.
[441] W. Wang, C. Yan, T.-K. Lau, J. Wang, K. Liu, Y. Fan, X. Lu, X. Zhan, Fused Hexacyclic Nonfullerene Acceptor with Strong Near-Infrared Absorption for Semitransparent Organic Solar Cells with 9.77% Efficiency, Adv. Mater. 29 (2017) 1701308. doi:10.1002/adma.201701308.
[442] W. Zhao, D. Qian, S. Zhang, S. Li, O. Inganäs, F. Gao, J. Hou, Fullerene-Free Polymer Solar Cells with over 11% Efficiency and Excellent Thermal Stability, Adv. Mater. 28 (2016) 4734–4739. doi:10.1002/adma.201600281.
[443] Y. Yang, Z.-G. Zhang, H. Bin, S. Chen, L. Gao, L. Xue, C. Yang, Y. Li, Side-Chain Isomerization on an n-type Organic Semiconductor ITIC Acceptor Makes 11.77% High Efficiency Polymer Solar Cells, J. Am. Chem. Soc. 138 (2016) 15011–15018. doi:10.1021/jacs.6b09110.
[444] L. Gao, Z.-G. Zhang, H. Bin, L. Xue, Y. Yang, C. Wang, F. Liu, T.P. Russell, Y. Li, High-Efficiency Nonfullerene Polymer Solar Cells with Medium Bandgap Polymer Donor and Narrow Bandgap Organic Semiconductor Acceptor, Adv. Mater. 28 (2016) 8288–8295. doi:10.1002/adma.201601595.
[445] B. Kan, H. Feng, X. Wan, F. Liu, X. Ke, Y. Wang, Y. Wang, H. Zhang, C. Li, J. Hou, Y. Chen, Small-Molecule Acceptor Based on the Heptacyclic Benzodi(cyclopentadithiophene) Unit for Highly Efficient Nonfullerene Organic Solar Cells, J. Am. Chem. Soc. 139 (2017) 4929–4934. doi:10.1021/jacs.7b01170.
[446] F. Liu, Z. Zhou, C. Zhang, T. Vergote, H. Fan, F. Liu, X. Zhu, A Thieno[3,4-*b*]thiophene-Based Non-fullerene Electron Acceptor for High-Performance Bulk-Heterojunction Organic Solar Cells, J. Am. Chem. Soc. 138 (2016) 15523–15526. doi:10.1021/jacs.6b08523.
[447] S. Li, L. Ye, W. Zhao, S. Zhang, S. Mukherjee, H. Ade, J. Hou, Energy-Level Modulation of Small-Molecule Electron Acceptors to Achieve over 12% Efficiency in Polymer Solar Cells, Adv. Mater. 28 (2016) 9423–9429. doi:10.1002/adma.201602776.
[448] S. Dai, F. Zhao, Q. Zhang, T.-K. Lau, T. Li, K. Liu, Q. Ling, C. Wang, X. Lu, W. You, X. Zhan, Fused Nonacyclic Electron Acceptors for Efficient Polymer Solar Cells, J. Am. Chem. Soc. 139 (2017) 1336–1343. doi:10.1021/jacs.6b12755.
[449] H. Yao, L. Ye, J. Hou, B. Jang, G. Han, Y. Cui, G.M. Su, C. Wang, B. Gao, R. Yu, H. Zhang, Y. Yi, H.Y. Woo, H. Ade, J. Hou, Achieving Highly Efficient Nonfullerene Organic Solar Cells with Improved Intermolecular Interaction and Open-Circuit Voltage, Adv. Mater. 29 (2017) 1700254. doi:10.1002/adma.201700254.
[450] D. Xie, T. Liu, W. Gao, C. Zhong, L. Huo, Z. Luo, K. Wu, W. Xiong, F. Liu, Y. Sun, C. Yang, A Novel Thiophene-Fused Ending Group Enabling an Excellent Small Molecule Acceptor for High-Performance Fullerene-Free Polymer Solar Cells with 11.8% Efficiency, Sol. RRL. 1 (2017) 1700044. doi:10.1002/solr.201700044.
[451] Y. Lin, F. Zhao, Q. He, L. Huo, Y. Wu, T.C. Parker, W. Ma, Y. Sun, C. Wang, D. Zhu, A.J. Heeger, S.R. Marder, X. Zhan, High-Performance Electron Acceptor with Thienyl Side Chains for Organic Photovoltaics, J. Am. Chem. Soc. 138 (2016) 4955–4961.

doi:10.1021/jacs.6b02004.
[452] F. Zhao, S. Dai, Y. Wu, Q. Zhang, J. Wang, L. Jiang, Q. Ling, Z. Wei, W. Ma, W. You, C. Wang, X. Zhan, Single-Junction Binary-Blend Nonfullerene Polymer Solar Cells with 12.1% Efficiency, Adv. Mater. 29 (2017) 1700144. doi:10.1002/adma.201700144.
[453] J. Wang, W. Wang, X. Wang, Y. Wu, Q. Zhang, C. Yan, W. Ma, W. You, X. Zhan, Enhancing Performance of Nonfullerene Acceptors via Side-Chain Conjugation Strategy, Adv. Mater. 29 (2017) 1702125. doi:10.1002/adma.201702125.
[454] Y. Lin, F. Zhao, Y. Wu, K. Chen, Y. Xia, G. Li, S.K.K. Prasad, J. Zhu, L. Huo, H. Bin, Z.-G. Zhang, X. Guo, M. Zhang, Y. Sun, F. Gao, Z. Wei, W. Ma, C. Wang, J. Hodgkiss, Z. Bo, O. Inganäs, Y. Li, X. Zhan, Mapping Polymer Donors toward High-Efficiency Fullerene Free Organic Solar Cells, Adv. Mater. 29 (2017) 1604155. doi:10.1002/adma.201604155.
[455] H. Yao, Y. Cui, R. Yu, B. Gao, H. Zhang, J. Hou, Design, Synthesis, and Photovoltaic Characterization of a Small Molecular Acceptor with an Ultra-Narrow Band Gap, Angew. Chemie Int. Ed. 56 (2017) 3045–3049. doi:10.1002/anie.201610944.
[456] H.R. Stuart, D.G. Hall, Island size effects in nanoparticle-enhanced photodetectors, Appl. Phys. Lett. 73 (1998) 3815. doi:10.1063/1.122903.
[457] J.-D. Chen, C. Cui, Y.-Q. Li, L. Zhou, Q.-D. Ou, C. Li, Y. Li, J.-X. Tang, Polymer Solar Cells: Single-Junction Polymer Solar Cells Exceeding 10% Power Conversion Efficiency (Adv. Mater. 6/2015), Adv. Mater. 27 (2015) 1132–1132. doi:10.1002/adma.201570040.
[458] R. Wang, L.-H. Xu, Y.-Q. Li, L. Zhou, C. Li, Q.-D. Ou, J.-D. Chen, S. Shen, J.-X. Tang, Broadband Light Out-Coupling Enhancement of Flexible Organic Light-Emitting Diodes Using Biomimetic Quasirandom Nanostructures, Adv. Opt. Mater. 3 (2015) 203–210. doi:10.1002/adom.201400391.
[459] J.-D. Chen, L. Zhou, Q.-D. Ou, Y.-Q. Li, S. Shen, S.-T. Lee, J.-X. Tang, Enhanced Light Harvesting in Organic Solar Cells Featuring a Biomimetic Active Layer and a Self-Cleaning Antireflective Coating, Adv. Energy Mater. 4 (2014) 1301777. doi:10.1002/aenm.201301777.
[460] P.-P. Cheng, L. Zhou, J.-A. Li, Y.-Q. Li, S.-T. Lee, J.-X. Tang, Light trapping enhancement of inverted polymer solar cells with a nanostructured scattering rear electrode, Org. Electron. 14 (2013) 2158–2163. doi:10.1016/J.ORGEL.2013.05.020.
[461] S.-I. Na, S.-S. Kim, J. Jo, S.-H. Oh, J. Kim, D.-Y. Kim, Efficient Polymer Solar Cells with Surface Relief Gratings Fabricated by Simple Soft Lithography, Adv. Funct. Mater. 18 (2008) 3956–3963. doi:10.1002/adfm.200800683.
[462] J. You, X. Li, F. Xie, W.E.I. Sha, J.H.W. Kwong, G. Li, W.C.H. Choy, Y. Yang, Surface Plasmon and Scattering-Enhanced Low-Bandgap Polymer Solar Cell by a Metal Grating Back Electrode, Adv. Energy Mater. 2 (2012) 1203–1207. doi:10.1002/aenm.201200108.
[463] Y.-S. Hsiao, F.-C. Chien, J.-H. Huang, C.-P. Chen, C.-W. Kuo, C.-W. Chu, P. Chen, Facile Transfer Method for Fabricating Light-Harvesting Systems for Polymer Solar Cells, J. Phys. Chem. C. 115 (2011) 11864–11870. doi:10.1021/jp201504z.
[464] A. Peer, R. Biswas, Nanophotonic Organic Solar Cell Architecture for Advanced Light Trapping with Dual Photonic Crystals, ACS Photonics. 1 (2014) 840–847. doi:10.1021/ph500124q.
[465] W.E.I. Sha, W.C.H. Choy, Y. Wu, W.C. Chew, Optical and electrical study of organic solar cells with a 2D grating anode, Opt. Express. 20 (2012) 2572. doi:10.1364/OE.20.002572.

[466] Y. Jin, J. Feng, M. Xu, X.-L. Zhang, L. Wang, Q.-D. Chen, H.-Y. Wang, H.-B. Sun, Matching Photocurrents of Sub-cells in Double-Junction Organic Solar Cells via Coupling Between Surface Plasmon Polaritons and Microcavity Modes, Adv. Opt. Mater. 1 (2013) 809–813. doi:10.1002/adom.201300223.
[467] J.-L. Wu, F.-C. Chen, Y.-S. Hsiao, F.-C. Chien, P. Chen, C.-H. Kuo, M.H. Huang, C.-S. Hsu, Surface Plasmonic Effects of Metallic Nanoparticles on the Performance of Polymer Bulk Heterojunction Solar Cells, ACS Nano. 5 (2011) 959–967. doi:10.1021/nn102295p.
[468] J.D. Myers, W. Cao, V. Cassidy, S.-H. Eom, R. Zhou, L. Yang, W. You, J. Xue, A universal optical approach to enhancing efficiency of organic-based photovoltaic devices, Energy Environ. Sci. 5 (2012) 6900. doi:10.1039/c2ee21254d.
[469] S.Y. Chou, W. Ding, Ultrathin, high-efficiency, broad-band, omni-acceptance, organic solar cells enhanced by plasmonic cavity with subwavelength hole array, Opt. Express. 21 (2013) A60. doi:10.1364/OE.21.000A60.

Appendix I Resources for adaption in Figure 1:

http://www.tindosolar.com.au/learn-more/poly-vs-mono-crystalline/;
https://phys.org/news/2011-06-efficiency-flexible-cdte-solar-cell.html;
http://www.robaid.com/tech/epfls-new-convention-center-west-facade-features-dye-solar-cells.htm; https://www.ofdesign.net/interior-design/transparent-organic-solar-cells-the-source-of-energy-of-the-future-2170;
https://www.lanl.gov/discover/news-release-archive/2017/March/03.22-quantum-dot-voltage.php; http://pubs.rsc.org/en/content/articlepdf/2015/ta/c5ta90089a;
http://news.ufl.edu/articles/2016/07/setting-the-gold-standard.php;
https://yunwang.wordpress.com/2010/06/19/synthesis-of-aligned-zno-nanorods-with-different-parameters-and-their-effects-on-the-humidity-sensing-property/;
http://novarials.com/ProductsTiONWs.html;
https://www.azonano.com/article.aspx?ArticleID=4600;
https://www.nano.gov/node/1824;
https://pubs.rsc.org/en/content/articlelanding/2017/nr/c7nr03789a#!divAbstract;
https://www.sciencedaily.com/releases/2012/07/120717084831.htm.
https://phys.org/news/2012-12-nanostructures-triple-solar-cells-efficiency.html;
Zsiborács, H., Pályi, B., Baranyai, H.N., Veszelka, M., Farkas, I. and Pintér, G., 2017. Energy performance of the cooled amorphous silicon photovoltaic (PV) technology. Quarterly Journal of the Hungarian Meteorological Service, 121(1), pp.415-430;
Liang, J., Zhang, G., Sun, W. and Dong, P., 2015. High efficiency flexible fiber-type dye-sensitized solar cells with multi-working electrodes. Nano Energy, 12, pp.501-509.
Tong, X., Lin, F., Wu, J. and Wang, Z.M., 2016. High performance perovskite solar cells. Advanced Science, 3(5), p.1500201.